Ludwig-Maximilians-Universität München
Department Biologie I
Bereich Genetik

Functional analysis of DOT1-dependent histone H3 lysine 76 methylation during cell cycle progression in *Trypanosoma brucei*

Alwine Gassen

Dissertation der Fakultät für Biologie
der Ludwig-Maximilians-Universität München
eingereicht am 18. Oktober 2012

Functional analysis of DOT1-dependent histone H3 lysine 76 methylation during cell cycle progression in *Trypanosoma brucei*

Alwine Gassen

Betreut von Prof. Dr. Christian Janzen

Erster Gutachter:

Prof. Dr. Michael Boshart
Biozentrum der Ludwig-Maximilians-Universität München
Bereich Genetik

Zweiter Gutachter:

Prof. Dr. Peter Becker
Adolf-Butenandt-Institut der Ludwig-Maximilians-Universität München
Lehrstuhl für Molekularbiologie

Eingereicht am 18.10.2012
Tag der mündlichen Prüfung: 03.12.2012

Eidesstattliche Erklärung

Ich erkläre hiermit an Eides statt, dass die vorgelegte Dissertation von mir selbständig und ohne unerlaubte Hilfe angefertigt wurde.

München, den 18.10.2012

_____

Alwine Gassen

Erklärung

Hiermit erkläre ich, dass die Dissertation nicht ganz oder in wesentlichen Teilen einer anderen Prüfungskommission vorgelegt wurde.

Des Weiteren erkläre ich, dass ich mich anderweitig noch keiner Doktorprüfung unterzogen habe.

München, den 18.10.2012

_____

Alwine Gassen

Contents

Abbreviations

ac	acetylation
ARS	autonomously replicating sequence
ATP	adenosine triphosphat
BLE	bleomycin resistance gene
bp	base pair(s)
BrdU	5-bromo-2'deoxyuridine
BSA	bovine serum albumin
BSF	bloodstream form
C	cytokinesis
Cdc	cell division cycle protein
CDK	cyclin-dependent kinase
cDNA	copy DNA
Cdt1	Cdc10-dependent transcript 1 protein
ChIP	chromatin immunoprecipitation
Cy3/5	cyanine dye 3/5
Dam	DNA adenine methyltransferase
DAPI	4'-6-diamidino-2-phenylindole
dH_2O	distilled water
DMSO	dimethyl sulfoxide
DNA	deoxyribonucleic acid
DNase	deoxyribonuclease
dNTP	deoxyribonucleotide
Dot1	disruptor of telomeric silencing 1
DSB	double-strand breaks
DTT	dithiothreitol
EDTA	ethylenediamine tetraacetate
EdU	5-ethynyl-2'-deoxyuridine
ENL	eleven-nineteen-leukemia protein
ER	endoplasmic reticulum
ES	expression site
ESAG	expression site associated genes
ESB	expression site body

EtBr	ethidium bromide
FACS	fluorescence activated cell sorting
FCS	fetal calf serum
FISH	fluorescence *in situ* hybridization
G1	gap1 phase
G2	gap2 phase
G418	geneticin
gDNA	genomic DNA
GFP	green fluorescent protein
GPI	glycosylphosphatidylinositol
H3K76	lysine 76 of histone H3
H3V	histone H3 variant
HDAC	histone deacetylase
HP1	heterochromatin protein 1
HPH	hygromycin phosphotransferase gene
IFA	indirect immunofluorescence analysis
IP	immunoprecipitation
JBP2	base J binding protein 2
KAT	lysine acetyltransferase
kDa	kilo Dalton
KMT	lysine methyltransferase
LB	Luria Bertani medium
LTQ	linear quadrupole ion trap
M	mitosis
Mcm	mini-chromosome maintenance protein
me1/2/3	mono-/di-/tri-methylation
MiTat	Molteno institute trypanozoon antigen type
MLL	mixed-lineage leukemia
mRNA	messenger RNA
MS	mass spectrometry
NEO	aminoglycoside phosphotransferase gene
NP-40	nonidet P-40
ORC	origin recognition complex
ORF	open reading frame

PAC	puromycin N-acetyl-transferase gene
PAGE	polyacrylamide gel electrophoresis
PBS	phosphate-buffered saline
PCF	procyclic form
PCNA	proliferating cell nuclear antigen
PCR	polymerase chain reaction
PFR	paraflagellar rod
PI	propidium iodide
PMSF	phenylmethylsulfonyl fluoride
Pol	polymerase
Pre-RC	pre-replicative complex
PTM	post translational modification
PVDF	polyvinylidene fluoride
rDNA	ribosomal DNA
RIPA	radio immunoprecipitation assay buffer
RNA	ribonucleic acid
RNAi	RNA interference
RNase	ribonuclease
RT	room temperature
S	synthesis phase
SDS	sodium dodecyl sulfate
SET	Su(var)3-9, enhancer of zeste, trithorax
Sir	silent information regulator
SM	single marker
SSC	saline sodium citrate buffer
SWI2/SNF2	SWItch/Sucrose non fermentable
T7RNAP	T7 RNA polymerase
Tet	tetracycline
TETR	tetracycline repressor
Ti	tetracycline inducible
TSS	transcription start site
TTS	transcription termination site
ub	ubiquitination
UTR	untranslated region

VSG	variable surface glycoprotein
w/v	weight/volume
WHO	World Health Organization
WT	wild-type
Δ	deletion
53BP1	p53 binding protein

Abstract

Trypanosomes are ancient eukaryotic parasites with some unusual biological features. They diverged from the eukaryotic lineage several hundred million years ago and developed some unique mechanisms to regulate basic biological processes such as gene expression. The majority of their genes is organized in large polycistronic units and regulation of individual transcripts occurs mostly post-transcriptionally and not on the level of transcription initiation. Thus, complex patterns of post-translational histone modifications (PTMs), which regulate promoter activity in higher eukaryotic cells, are unlikely to exist in trypanosomes. Although the epigenetic machinery seems to be rather simple, a variety of PTMs have been identified in trypanosomes and only a few seem to be involved in transcription regulation. Together with easy genetic manipulation, this qualifies trypanosomes as a perfect model organism to study epigenetic mechanisms that are not associated with transcription regulation. Furthermore, their evolutionary divergence can be exploited to investigate how PTMs and the corresponding histone modifying enzymes develop new biological functions.

This thesis explored the methylation of histone H3 on lysine 76 (H3K76me) and its function during DNA replication in *Trypanosoma brucei.* Imaging techniques as well as mass spectrometry analyses revealed that H3K76 mono- and dimethylation (me1 and me2) were strictly cell cycle-regulated and restricted to G2 phase and mitosis. The regulation and function of H3K76me was thoroughly analyzed by genetic manipulation of the corresponding histone methyltransferases DOT1A and DOT1B. Depletion of *DOT1A* by RNAi abolished DNA replication, whereas over-expression of DOT1A and DOT1B caused continuous replication of the nuclear DNA. Furthermore, chromatin immunoprecipitation was employed to investigate the genome-wide distribution of H3K76me1 and -me2, which unraveled an association to putative origins of replication.

In summary, this study suggests that H3K76 methylation regulates DNA replication in *T. brucei*. This is a novel function for DOT1 methyltransferases, which might not be unique to trypanosomes. Furthermore, putative replication origins were identified in *T. brucei.* These findings provide the basis for future experimental approaches to understand how trypanosomes developed this new regulatory system for DNA replication.

1 Introduction

1.1 Trypanosoma brucei as a model organism

Trypanosomatids are unicellular flagellates that diverged several hundred million years ago from the main eukaryotic lineage (Fernandes *et al.*, 1993; Stevens *et al.*, 2001). All representatives of this group live widely spread as mostly harmless parasites in various hosts including insects, vertebrates and plants. However, some of the members such as *Leishmania major*, *Trypanosoma brucei* and *Trypanosoma cruzi* are pathogenic and cause major diseases in humans and livestock. *T. brucei* is responsible for the human sleeping sickness as well as nagana disease in livestock, in sub-Saharan Africa. Their impact as pathogens creates great interest to study these organisms in order to understand their cell biology and to find more efficient treatment of the diseases. Trypanosomes have therefore been investigated intensively for biomedical research purposes. These studies have allowed the discovery of unusual gene regulation mechanisms.

For example, RNA-editing occurs to a great extent in the mitochondria of trypanosomes and was first discovered in these organisms (Stuart *et al.*, 2005). During this process, precursor mRNA sequences are changed by insertion or deletion of uridine nucleotides. Guide RNAs specify the editing mechanism. Another unusual feature of trypanosome biology is that genes are transcribed genome-wide via polycistronic units (Fig 1; Martinez-Calvillo *et al.*, 2010). Complex promoter elements have not been described in trypanosomes and polycistronic units are thought to be expressed in a constitutive manner. Consequently, regulation of gene expression happens mainly post-transcriptionally. Only one RNA polymerase II (RNA Pol II) promoter has been found, which regulates transcription of the spliced-leader array (Gilinger and Bellofatto, 2001). Due to the polycistronic organization of genes, trypanosomes process RNA transcripts in a fundamentally different way compared to most other eukaryotes. A 39-nucleotide capped spliced-leader RNA is transferred to the 5´-end of mRNA by *trans*-splicing (Clayton, 2002). In trypanosomes, cellular mechanisms often involve evolutionarily conserved players, which adopted novel roles compared to other eukaryotes. One example is RNA Pol I, which transcribes some protein-coding genes including the *VSG* (variant surface glycoprotein) genes in trypanosomes (Gunzl *et al.*, 2003).

Epigenetics in trypanosomes is a recent field of research. The function of chromatin structure in transcription regulation is most likely less complex, because there is no need for differential regulation of individual genes. Instead, epigenetic mechanisms are more likely involved in

transcription-independent processes like DNA repair, segregation of chromosomes and DNA replication in trypanosomes.

In this thesis, histone methylation on H3K76 (histone H3, lysine 76) is examined in *T. brucei* and reveals some unexpected function in DNA replication regulation, which has not been found in other eukaryotes so far. Exploring epigenetic regulation in *T. brucei*, which is an early branched eukaryote, may contribute to the comprehension of essential mechanisms like replication regulation in higher eukaryotes. In combination with a variety of tools for genetic manipulations, *T. brucei* is a perfect model organism to study the function of chromatin and histone modifications in transcription-independent processes.

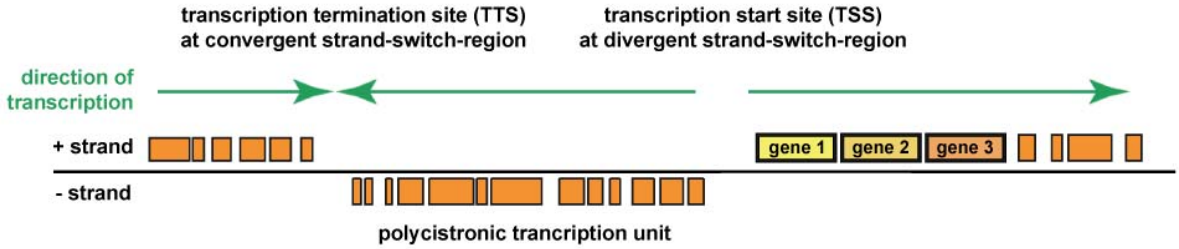

Figure 1: Polycistronic transcription in trypanosomes. Most of the genes (orange or yellow boxes) are arranged as convergent or divergent polycistronic units transcribed by RNA Pol II. Direction of transcription is indicated with green arrows. The "strand-switch-region" is the region between two neighboring units located on opposite strands, where transcription is initiated or terminated. Figure modified from (Siegel *et al.*, 2011).

1.1.1 Genome organization, antigenic variation and life cycle of *T. brucei*

Exploration of cellular mechanisms in *T. brucei* is greatly facilitated, because its genome is completely sequenced (Berriman *et al.*, 2005). The genome consists of 11 pairs of megabase-size chromosomes and additionally 1 to 5 intermediate-size chromosomes and over 100 minichromosomes of uncertain ploidy (Ersfeld *et al.*, 1999). Gene deletion mutants can be easily obtained using homologous recombination. Forward genetic approaches and high throughput RNAi screens (Alsford *et al.*, 2012) have been developed as well.

RNA Pol II-dependent transcription is constitutive and occurs via polycistronic units as mentioned above. Transcription of two neighboring polycistronic units located on opposite strands can be convergent or divergent (Fig 1). On the other hand, RNA Pol I-dependent transcription is regulated and some of the Pol I-transcribed genes are expressed in a strictly monoallelic fashion. The bloodstream form (BSF) of *T. brucei* (Fig 2A) is covered by a dense

coat of a glycosylphosphatidylinositol (GPI)-anchored VSG (Cross, 1975). A *VSG* gene is transcribed from a specialized subtelomeric locus called the expression site (ES; Hertz-Fowler *et al.*, 2008). About 20 of such ES exist in each cell, but only one is active at any given time resulting in monoallelic expression of the VSG (Horn and McCulloch, 2010). The active ES is localized to a specialized nuclear structure called the expression site body (ESB; Navarro and Gull, 2001).

The parasite periodically changes its surface proteins to escape the host immune response, a process known as antigenic variation (Rudenko *et al.*, 1998). Switching of VSG expression can happen first by homologous recombination of the *VSG* gene in the active ES with other *VSG* genes (~1000 different *VSG* genes and pseudogenes are present in the genome), or second by *in situ* switching, where another ES is activated and the previously active one is silenced (Borst *et al.*, 1998). By means of antigenic variation the parasites survives and proliferates in the bloodstream of the mammalian host. However, in its complex life cycle *T. brucei* alternates between its mammalian and its insect host, the tsetse fly of the genus *Glossina* (Vickerman, 1985). When parasites reach a threshold density in the bloodstream of the mammalian host, they differentiate to the cell cycle-arrested short stumpy form (Fig 2B), which is the insect-preadapted quiescent stage, irreversibly committed to differentiation to the procyclic form (PCF). They die within days, when they are not taken up by a tsetse fly during its bloodmeal on an infected mammal. Upon transmission to the insect's gut, the parasite completes the differentiation into the proliferating PCF (Fig 2B). PCF adapt to the new environment in the fly by changing their metabolism and by expressing another surface protein, the procyclin (Roditi *et al.*, 1989). After migration into the salivary glands, *T. brucei* transforms into epimastigote forms, which are attached to the microvilli of the epithelial cells by their flagella (not shown in the figure). Cells undergo genetic exchange in this developmental stage as experiments with fluorescently labeled cells have revealed (Gibson *et al.*, 2008). The exact mechanism is still unclear, but expression of meiotic proteins could be detected in this stage (Peacock *et al.*, 2011) supporting the hypothesis that meiosis is involved. Later in the life cycle *T. brucei* differentiates into the cell cycle-arrested metacyclic form (Fig 2B), which is preadapted to the mammalian environment and expresses VSG. The life cycle is completed with the transmission of the metacyclic form to the mammalian host during another bloodmeal of the tsetse fly.

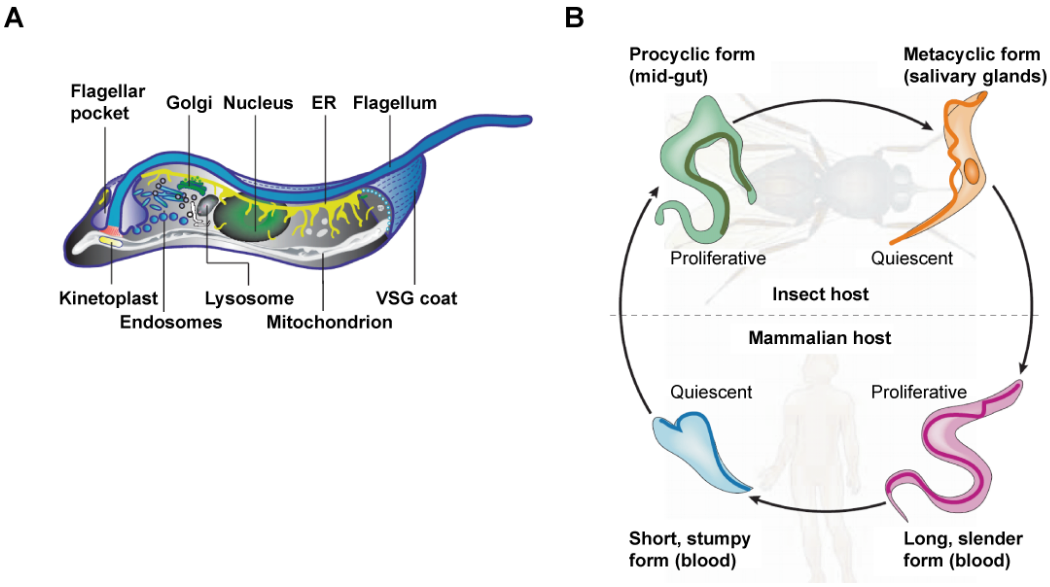

Figure 2: **Cell morphology and life cycle of *T. brucei*.** (**A**) Cellular structure and organelles of *T. brucei*. ER: Endoplasmatic Reticulum (Figure from Overath and Engstler, 2004) (**B**) Schematic view of its life cycle. Trypanosomes shuttle between the tsetse fly and the mammalian host and proliferate in the mid-gut of the insect or the bloodstream of the mammal. To adapt to the different environments, parasites undergo transformation into quiescent forms before they differentiate upon transfer to the new host (Figure from Pays *et al.*, 2006).

1.1.2 Cell cycle regulation

The cell cycle of trypanosomes is like in other eukaryotes divided into G1, S, G2 and M phase, followed by cytokinesis. In contrast to higher eukaryotes, each trypanosome cell possesses a single mitochondrion, which divides synchronously with the nucleus. The mitochondrial DNA, the kinetoplast (Fig 2A), is replicated in a distinct phase during the cell cycle (Woodward and Gull, 1990). The S phase of the kinetoplast is initiated before onset of nuclear DNA replication and its segregation precedes nuclear mitosis. Thus, the configuration and morphology of nucleus and kinetoplast act as a cytological marker for the position of an individual cell in the cell cycle (Fig 3).

Unlike higher eukaryotes, the nuclear envelope persists during all stages of the cell cycle in trypanosomes, which is characteristic for a closed mitosis. Furthermore, chromosomes do not condense into discrete visible interphase chromosomes during mitosis (Ogbadoyi *et al.*, 2000; Vickerman and Preston, 1970). Many orthologs of known cell cycle regulators like the cyclin-dependent kinases (CDKs) are found in trypanosomes, but key enzymes as well as some cell cycle checkpoints are missing (Hammarton, 2007). For example, treatment of procyclic trypanosomes with the anti-microtubuli agent rhizoxin results in cytokinesis in the absence of

mitosis, suggesting the lack of a mitosis to cytokinesis checkpoint in PCF (Ploubidou *et al.*, 1999).

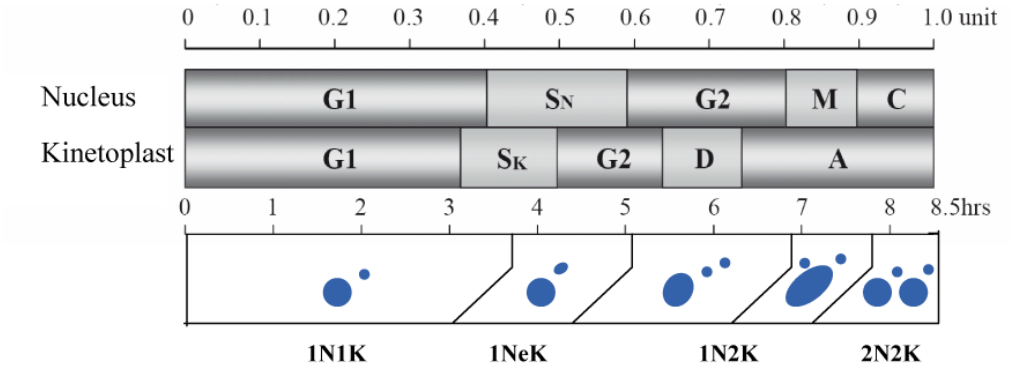

Figure 3: Phases of nucleus and kinetoplast during the cell cycle of *T. brucei*. Cell cycle duration of PCF is 8.5 hours, but is extended to 12 hours depending on culture conditions. Kinetoplast replication (S_K) initiates before nuclear S phase and finishes earlier leading to kinetoplast segregation (D) before the onset of nuclear mitosis. Phase A refers to "apportioning", in which kinetoplasts move further apart. Nucleus to kinetoplast configuration is shown below, which is used as marker for the cell cycle position of individual cells. 1N1K: 1 nucleus, 1 kinetoplast; 1NeK: 1 nucleus, elongated kinetoplast; 1N2K: 1 nucleus, 2 kinetoplasts; 2N2K: 2 nuclei, 2 kinetoplasts. Figure modified from McKean, 2003).

1.2 DNA replication

1.2.1 Basic principles in eukaryotes

Replication of DNA has to be precisely coordinated to maintain stability and integrity of the genome, before segregation to the daughter cell takes place. To enable DNA replication, the pre-replicative complex (pre-RC) has to assemble at defined DNA sites, known as the origins of replication (Fig 4). In *Saccharomyces cerevisiae*, these origins consist of 11 bp of a conserved autonomously replicating sequence (ARS) and several less conserved elements (Marahrens and Stillman, 1992). However in *Schizosaccharomyces pombe*, the origins of replication are much larger and less defined but contain AT-stretches (Okuno *et al.*, 1999). In higher eukaryotes, the origins are not conserved and replication is initiated randomly without sequence specificities (Cvetic and Walter, 2005). On the other hand, the components of the pre-RC are conserved among eukaryotes and include the origin recognition complex (Orc1-6), cell division cycle 6 (Cdc6), the replication factor Cdt1 and the mini-chromosome maintenance proteins (Mcm2-7). The pre-RC is formed by ordered assembly of these different replication factors and by its formation the origin is licensed for replication (Fig 4). After

licensing, additional factors are recruited and full activation of the origin is achieved by unwinding of DNA, formation of the replication fork and association of replicative DNA polymerases. Licensing of origins and the loading of Mcm2-7 onto DNA is restricted to late mitosis and G1 phase, which is important to coordinate DNA replication with the cell cycle (Bell and Dutta, 2002).

Eukaryotic cells have developed multiple redundant mechanisms to prevent re-initiation of replication from the same origin (Arias and Walter, 2007; Blow and Dutta, 2005). CDKs play an important role in preventing re-replication by phosphorylation of ORC, Cdc6 and the Mcms. For example, Cdc6 is degraded after phosphorylation in yeast cells leading to inhibition of pre-RC re-assembly. Metazoans inhibit re-replication mainly by downregulation of Cdt1 activity. Cdt1 is bound by an inhibitory protein called geminin, whose regulation is cell cycle-dependent (geminin appears in S phase and accumulates until late M phase). Inactivation of Cdt1 impairs the loading of Mcm proteins onto chromatin, thus preventing licensing.

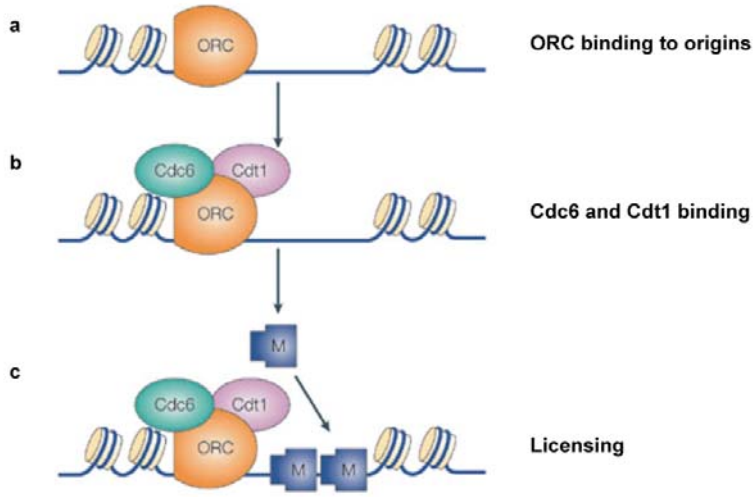

Figure 4: Assembly of pre-replicative complex proteins during origin licensing. (**a**) The origin recognition complex (ORC) is recruited to replication origins. (**b**) Cdc6 and Cdt1 bind. (**c**) Multiple Mcm2-7 protein hexamers are loaded onto the origin, which license the origin for replication. Figure from Blow and Dutta, 2005).

1.2.2 The replication machinery in *T. brucei* and other trypanosomatids

Very little is known about nuclear replication in trypanosomatids. In *T. cruzi* an Orc1 homologue (Orc1/Cdc6) seems to be constitutively expressed and is associated with chromatin throughout the cell cycle (Godoy *et al.*, 2009). Replication sites, identified by

incorporation of BrdU, are in the nuclear periphery at the beginning of S phase. Later in the cell cycle, these sites are observed in the interior of the nucleus due to a chromosome rearrangement as concluded by the authors (Elias *et al.*, 2002). In accordance with peripheral replication sites, the proliferating cell nuclear antigen of *T. cruzi* (TcPCNA) is constrained to the nuclear periphery during S phase where it co-localizes in distinguishable foci with TcOrc1/Cdc6 (Calderano *et al.*, 2011). During all other phases of the cell cycle TcPCNA and TcOrc1/Cdc6 are visible in a dispersed pattern throughout the nucleus.

In *Leishmania donovani*, PCNA can be detected primarily in the nucleus throughout the cell cycle although expression levels and pattern seem to vary (Kumar *et al.*, 2009). Maximum expression is observed in G1 and S phase showing sub-nuclear foci, which suggests the existence of replication factories as in higher eukaryotes. In G2/M phase and after mitosis a more diffuse pattern of PCNA is detectable. Additionally, MCM4 has been characterized in *L. donovani,* revealing nuclear localization throughout the cell cycle and a potential interaction with PCNA in S phase cells (Minocha *et al.*, 2011).

In *T. brucei,* PCNA is clearly detectable during S phase of the cell cycle but in contrast to observations in *T. cruzi* and *L. donovani*, TbPCNA seems to be degraded when cells enter G2 phase (Kaufmann *et al.*, 2012). Furthermore, replication sites are not restricted to the nuclear periphery in *T. brucei,* as it is observed in *T. cruzi*. Altogether, these findings suggest that a different mechanism of replication regulation may have evolved within the group of trypanosomatids. Recently, Dang and colleagues characterized many components of the regulatory complex at origins of replication in *T. brucei* including Cdc45, Mcm2-7, Sld5, Psf1-3 and a novel Orc1-like protein, Orc1b (Dang and Li, 2011). Interestingly, Cdc45 is exported out of the nucleus after DNA replication, whereas the other components are confined to the nucleus throughout the cell cycle. This indicates a potential mechanism for preventing re-replication in trypanosomes. Another group identified three novel Orc1/Cdc6 interacting factors, one of these as putative orthologue of eukaryotic Orc4 (Tiengwe *et al.*, 2012b). The other two lack homology to known proteins in higher eukaryotes, suggesting a kinetoplastid-specific function.

1.3 Chromatin organization

1.3.1 Characteristics of chromatin and histone modifications

Eukaryotic DNA is packaged in the nucleus through its association with histone proteins. 147 bp of DNA are wrapped around a histone octamer, which is composed of one H3/H4 tetramer

and two H2A/H2B dimers. This complex, the nucleosome, is the basic unit of DNA packaging (Fig 5). The less conserved histone H1 protein binds to the DNA loop between two neighboring nucleosomes. A striking feature of histone proteins is that they are subject to reversible post-translational modifications (PTMs) such as acetylation, methylation, phosphorylation, ubiquitination and sumoylation (Kouzarides, 2007).

Originally, chromatin has been categorized into euchromatin, which is decondensed in interphase nuclei, and heterochromatin, the condensed form. Heitz classified chromatin with the help of chromosomal stains of moss nuclei and proposed that heterochromatin reflects a functionally inactive state of the genome, whereas euchromatin is a marker for active transcription (Heitz, 1928; Passarge, 1979).

Today, this classification appears to be more complex because at least five distinct states of chromatin have been identified by a unique combination of chromatin proteins and PTMs (Filion *et al.*, 2010). Binding sites of chromatin-associated proteins were detected with the help of a DNA adenine methyltransferase (Dam) from bacteria. Dam was fused to chromatin proteins and local methyltransferase activity was determined. A genome-wide location map of 53 chromatin proteins in *Drosophila melanogaster* was generated revealing the chromatin composition along the genome. Five chromatin types, named BLACK, GREEN, BLUE, RED and YELLOW, were defined by computational analysis (Filion *et al.*, 2010). Interestingly, BLACK chromatin is a type of repressive chromatin that covers more than half of the genome, but seems to be devoid of HP1 association, a known heterochromatic protein (Eissenberg *et al.*, 1990), which can be found in GREEN chromatin. YELLOW and RED regions contain active genes but differ in the trimethylation on lysine 36 of histone H3 (H3K36me3), which is specific for YELLOW chromatin. Developmental genes are more often found in RED regions indicating specific roles in gene regulation for the different chromatin states.

PTMs of histones generate binding platforms for regulatory factors or alter higher order chromatin compaction by affecting the interaction between histones in adjacent nucleosomes (cross-talk; Fischle *et al.*, 2003). Acetylation, for example, neutralizes the positive charge of lysines resulting in looser interaction between nucleosome and DNA (Hong *et al.*, 1993). In general, PTMs play crucial roles that are linked to gene expression (Kouzarides, 2007). The "histone code hypothesis" proposes that different combinations of modifications establish epigenetic information that can be propagated from one generation to the next (Strahl and Allis, 2000). Histone-modifying enzymes set specific modifications to either one or more histone residues. Lysine methyltransferases (KMTs) are more specific than acetyltransferases

(Kouzarides, 2007) and often catalyze three levels of methylation: mono- di- and trimethylation (me1, me2, me3). The KMTs can be divided into two classes: enzymes with a conserved SET domain (Su(var)3-9, Enhancer of Zeste, Trithorax; Jenuwein *et al.*, 1998) and enzymes without SET domain such as Dot1. Lysine methylation is associated with either activation or repression of transcription, depending on the modified residue. Lysine 9 of histone H3 (H3K9) methylation, H3K27 methylation and H4K20me3 are associated with transcriptional repression in mammals (Peters *et al.*, 2003; Cao *et al.*, 2002; Schotta *et al.*, 2004), whereas actively transcribed chromatin shows high level of H3K4me3, H3K79me3 (Schubeler, 2004) and H3K36me3 (Santos-Rosa *et al.*, 2002; Schubeler, 2004; Krogan *et al.*, 2003b).

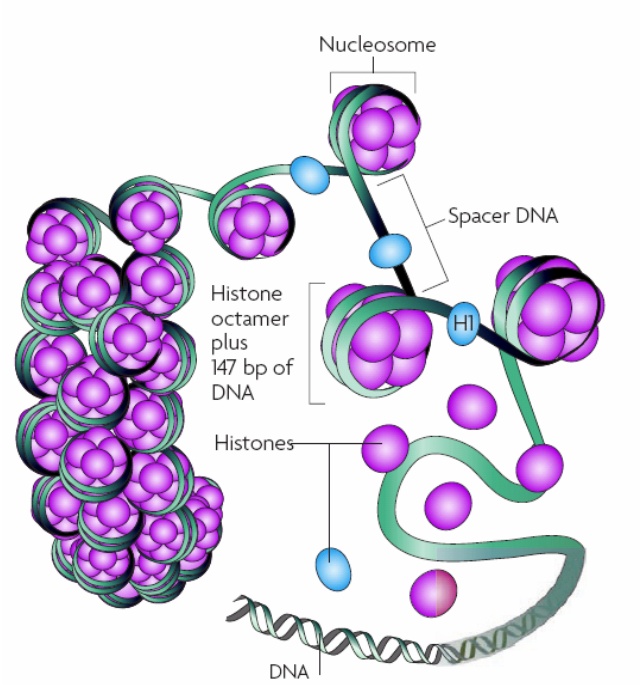

Figure 5: Chromatin structure. Nucleosomes are composed of 147 bp DNA wrapped around an octamer of two H2A/H2B dimers and one H3/H4 tetramer. Histone H1 (light blue) interacts with the linker DNA. Figure from Figueiredo *et al.*, 2009.

1.3.2 Chromatin in *T. brucei*

T. brucei possesses four canonical histones (H2A, H2B, H3 and H4), which are highly divergent from other organisms (Alsford and Horn, 2004; Sullivan *et al.*, 2006). This is unusual, because histones are some of the most conserved proteins in eukaryotes. Additionally, H1 linker histones and four histone variants (H2AZ, H2BV, H3V and H4V) exist in *T. brucei*. The histone variants H2AZ and H2BV dimerize (Lowell *et al.*, 2005) and

are enriched at RNA polymerase II transcription start sites (TSS; Siegel *et al.*, 2009) indicating a function in transcription initiation. The histone variant H3V is enriched at telomeric repeats (Lowell and Cross, 2004) and transcription termination sites (TTS), together with the variant H4V (Siegel *et al.*, 2009). H2AZ and H2BV are essential for viability, whereas H3V and H4V are not (Lowell and Cross, 2004; Lowell *et al.*, 2005; Siegel *et al.*, 2009). Hence, transcription of polycistronic units appears to be regulated by incorporation of histone variants suggesting that chromatin structure plays an important role in *T. brucei*.

The set of histone PTMs is smaller in *T. brucei*, some well conserved modifications are absent and some are trypanosome-specific. Significant progress has been made in mapping methylation and acetylation of trypanosomatid histones (da Cunha *et al.*, 2006; Janzen *et al.*, 2006a; Mandava *et al.*, 2007). Using Edman degradation and mass spectrometry several unusual PTMs could be found: The N-termini of H2A, H2B and H4 show methylated alanines and the C-terminus of H2A displays hyperacetylation of unknown function. 4 probable trypanosome-specific modifications have been detected on H2B: methylation of A1 (alanine residue 1) and acetylation of K4, K12 and K16. The modifications of histone H3´ N-terminal tail, mostly involved in transcriptional regulation in humans, are absent in *T. brucei,* except for H3K4me3, H3K23ac (homologous to H3K27) and H3K32me3 (homologous to H3K36), but the function of these histone modifications in trypanosomes is unknown. H3K76 methylation is homologous to K79 methylation in other organisms and the subject of this thesis. Histone H4 exhibits acetylation and methylation of K2, acetylation of K4 by histone acetyltransferase 3 (HAT3) and K10 by HAT2. H4K10 is an essential modification and shows enrichment at probable RNA polymerase II TSS, together with the histone variants H2AZ and H2BV. H4K14ac (homologous to the euchromatin marker H4K16ac in mammals) and H4K18me3 (homologous to H4K20me3, which is involved in heterochromatin formation in humans) have been found in trypanosomes, but have not been characterized so far.

The responsible enzymes are also sparsely represented in trypanosomes owing to the small set of histone modifications. 5 lysine acetyltransferases (KATs) and 7 histone deacetylases (HDACS) have been detected in *T. brucei* (Ingram and Horn, 2002; Kawahara *et al.*, 2008; Siegel *et al.*, 2008b), 3 of them are Sir2-related histone deacetylases (Alsford *et al.*, 2007; Garcia-Salcedo *et al.*, 2003). About 20 lysine methyltransferases containing a SET domain are annotated in the *T. brucei* genome, but none of them has yet been characterized. In contrast, the two Dot1 like proteins are well characterized (Janzen *et al.*, 2006b) and subject of this thesis. Putative demethylases of the Jumonji family have been annotated as well in *T. brucei* but not yet characterized. Arginine methylation has not been detected so far in trypanosomes,

although 5 candidates of arginine methyltransferases are present in the genome (Pelletier *et al.*, 2005). In addition to these modifying enzymes, two chromatin remodeling enzymes are characterized in *T. brucei*: ISWI, which is involved in ES silencing (Hughes *et al.*, 2007), and JBP2 (base J binding protein 2), which binds chromatin via the SWI2/SNF2 domain and hydroxylates thymidine residues (base J synthesis) at specific sites in BSF (DiPaolo *et al.*, 2005).

In summary, trypanosomes exhibit a smaller repertoire of histone modifications and chromatin associated enzymes compared to higher eukaryotes. The histone code is probably less complicated. This fact may help to discover the function and evolution of the histone code. Only few PTMs of histones seem to regulate Pol II-dependent transcription as Pol II transcribes constitutively via polycistronic units. Therefore, *T. brucei* may serve as a useful model organism to study PTMs that are not associated with Pol II transcription but regulate other evolutionarily conserved processes, such as DNA replication.

1.4 The DOT1 histone methyltransferase

DOT1 (disruptor of telomeric silencing; also *KMT4*) was discovered in a genetic screen for genes whose over-expression disrupt telomeric silencing (Singer *et al.*, 1998). The enzyme Dot1 is evolutionarily conserved and catalyzes the methylation of H3K79. This histone residue is located in the loop between the first and second alpha helix in the globular domain of the H3 core, where it is exposed on the surface of the nucleosome (Luger *et al.*, 1997). The yeast Dot1 and its human homolog DOT1L are responsible for me1, me2 and me3 of H3K79 in a distributive manner (Frederiks *et al.*, 2008; Min *et al.*, 2003) suggesting redundant roles of the three methylation states (Frederiks *et al.*, 2008). However, other studies indicated that there are different distributions and functions of H3K79me2 and H3K79me3 (Ooga *et al.*, 2008; Schulze *et al.*, 2009).

DOT1L methylates H3K79 only in a nucleosomal context (Feng *et al.*, 2002) suggesting the existence of a cross-talk between histones or histone modifications. Indeed, H3K79 methylation requires Rad6/Bre1-dependent ubiquitination of histone H2B on lysine 123 (H2BK123ub) in yeast (Briggs *et al.*, 2002; Ng *et al.*, 2002). The inhibition of H2B ubiquitination by deletion of Rad6 as well as mutation of H2BK123 prevents methylation of H3K79 (Briggs *et al.*, 2002). DOT1L methylation activity is robustly stimulated by ubiquitination of H2BK120 (human homolog to H2BK123 in yeast) as detected by *in vitro* constitution of nucleosomes (McGinty *et al.*, 2008). In addition, an acidic patch located in the

C-terminal region of Dot1 was shown to interact with a stretch of basic residues in the histone H4 tail (Fingerman *et al.*, 2007). This interaction is required for H3K79me2 and H3K79me3 *in vivo* reflecting another *trans*-histone regulatory mechanism.

Studies of enzymatic activity and regulation of Dot1 in many organisms revealed roles in different biological processes like transcription, cell cycle regulation and DNA damage response (reviewed in Nguyen and Zhang, 2011).

H3K79 methylation is correlated with active transcription

Over-expression and deletion of Dot1 in yeast disrupt silencing at telomere-proximal reporter genes (van Leeuwen *et al.*, 2002). Silent information regulator (Sir) proteins are required for telomeric silencing and their association to chromatin is prevented by H3K79 methylation. Hypermethylation of H3K79 by Dot1 over-expression reduces Sir binding globally, which abolishes silencing at telomeres. If H3K79 is hypomethylated after deletion of Dot1, Sir proteins disperse along the chromosome leading to reduced levels of Sir proteins at telomeres, which causes the disruption of telomeric silencing as well. Thus, methylated H3K79 seems to be a marker for euchromatic regions.

H3K79 methylation is associated with transcription in other studies as well. The genome-wide distribution of this modification was analyzed in different organisms. In *Drosophila,* ChIP-chip (Chromatin immunoprecipitation coupled with gene expression microarrays) revealed a correlation between H3K79me2 and active gene transcription (Schubeler, 2004). In line with these findings, Steger and colleagues revealed that H3K79 methylation is linked to gene transcription in mouse (Steger *et al.*, 2008). In human cells, ChIP-seq (Chromatin immunoprecipitation coupled with deep sequencing) experiments indicated that H3K79 methylation is enriched at transcribed genes (Wang *et al.*, 2008). Furthermore, H3K79 methylation is enriched on H3.3, a histone variant found at transcriptional active loci in *Drosophila* and mammals (Hake *et al.*, 2006; McKittrick *et al.*, 2004).

DOT1L was also purified in RNA polymerase II-associated transcription elongation complexes (Bitoun *et al.*, 2007; Krogan *et al.*, 2003a; Mohan *et al.*, 2010; Mueller *et al.*, 2007). A multi-subunit complex associated with Dot1 (called DotCom) was isolated and comprised the transcription factors AF9, AF10, AF17, ENL plus members of the Wnt pathway (Mohan *et al.*, 2010). Knockdown of ENL reduces H3K79me2 and inhibits global transcriptional elongation activity (Mueller *et al.*, 2007). Over-expression of several DotCom members increases H3K79 methylation levels and transcription elongation (Bitoun *et al.*, 2007). Therefore, a role for DOT1L in transcriptional elongation is suggested.

The first direct evidence that DOT1L is able to activate gene transcription comes from studies of leukemia, caused by chromosomal rearrangements.

Role of DOT1L in cancer and embryogenesis

Translocation of the *MLL* (mixed-lineage leukemia) gene, which codes for a H3K4 methyltransferase, results in the expression of oncogenic fusion proteins and is a common cause of acute leukemia. The MLL methyltransferase normally activates *Hox* genes, important during embryogenesis and hematopoiesis. In leukemic cells, the N-terminus of MLL without its methyltransferase domain is fused to more than 50 interaction partners leading to constitutive activation of *Hox* genes (Krivtsov and Armstrong, 2007). Several studies identified MLL fusion partners as interaction partners of DOT1L. AF10, ENL (Okada *et al.*, 2005), AF4 (Bitoun *et al.*, 2007) and AF9 (Zhang *et al.*, 2006) are some examples. The interaction between DOT1L and the MLL fusion partners causes mistargeting of DOT1L and aberrant H3K79 methylation at *Hox* genes, which leads to constitutive transcriptional activation and leukemogenesis (Chang *et al.*, 2010; Krivtsov *et al.*, 2008; Mueller *et al.*, 2009).

Another important role of DOT1L was demonstrated in embryogenesis of higher eukaryotes. In *Drosophila, grappa* (an ortholog of *DOT1*) seems to be important in parasegmentation, similar to *polycomb* and *trithorax* genes (Shanower *et al.*, 2005). *Grappa* is also involved in Wnt-signaling, which is essential for the wing morphogenesis of the fly (Mohan *et al.*, 2010). In mice, DOT1L plays an important role in organogenesis of the cardiovascular system during the development since *DOT1L* knockout embryos die by day 10.5 (Jones *et al.*, 2008).

Function of H3K79 methylation in DNA repair and meiotic checkpoint control

A breakthrough in understanding the function of H3K79 methylation was the discovery of the first protein that interacts with this modification. The human protein 53BP1 binds to methylated H3K79, an essential interaction for the recruitment of 53BP1 to DNA double-strand breaks (DSBs; Huyen *et al.*, 2004). The same association was detected in yeast, where Rad9, the ortholog of 53BP1, interacts with methylated H3K79 (Wysocki *et al.*, 2005). Dot1 mutants loose G1- and S phase checkpoint control and progress through the cell cycle even after ionizing radiation-induced DNA damage (Wysocki *et al.*, 2005). Furthermore, interaction between methylated H3K79 and Rad9 inhibits the accumulation of single-stranded DNA (ssDNA) at DSBs and at uncapped telomeres. This controls the mechanism of resection

by homologous recombination during DNA repair (Lazzaro *et al.*, 2008). In addition, Dot1 and Rad9 promote DSB-induced loading of cohesion onto chromatin (Conde *et al.*, 2009).
Besides its function in DNA repair, Dot1 plays a role in meiotic checkpoint control in yeast. The pachytene checkpoint prevents premature nuclear division in case of defective chromosome synapsis and thereby ensures proper chromosome segregation. Yeast mutants, defective in meiotic recombination, arrest at this checkpoint but fail to arrest in the absence of Dot1 resulting in unviable meiotic products (San-Segundo and Roeder, 2000). A mislocalization of the nucleolar proteins Pch2 and Sir2, which are important for the pachytene checkpoint, is observed in Dot1-depleted cells (San-Segundo and Roeder, 2000).

Cell cycle regulation of H3K79

H3K79 methylation levels fluctuate within the cell cycle in yeast and human cells suggesting a potential role in cell cycle regulation. In yeast, H3K79me2 level is low in G1 and S phases and increases in G2 and M phases (Schulze *et al.*, 2009; Zhou *et al.*, 2006). However, cell cycle-dependent appearance is different in HeLa cells. Here, H3K79me2 level is high in G1 and shows the lowest level in G2, before it increases again in M phase (Feng *et al.*, 2002).
A direct link of this histone modification to cell cycle-dependent gene regulation was found by discovering that H3K79me2 is enriched at genes, which are specifically expressed in G1 (Schulze *et al.*, 2009). Paradoxically, levels of H3K79me2 increase when these genes are inactive, during G2/M phases. The establishment of H3K79me2 requires the Swi4/Swi6 complex that regulates genes involved in the G1/S-transition. Additionally, this study challenges the functional redundancy of the three different methylation states of H3K79 suggested by Frederiks and colleagues (Frederiks *et al.*, 2008). ChIP-chip analysis revealed that H3K79me2 and H3K79me3 reside in different regions of the genome and show mutually exclusive patterns. H3K79me3 but not H3K76me2 colocalizes with H2BK123ub (Schulze *et al.*, 2009). Hence, pattern of H2B123ub may control the genome-wide establishment of H3K79me2 versus -me3.
Although H3K79me2 is enriched at cell-cycle regulated genes, it does not seem to be essential for cell cycle regulation and a distinct function could not been shown in yeast. Recently, a function of H3K79 in cell proliferation was detected in lung cancer cells (Kim *et al.*, 2011). DOT1L depletion leads to multi-nucleation, abnormal mitotic spindle formation and finally an irreversible G1 arrest in these cancer cells.
De Vos and colleagues introduced a novel aspect about the dynamic behaviour of H3K79 methylation in yeast (De Vos *et al.*, 2011). The pattern of H3K79 is affected by Dot1 activity,

but also by histone dilution during replication. Slowly growing cells accumulate more methyl groups on H3K79 indicating that cell-cycle length influences the average methylation pattern (De Vos *et al.*, 2011). A model was suggested in which H3K79 methylation functions as a timer and couples cell-cycle length to a biological response through quantitative changes in chromatin modifications.

In summary, there are some hints that H3K79 methylation might influence cell cycle-dependent gene regulation or cell cycle progression but the specific function in these processes remains unclear.

1.4.1 DOT1A and DOT1B

Trypanosoma brucei possesses two Dot1 homologs, DOT1A and DOT1B (Janzen *et al.*, 2006b), which probably arose from gene duplication. DOT1A is essential for viability and catalyzes H3K76me1 and -me2 (homologous to H3K79 in other organisms). DOT1B is not essential and exclusively mediates H3K76me3. In addition, DOT1B is also capable of adding the lower H3K76-methylation states. *In vitro* assays showed that unmodified recombinant nucleosomes become successively methylated by DOT1B independent of DOT1A activity (Gülcin Dindar, personal communication). Furthermore, expression of DOT1B in a yeast mutant lacking endogenous Dot1 enzyme leads to H3K79me2 and -me3 in the absence of DOT1A (Frederiks *et al.*, 2010). These *in vivo* data from a heterologous system indicate that DOT1A and DOT1B methylate independently from each other.

The function of the different H3K76 methylation states is largely unclear. However, initial analyses of H3K76me3 have revealed some functional hints. H3K76me3 is required for differentiation from BSF to PCF (Janzen *et al.*, 2006a). Differentiation of trypanosomes can be triggered *in vitro* by lowering of temperature from 37°C to 27°C and addition of citrate or *cis*-aconitate (Brun and Schonenberger, 1981; Engstler and Boshart, 2004). ΔDOT1B cells suffer growth arrest and die several days after induction of the differentiation process (Janzen *et al.*, 2006b). In addition, ES silencing is impaired in cells lacking *DOT1B* and H3K76me3 (Figueiredo *et al.*, 2008). *VSG* mRNAs originated from the silent ESs are ~10fold more abundant in ΔDOT1B mutants and the ES switching process is delayed resulting in cells expressing simultaneously two different VSGs on their surface (Figueiredo *et al.*, 2008). In summary, DOT1B seems to have a role in monoallelic VSG expression and differentiation in trypanosomes (Stockdale *et al.*, 2008).

The function of DOT1A is even less explored, although this enzyme harbors interesting characteristics and is essential for the parasite. H3K76me2 is regulated in a cell cycle-

dependent manner and can be detected mainly during mitosis and cytokinesis (Janzen *et al.*, 2006b). Depletion of *DOT1A* by RNAi causes a cell cycle phenotype, which is characterized by the emergence of cells with reduced DNA content (Janzen *et al.*, 2006b). The origin of this cell population is completely unknown. The data suggest a role for DOT1A and H3K76me2 in mitotic cell cycle regulation. However, many questions are open and need to be answered.

1.5 Aim of this thesis

Various experiments described in the literature indicate that H3K79 methylation is involved in transcriptional regulation, DNA repair, control of accurate chromosome segregation and possibly cell cycle regulation. However, the specific function of H3K79 methylation in these processes in yeast or other organisms is still not well understood and phenotypes after genetic manipulation of Dot1 are often difficult to decipher. For example, neither over-expression nor deletion of Dot1 in yeast causes any cell cycle-related phenotype, although a function in cell cycle-dependent transcription regulation has been suggested (Schulze *et al.*, 2009). Remarkably, trypanosomes develop a clear cell cycle-related phenotype after depletion of *DOT1A*, resulting in cells with half of the DNA content of a diploid cell and subsequent lethality (Janzen *et al.*, 2006b). Furthermore, H3K76me2 is only detectable in mitotic and cytokinetic cells (Janzen *et al.*, 2006b). Therefore, the function of H3K76 methylation in cell cycle progression, and the cell cycle-dependent regulation of this epigenetic mark were explored in detail in this thesis.

In order to understand the role of H3K76 methylation, the occurrence of H3K76me1 in the course of the cell cycle as well as the nuclear localization of all H3K76 methylation states were addressed. The regulation of the DOT1 enzymes during the cell cycle was analyzed with the help of a luciferase reporter system. To directly test their function, *DOT1A* and *DOT1B* were genetically manipulated by RNA interference and tetracycline-inducible over-expression systems. First, *DOT1A* was depleted and the observed cell cycle defect was characterized thoroughly to unravel the source of the cells with decreased DNA content, and second, over-expression systems of DOT1A and DOT1B were established in *T. brucei* to explore potential reciprocal phenotypes. Finally, a genome-wide study by chromatin immunoprecipitation was performed to find associations of H3K76me1 and -me2 to DNA sequences or genomic domains in order to understand the role of H3K76 methylation in a chromosomal context in *T. brucei*.

2 Materials and methods

2.1 Materials

2.1.1 *Escherichia coli*

E. coli SURE — *e14⁻(McrA⁻) Δ(mcrCB-hsdSMR-mrr) 171 endA1 supE44 thi-1 gyrA96 relA1 lac recB recJ sbcC umuC::Tn5 (Kan^r) uvrC [F´ proAB lacI^q ZΔM15 Tn10 (Tet^r)]* (Stratagene, Amsterdam)

E. coli XL10-Gold — *endA1 glnV44 recA1 thi-1 gyrA96 relA1 lac Hte Δ(mcrA)183 Δ(mcrCB-hsdSMR-mrr)173 tetR F'[proAB lacIqZΔM15 Tn10(TetR Amy CmR)]* (Stratagene, Amsterdam)

2.1.2 *Trypanosoma brucei brucei*

2.1.2.1 Wild-type strains

T. brucei MITat 1.2 — (Molteno Institute Trypanozoon antigen type 1.2) Stock 427, clone 221, monomorphic bloodstream form (BSF), G. Cross, New York (USA; Cross, 1975)
The origin of strain Lister 427 is unclear. For detailed information see pedigree of G. Cross
(http://tryps.rockefeller.edu/DocumentsGlobal/lineage_Lister427.pdf).

T. brucei AnTat 1.1 — (Antwerp Trypanozoon antigen type 1.1) Clone of EATRO 1125 from E. Pays (Brussels, Belgium) and P. Overath (Tübingen)
(Geigy *et al.*, 1975)

2.1.2.2 Transgenic strains

Genotypes of cell lines have been named according to the nomenclature of Clayton *et al.* (Clayton *et al.*, 1998). All transgenic lines used in this project are listed in table 1.

Table 1: Transgenic cell lines. Abbreviations: (TETR) tetracycline repressor, (T7RNAP) T7 RNA polymerase, (*NEO*) aminoglycoside phosphotransferase gene, (*BLE*) bleomycin resistance gene, (*HPH*) hygromycin phosphotransferase gene, (*BLAS*) blasticidin deaminase gene, (*PUR*) puromycin N-acetyl-transferase gene, (*RDNA*) ribosomal DNA, (Ti) tetracycline inducible

name	**29-13**
made by	(Wirtz *et al.*, 1999)
genotype	TETR T7RNAP *NEO HPH*
clone / pool	clone
constructs	pLew29, pLew13
selection markers	G418 [15 µg/ml], hygromycin [25 µg/ml]
note	PCF

name	**MITat1.2_sm**
made by	(Wirtz *et al.*, 1999)
genotype	TETR T7RNAP *NEO*
clone / pool	clone
constructs	pHD328, pLew114hyg5′
selection markers	G418 [2 µg/ml]
note	BSF

name	**29-13_DOT1B-TY**
made by	A. Gassen
genotype	TETR T7RNAP *NEO HPH RDNA::DOT1B-TY* ^{Ti} *BLE*
clone / pool	pool
constructs	pLew29, pLew13, pLew100_DOT1B-TY (CJ40)
selection markers	G418 [15 µg/ml], hygromycin [25 µg/ml], bleomycin [2,5 µg/ml]
note	PCF

name	**ΔDOT1B**
made by	(Janzen *et al.*, 2006b)
genotype	Δ*dot1b::NEO* / Δ*dot1b::HPH*
clone / pool	clone
constructs	PCR products
selection markers	G418 [15 µg/ml], hygromycin [25 µg/ml]
note	PCF

name	**ΔDOT1B_DOT1B-Luciferase**
made by	A. Gassen
genotype	Δ*dot1b::NEO* / Δ*dot1b::HPH tubulin::*DOT1B-Luciferase *PUR*
clone / pool	pool
constructs	CJ44_DOT1B-Luciferase_PUR
selection markers	puromycin [1 µg/ml]
note	PCF

name	**ΔDOT1B_DOT1B-Luciferase**
made by	A. Gassen
genotype	Δ*dot1b::NEO* / Δ*dot1b::HPH tubulin::*DOT1B-Luciferase *BLAS*
clone / pool	pool
constructs	CJ44_DOT1B-Luciferase_BLAS
selection markers	blasticidin [10 µg/ml]
note	PCF

name	**29-13_DOT1A-RNAi_pHD615**
made by	A. Gassen
genotype	TETR T7RNAP *NEO HPH tubulin::*DOT1A-RNAi^{Ti} *PUR*
clone / pool	pool
constructs	pLew29, pLew13, pHD615_DOT1A
selection markers	G418 [15 µg/ml], hygromycin [25 µg/ml], puromycin [1 µg/ml]
note	PCF

name	**MITat1.2_sm_DOT1A-RNAi_p2T7**
made by	A. Gassen
genotype	TETR T7RNAP *NEO RDNA*::DOT1A-RNAi^{Ti} *HPH*
clone / pool	clone
constructs	pHD328, pLew114hyg5′, p2T7-DOT1A (CJ38)
selection markers	G418 [2 µg/ml], hygromycin [2,5 µg/ml]
note	BSF

name	**MITat1.2_sm_DOT1A-RNAi_pHD615**
made by	A. Gassen
genotype	TETR T7RNAP *NEO RDNA*::DOT1A-RNAi^{Ti} *PUR*
clone / pool	clone
constructs	pHD328, pLew114hyg5′, pHD615_DOT1A
selection markers	G418 [2 µg/ml], puromycin [0,1 µg/ml]
note	BSF

name	**ANTat1.1_DOT1A-Luciferase**
made by	A. Gassen
genotype	*DOT1A*::DOT1A-Luciferase *BLE*
clone / pool	pool
constructs	PCR product; *in situ* tagging (Oberholzer *et al.*, 2006)
selection markers	bleomycin [2,5 µg/ml]
note	PCF

name	**29-13_DOT1A-TY**
made by	A. Gassen
genotype	TETR T7RNAP *NEO HPH RDNA::DOT1A-TY^{Ti} BLE*
clone / pool	pool
constructs	pLew29, pLew13, pLew100V5_DOT1A-TY
selection markers	G418 [15 µg/ml], hygromycin [25 µg/ml], blasticidin [10 µg/ml]
note	PCF

name	**29-13_PCNA-TY**
made by	(Kaufmann *et al.*, 2012)
genotype	TETR T7RNAP *NEO HPH pcna::pcna-TY PUR*
clone / pool	pool
constructs	pLew29, pLew13, PCR product, *in situ* tagging (Oberholzer *et al.*, 2006)
selection markers	G418 [15 µg/ml], hygromycin [25 µg/ml], puromycin [1 µg/ml]
note	PCF

2.1.3 Plasmids

Complete sequences of all constructs are available on the attached DVD as GCK files.

Table 2: Description and construction of plasmids used in this thesis.

name	**pLew100_DOT1B-TY (CJ40)**
made by	Christian Janzen
short description	inducible over-expression of DOT1B-TY from rDNA spacer gene locus
construction	The ORF of DOT1B was amplified from genomic DNA. The TY-epitope was introduced by PCR. Insert was cloned via *Bam*HI / *Hind*III.
digest for transfection	*Not*I
selection marker	bleomycin

name	**pLew100_v5b1d_DOT1A-TY**
made by	A. Gassen
short description	inducible over-expression of DOT1A-TY from rDNA spacer gene locus
construction	The ORF of DOT1A was amplified from genomic DNA using primers AG51 and AG52. The TY-epitope was introduced by PCR. Insert was cloned via *Bam*HI and *Hin*dIII.
digest for transfection	*Not*I
selection marker	bleomycin

name	**pHD309_CJ44_BSD**
made by	Christian Janzen
short description	constitutive expression vector, contains GFP under control of *DOT1B*-UTRs
construction	unpublished
digest for transfection	*Not*I
selection marker	blasticidin

name	**pHD309_CJ44_DOT1B-Luciferase**
made by	A. Gassen
short description	constitutive transcription of fusion gene DOT1B-Luciferase with *DOT1B*-UTRs from tubulin gene locus
construction	The ORF of DOT1B was amplified from genomic DNA using primers AG62 and AG63. The ORF of Luciferase was amplified from the plasmid pLew82. Insert was cloned via *Spe*I and *Bam*HI by three component ligation reaction.
digest for transfection	*Not*I
selection marker	puromycin or blasticidin

name	**pHD615_DOT1A**
made by	A. Gassen
short description	inducible DOT1A-RNAi hairpin vector (integration in rDNA spacer locus); RNAi directed against 460 bp of the DOT1A-ORF
construction	Sense and antisense fragments for RNAi hairpin were amplified from gDNA with primers MK3S, MK5S; MK3AS and MK5AS. Insert was cloned via *Hind*III, *Xho*I and *Bam*HI including a three component ligation reaction.
digest for transfection	*Not*I
selection marker	puromycin

name	**p2T7_DOT1A (CJ38)**
made by	Christian Janzen
short description	inducible DOT1A-RNAi vector (integration in rDNA spacer locus); transcription of *DOT1A* from two opposing T7 promotors
construction	The ORF of DOT1A was amplified from gDNA with primers CJ84 and CJ85. Insert was cloned via *Hind*III and *Bam*HI.
digest for transfection	*Not*I
selection marker	hygromycin

2.1.4 Primer

All oligonucleotides were synthesized by Sigma-Aldrich.

Table 3: Primer used in this thesis. Restriction sites are underlined and enzymes are mentioned.

name	sequence	application
AG 51	CGA ATT CCC CAA GCT TTA TGG AAG TCC ATA CTA ACC AGG ACC CAC TTG ACC CTG GAT TGC TAA TAT CCC G	amplification of *TY-DOT1A*, *Eco*RI and *Hind*III restriction sites
AG 52	CGA ATT CCA GGA TCC CGT TCA TCT CCG TCG GTG AAT G	amplification of *DOT1A*, *Eco*RI and *Bam*HI restriction sites
AG 56	CAG GAG TGC AGC GTG GAA TGG TGT ACG AGG GAT GGC CCT TTT TTC ATT CAC CGA CGG AGA CCG GGA CCG ATG GAA GAC GCC AAA AAC ATA	*in situ* tagging DOT1A-Luciferase
AG 57	ACT TGA TAA GTT GAA TAG CTG AAG TGA GCT ATC CAA AAA GAT ATA TGT CAG ACG TGT GGT AAT ACT GCA TAG ATA ACA AAC	*in situ* tagging DOT1A-Luciferase
AG 60	CCG GGA TCC ATG GAA GAC GCC AAA	amplification Luciferase gene, *Bam*HI restriction site
AG 61	CCG ACT AGT TTA CAA TTT GGA CTT TCC	amplification Luciferase gene, *Spe*I restriction site
AG 62	GAC TAG TAT GGA AGT CCA TAC TAA CCA GGA CCC ACT TGA CGA CGC ACG TGT TCA TCG TAG	amplification *TY-DOT1B*, *Spe*I restriction site
AG 63	CCG GGA TCC CGG TCC CGG CGA TCG CTT GAT GTA AAG ATA A	amplification *TY-DOT1B*, *Bam*HI restriction site
AG 66	CCA CTT GAT AAG TTG AAT AGC	integration check from 3´UTR-*DOT1A*
AG 69	CTT ATT GTT TTT CTG ATG TCA T	integration check from 5´UTR-*DOT1A*
AG 70	AGG AGA TAC ACA ATG GAT AC	integration check from 3´UTR-*DOT1A*

CJ 84	CCC AAG CTT TAT GGA AGT CCA TAC TAA CCA GGA CCC ACT TGA CCC TGG ATT GCT AAT ATC CCG	amplification of *DOT1A*, *Hind*III restriction site
CJ 85	AGG ATC CCG TTC ATC TCC GTC GGT GAA TG	amplification of *DOT1A*, *Bam*HI restriction site
CJ 116	AGA GCC ACG GAT AGT AGA GG	amplification of the tubulin gene locus (alpha + beta tubulin)
CJ 117	TCC GCG TCT AGT ATT GCT CC	amplification of the tubulin gene locus (alpha + beta tubulin)
MK 3S	GGG TAA GCT TGG AGC TGG GAC ACC TCA	amplification of sense fragment of *DOT1A*, *Hind*III restriction site
MK 5S	AAG ACT CGA GCT CAA GTT CCG GTC TGA	amplification of sense fragment of *DOT1A*, *Xho*I restriction site
MK 5AS	GGG TGG ATC CGG AGC TGG GAC ACC TCA	amplification of antisense fragment of *DOT1A*, *Bam*HI restriction site
MK 3AS	ATC CCT CGA GAT CTT TGT CAT ATC GGA	amplification of antisense fragment of *DOT1A*, *Xho*I restriction site

2.1.5 Antibodies

Table 4: Primary and secondary antibodies used in this thesis. Antibodies were diluted for western analysis or immunofluorescence analysis (IFA) as indicated below**.**

name	source	type	origin	western	IFA
primary antibodies					
anti-H3K76me1	rabbit	polyclonal	peptide (VSGAQK[Me1]EGLRFC) antibody, affinity purified	1:500	1:500
anti-H3K76me2	rabbit	polyclonal	peptide (VSGAQK[Me2]EGLRFC) antibody, affinity purified (Janzen *et al.*, 2006b)	1:2000	1:2000
anti-H3K76me3	rabbit	polyclonal	peptide (VSGAQK[Me3]EGLRFC) antibody, affinity purified (Janzen *et al.*, 2006b)	1:4000	1:2000
anti-H3	rabbit	polyclonal	recombinant full length protein from *T. brucei* (Pineda)	1:100,000	1:50,000
anti-H3	guinea-pig	polyclonal	recombinant full length protein from *T. brucei* (Pineda)		1:5000
anti-H4	rabbit	polyclonal	peptide (AKGKKSGEAC) antibody, affintiy purified (Siegel *et al.*, 2008b)	1:2000	1:2000
anti-tubulin (Tat1)	mouse	monoclonal	gift from Keith Gull (Woods *et al.*, 1989)	1:1000	1:1000
anti-TY (BB2)	mouse	monoclonal	gift from Keith Gull (Bastin *et al.*, 1996)	1:1000	1:1000
anti-PFR A/C	mouse	monoclonal	gift from Keith Gull (Woods *et al.*, 1989)	1:2000	
anti-BrdU	mouse	monoclonal	Caltag, clone JU-4		1:1000

secondary antibodies					
Alexa Fluor 488 anti-guinea pig IgG	goat	polyclonal	Invitrogen		1:2000
Alexa Fluor 488 anti-rabbit IgG	goat	polyclonal	Invitrogen		1:2000
Alexa Fluor 594 anti-mouse IgG	goat	polyclonal	Invitrogen		1:2000
Alexa Fluor 488 anti-mouse IgG	goat	polyclonal	Invitrogen		1:2000
Alexa Fluor 594 anti-rabbit IgG	goat	polyclonal	Invitrogen		1:2000
Alexa Fluor 680 anti-rabbit lgG	goat	polyclonal	Invitrogen	1:5000	
IRdye 800 anti-mouse IgG	goat	polyclonal	Invitrogen	1:20,000	
IRdye 680 LT anti-rabbit IgG	goat	polyclonal	Invitrogen	1:50,000	

2.1.6 Enzymes

Calf intestinal alkaline phosphatase (CIP)	NEB, Frankfurt
Phusion DNA polymerase	NEB, Frankfurt
Restriction endonucleases	NEB, Frankfurt
T4 DNA ligase	NEB, Frankfurt
Taq DNA polymerase	NEB, Frankfurt

2.1.7 Chemicals

Acids and bases	Roth, Karlsruhe; AppliChem, Darmstadt
Acrylamide	Roth, Karlsruhe
Agarose	Biozym, Hess.Oldendorf
Amino acids	AppliChem, Darmstadt; Sigma, Taufkirchen
BrdU (5-bromo-2'deoxyuridine)	Sigma, Taufkirchen
BSA	AppliChem, Darmstadt
DAPI (4,6-diamidino-2-phenylindole)	Sigma, Taufkirchen
Dialyzed FCS	PAA, Pasching
D-Luciferin	PJK, Kleinblittersdorf
dNTPs	Roche, Mannheim
Dynabeads coupled to sheep anti-rabbit IgG	Invitrogen, Karlsruhe

EdU (5-ethynyl-2'-deoxyuridine)	Invitrogen, Karlsruhe
Ethidium bromide	Roth, Karlsruhe
ExtrAvidin-Cy3	Sigma, Taufkirchen
Immersion Oil N=1.520	Applied Precision, Issaquah (USA)
Immersion Oil Immersol 518N	Thermo Scientic, Dreieich
Media additives	AppliChem, Darmstadt; Invitrogen, Karlsruhe; Sigma, Taufkirchen
Organic solvents	Roth, Karlsruhe; AppliChem, Darmstadt; Merck, Darmstadt
Pepstatin A	Serva, Heidelberg
Propidium iodide	Sigma, Taufkirchen
Standard and fine chemicals	AppliChem, Darmstadt; Merck, Darmstadt; Roche, Mannheim; Roth, Karlsruhe; Sigma, Taufkirchen
Size standards (DNA, Protein)	NEB, Frankfurt
Vectashield	Vector laboratories, Burlingame (USA)
Vybrant DyeCycle Orange stain	Invitrogen, Karlsruhe

2.1.8 Antibiotics

Ampicillin (10 mg/ml in H_2O)	Boehringer, Mannheim
Blasticidin (10 mg/ml in H_2O)	Merck, Darmstadt
Hygromycin (10 mg/ml in H_2O)	Calbiochem, Darmstadt
Neomycin , G418 (10 mg/ml in H_2O)	Sigma, Taufkirchen
Phleomycin (10 mg/ml in H_2O)	Cayla, Toulouse, France
Puromycin (10 mg/ml in H_2O)	Sigma, Taufkirchen
Tetracycline (10 mg/ml in EtOH)	Sigma, Taufkirchen

2.1.9 Kits

BigDye Terminator Mix v3.1	Applied Biosystems, Darmstadt
Biotin-Nick Translation Mix	Roche, Mannheim
Click-iT^{TM} EdU Alexa Fluor 594 Imaging Kit	Invitrogen, Karlsruhe
GenomePlex Amplification Kit	Sigma, Taufkirchen
Human T Cell Nucleofector Kit	Lonza, Köln

NucleoBond PC100 & 500	Macherey&Nagel, Düren
NucleoSpin Extract II	Macherey&Nagel, Düren
NucleoSpin Plasmid	Macherey&Nagel, Düren
NucleoSpin Tissue	Macherey&Nagel, Düren
QIAquick PCR Purification Kit	Qiagen, Hilden

2.1.10 Media and buffers

All media were prepared using ddH_2O and were filtrated for sterilization (pore size: 0.22 μm). FCS was heat-inactivated for 1h at 56°C before use.

HMI9	(Hirumi and Hirumi, 1989) modified by (Vassella and Boshart, 1996): Iscove's modified medium powder for 1 l; 3.024 g $NaHCO_3$; 136 mg hypoxanthine; 28.2 mg bathocuproine sulfonate; 0.2 mM β-mercaptoethanol; 39 mg thymidine; 100,000 U penicillin; 100 mg streptomycin; 182 mg cysteine; 10% (v/v) FCS
SDM79	SDM79 basic medium (Brun and Schonenberger, 1979), modified by G. Cross (SDM79 JRH57453, http://tryps.rockefeller.edu/trypsru2_culture_media_compositions.html), complemented with 7.5 mg/l hemin; 10 mM glycerol; 100,000 U/l penicillin; 100 mg/l streptomycin; 26 mM $NaHCO_3$ and 10% FCS
Conditioned SDM79	AnTat 1.1 PCF culture of 1-2x10^7 cells/ml was centrifuged (10 min; 900 g; 4 °C) and the supernatant was sterile filtrated.
Freezing medium	HMI9 or SDM79 containing 10-25% (v/v) FCS and 10% glycerol
Cytomix	10 mM K_2HPO_4/KH_2PO_4 pH 7.6; 25 mM HEPES; 2 mM EGTA; 120 mM KCl; 150 µM $CaCl_2$; 5 mM $MgCl_2$; 0.5% (w/v) glucose; 1 mM hypoxanthine; 100 µg/ml BSA
CASYton	135.7 mM NaCl; 1.3 mM EDTA-diNa; 5.36 mM KCl; 1.37 mM Na_2HPO_4; 5.44 mM NaH_2PO_4; 7.14 mM NaF
PBS	10 mM Na_2HPO_4; 1.8 mM KH_2PO_4; 140 mM NaCl; 2.7 mM KCl; pH 7.4

LB medium	10 g tryptone; 5 g yeast extract; 10 g NaCl; pH 7
LB agar plates	LB medium of 16 g/l agar
TAE	40 mM Tris-HCl pH 8; 40 mM NaOAc; 1 mM EDTA
TE-buffer	10 mM Tris-HCl pH 7.6; 1 mM EDTA
DNA loading dye (6x)	0.4% (w/v) Orange G; 15% (w/v) Ficoll 400
Separating gel buffer	1.5 M Tris-HCl pH 8.8; 0.4% (w/v) SDS
Stacking gel buffer	0.5 M Tris-HCl pH 6.8; 0.4% (w/v) SDS
Anode buffer	300 mM Tris pH 10.4; 20% (v/v) methanol
Cathode buffer	25 mM Tris pH 7.6; 20% (v/v) methanol; 40 mM ε-amino caproic acid
Laemmli running buffer	25 mM Tris-base pH 8.8; 0.1% (w/v) SDS; 0.192 M glycine
Laemmli loading dye (6x)	350 mM Tris-HCl pH 6.8; 0.28% (w/v) SDS; 10% (v/v) glycerol; 0.6 M DTT; 0.012% (w/v) bromphenol blue; 0.6% (w/v) β-mercaptoethanol
Coomassie stain	10% acetic acid; 0.006% CBB G250
Destain solution	50% methanol; 10% acetic acid

ChIP buffers

Formaldehyde solution	50 mM HEPES-KOH, pH 7.5; 100 mM NaCl; 1 mM EDTA; 0.5 mM EGTA; 11% formaldehyde
Lysis buffer 1	50 mM HEPES-KOH, pH 7.5; 140 mM NaCl; 1 mM EDTA; 10% glycerol; 0.5% NP-40; 0.25% Triton X-100; 1 mM PMSF; 1 mM TLCK; 1 µg/µl Leupeptin; 1 µg/µl Pepstatin
Lysis buffer 2	10 mM Tris-HCl, pH 8; 200 mM NaCl; 1 mM EDTA; 0.5 mM EGTA; 1 mM PMSF; 1 mM TLCK; 1 µg/µl Leupeptin; 1 µg/µl Pepstatin
Lysis buffer 3	10 mM Tris-HCl, pH 8; 100 mM NaCl; 1 mM EDTA; 0.5 mM EGTA; 0.1% Na-deoxycholate; 0.5% N-lauroylsarcosine; 1 mM PMSF; 1 mM TLCK; 1 µg/µl Leupeptin; 1 µg/µl Pepstatin
Wash buffer (RIPA)	50 mM HEPES-KOH, pKa 7.55; 500 mM LiCl; 1 mM EDTA; 1.0% NP-40; 0.7% Na-deoxycholate
Elution buffer	50 mM Tris-HCl, pH 8; 10 mM EDTA, 1% SDS

FISH solutions

SSC (20x)	3 M NaCl; 0.3 M NaCitrate; pH 7.0
SSPE (20x)	3 M NaCl; 0.2 M $NaH_2PO_4xH_2O$; 0.2 M Na_2EDTA; pH 7.4
Hybridization buffer	50% formamide; 10% dextran sulfate, 2x SSPE

Luciferase assay buffers

Lysis buffer	250 mM Tris-HCl, pH 7.8; 1 mM EDTA; 0.2% Saponin; 1 mM DTT; store at -20°C
Reaction buffer	20 mM Tris-HCl, pH 7.8; 5 mM $MgCl_2$; 0.1 mM EDTA; 33.3 mM DTT; 270 µM Coenzym A; 470 µM D-Luciferin; 530 µM rATP, pH 7.0; store at -80°C

2.1.11 Equipment

Amaxa Nucleofector II		Lonza, Köln
Bioruptor		Diagenode, Lüttich, Belgium
CASY I Cell Analyzer (model TTC)		Schärfe System, Reutlingen
Centrifuges	Sorvall RC5C (GSA, SS34)	Thermo Scientific, Dreieich
	Heraeus Varifuge 3.0R	Thermo Scientific, Dreieich
	Heraeus Varifuge 3.2RS	Thermo Scientific, Dreieich
	Rotixa/KS	Hettich, Tuttlingen
	2K15 (rotor 12145)	Sigma, Deisenhofen
	5417R	Eppendorf, Hamburg
	Ultra centrifuge (rotor TLA-45)	Beckman Instruments, München
Electro Cell Manipulator 630		BTX, San Diego, USA
FACSAriaII		Becton Dickinson, New Jersey, USA
FACSCalibur Dual Laser Flow Cytometer		Becton Dickinson, New Jersey, USA
Geldoc 2000		Bio-Rad, München
Gene Amp PCR System 2400		Perkin Elmer, Weiterstadt
Incubators	Forma Scientific 3121	Thermo Scientific, Dreieich
	Heraeus BB6060	Thermo Scientific, Dreieich
	Heraeus Cytoperm 8088	Thermo Scientific, Dreieich
	Thermo Heracell 240	Thermo Scientific, Dreieich
Lumat LB 9501		Berthold, Pforzheim
MALDI-LTQ-Orbitrap		Thermo Scientific, Dreieich

Microscopes	IM35, Axiovert, Axiophot2	Zeiss, Jena
	DeltaVision (IX71 Olympus)	Applied Precisions, Issaquah, USA
	DeltaVision OMX v3	Applied Precision, Issaquah, USA
MyCycler		Bio-Rad, München
Nano Drop-1000		Peqlab, Erlangen
Neubauer counting chamber (0.1 mm)		Brand Gläser, Wertheim
Odyssey IR Systems		LI-COR, Bad Homburg

Consumable Supplies

8-strips (0.2 ml)	VWR International, Darmstadt
Cell culture flasks	Greiner bio-one, Solingen
Cover slips (round, 12 mm)	VWR International, Darmstadt
Cover slips (square, 17 mm)	Roth, Karlsruhe
Electroporation cuvettes (EC)	BTX, Heidelberg; Lonza, Köln
Immobilion PVDF- Membrane	Millipore, Schwalbach
Microtiter plates	Greiner bio-one, Solingen
Multiwell culture plates	Greiner bio-one, Solingen
PCR/sequencing tubes (0.2 ml)	Bio-Rad, München
Petri dishes	Greiner bio-one, Solingen
Polypropylen tubes (15 and 50 ml)	Greiner bio-one, Solingen
Reaction tubes	Sarstedt, Nürnberg
Sterile filter 0.2 µM	Millipore, Schwalbach
Whatman filter paper	Schleicher und Schuell, Dassel

2.1.12 Software

4peaks	Mekentosj, Amsterdam, Netherlands
Adobe Illustrator CS3	Adobe Systems, San Jose, USA
Adobe Photoshop CS5	Adobe Systems, San Jose, USA
Bioconductor	http://www.bioconductor.org
BLAST	http://ncbi.nlm.nih.gov/
CellQuest 3.3	Becton Dickinson, New Jersey, USA
ClustalX 2.0	Conway Institute, Dublin, Ireland
EndNote X4	Thomson Reuters, Carlsbad, USA
FACSDiva 6.0	Becton Dickinson, New Jersey, USA

FlowJo 8.8.6	Tree Star, Oregon, USA
Gene Construction Kit 2.5	Texto, New Hampshire, USA
GeneDB	http://www.genedb.org/
ImageJ 1.42k	http://rsb.info.nih.gov/ij/
Integrated Genome Browser	http://bioviz.org/igb/download.shtml
Odyssey 2.1	Li-COR, Bad Homburg
Proteome Discoverer	Thermo Scientific, Dreieich
R	http://www.r-project.org
softWoRxTM 3.7.1	AppliedPrecision, Issaquah, USA
TriTryp	http://tritrypdb.org/tritrypdb/
Xcalibur	Thermo Scientific, Dreieich

2.2 Methods

2.2.1 Cultivation of BSF

Monomorphic BSF trypanosomes were cultivated in HMI9 medium at 37°C and 5% CO_2 under constant selection with appropriate drug(s). To ensure logarithmic growth, cells were counted regularly with a Neubauer-improved counting chamber and diluted if necessary. Cell densities never exceeded $1x10^6$ cells per ml.

To freeze established transgenic cell lines, $5x10^6$ cells were harvested and resuspended in 1 ml of cold freezing medium per stabilate and transferred to cryotubes. Cells were slowly cooled down to -80°C with a Stratacooler and transferred to -152°C for long time storage.

2.2.2 Transfection of BSF

BSF were transfected using the AMAXA Nucleofector II with the program X-001. 10 μg of plasmid DNA were linearized and precipitated by isopropanol. $1\text{-}2x10^7$ cells were resuspended in 100 μl of Nucleofector solution, mixed with the DNA, electroporated and immediately added to 50 ml HMI9 medium. To get clonal cell populations, 50 ml were split onto two 24-well-plates. Adequate antibiotics were added 6-8 hours post transfection for selection.

2.2.3 Cultivation of PCF

PCF trypanosomes were cultivated *in vitro* in SDM79 at 27°C under constant selection with appropriate drug(s). To ensure logarithmic growth cells were counted regularly with the CASY Cell Analyzer and were diluted if necessary. Cell densities never fell below $1x10^6$ cells per ml or exceeded $2x10^7$ cells per ml.

To freeze established transgenic cell lines, $5x10^7$ cells were harvested and resuspended in 1 ml of cold freezing medium per stabilate and transferred to cryotubes. Cells were slowly cooled down to -80°C with a Stratacooler and transferred to -152°C for long time storage.

2.2.4 Transfection of PCF

PCF were transfected using the Electro Cell Manipulator (BTX) with the settings: 1.2 kV, 25 µF and 186 Ω. $2x10^7$ cells were washed with cytomix, resuspended in 400 µl of 4°C cold cytomix, mixed with 10 µg linearized plasmid DNA and electroporated. Afterwards cells were added to 11 ml prewarmed 30% conditioned SDM79. 5 ml of cell culture were kept undiluted, while the rest of the cells were diluted 1:2, 1:4, 1:8 and 1:16 onto a 24-well-plate to get clonal populations. Antibiotics were added 12 to 18 hours later for selection.

2.2.5 *In situ* tagging of genes in *T. brucei*

In *T. brucei*, *in situ* tagging is greatly facilitated by high frequency of homologous recombination of tagging constructs into target genes. The PCR based method can be used to introduce C-terminal tags to proteins (Oberholzer *et al.*, 2006; Shen *et al.*, 2001). With this method the original 3´UTR of the target gene is replaced by another UTR introduced by the tagging construct. In this thesis C-terminal tagging of DOT1A with Luciferase was performed by such PCR-mediated approach. The Luciferase tag and the phleomycin resistance gene were amplified from pLew82 using primers containing homologous sequences to the target side at their end. The forward primer carried the last 60 bp of the *DOT1A* open reading frame without stop codon as target sequence and 20 nucleotides of the beginning of the Luciferase gene. The reverse primer contained 60 bp of the 3´UTR of *DOT1A* for targeting and 20 nucleotides of the pLew82 backbone binding to the UTR downstream of the phleomycin resistance gene. The construct was amplified and transfected in *T. brucei* and correct integration was confirmed by PCR of genomic DNA isolated from the transgenic clone. Homologous

recombination resulted in expression of a DOT1A-Luciferase fusion protein from the endogenous *DOT1A* gene locus.

2.2.6 RNAi systems in *T. brucei*

Two different systems were used for downregulation of *DOT1A* by RNA interference:

1. The tetracycline inducible system with two opposing T7 promoters leading to transcription from two sites by T7 polymerase and therefore production of sense and antisense RNA, which induce the RNAi (Alibu *et al.*, 2005). The vector is stably integrated into the *RDNA* spacer locus.
2. The tetracycline inducible hairpin system based on the vector pHD615_PAC (derivate of pHD615 with puromycin resistance gene (Biebinger *et al.*, 1997)). The vector is stably integrated into the *RDNA* spacer locus. RNAi was induced with 1 µg/ml tetracycline, which led to a derepression of the tetracycline repressor and transcription of the hairpin fragment by RNA polymerase I.

2.2.7 Over-expression in *T. brucei*

For ectopic expression of *DOT1A* and *DOT1B,* ORFs were amplified from genomic DNA introducing a C-terminal TY-epitope and were cloned into the vector pLew100v5, an improved version of the original pLew100 vector (Wirtz *et al.*, 1999). The construct was stably integrated into the *RDNA* spacer region and allowed inducible expression from a *RDNA* promoter with reduced leakiness. Introduction of two tetracycline operators and two T7 terminators improved this vector. Over-expression of DOT1A or DOT1B was induced by adding 1 µg/ml tetracycline to the medium.

2.2.8 Immunofluorescence analysis

2.2.8.1 Silanized cover slips

Cover slips were washed in 2 N HCl for 5 min, rinsed with dH_20 and washed with acetone. For silanization they were treated with 2% 3-aminopropyltriethoxysilane in acetone for 2 min, washed in dH_2O and dried.

2.2.8.2 Indirect immunofluorescence analysis (IFA)

$1x10^7$ cells were harvested (BSF: 1400 g; 10 min; 37°C or PCF: 900 g; 10 min; 27°C) in 1 ml of medium (HMI9 or SDM79) and fixed in 2% (w/v) formaldehyde for 5 min at RT following two wash steps with PBS and resuspension in 300 µl of PBS. 50 µl of resuspension were spread onto aminopropyltriethoxysilane-coated cover slips and cells were allowed to settle down for 10 minutes before washing with PBS twice. Trypanosomes were permeabilized for 5 min in 0.2% NP-40 / PBS. Two washing steps with PBS followed and the immobilized cells were blocked in 1% (w/v) BSA in PBS for 10 min before labeling with the primary antibody diluted in PBS for 1h at RT. After two washes with PBS cells were incubated with the secondary antibody diluted in PBS for 1 h at RT in the dark. The cellular DNA was stained with 1 µg/ml 4,6-diamidino-2-phenylindole (DAPI) in PBS for 5 min at RT. The cover slips were washed three times with PBS and once with dH_2O and embedded in Vectashield anti-fade medium.

2.2.8.3 DNA labeling and detection

5-Ethynyl-2-deoxyuridine (EdU) and/or 5-bromo-2-deoxyuridine (BrdU) were added to cell cultures at concentrations of 300 µM and 200 µM, respectively. Additionally, 100 µM of 2-deoxycytidine was supplemented. For double labeling experiments, cells were incubated for two hours with EdU, washed twice with medium to remove EdU and were cultivated in medium without any additive for 3 more hours before adding BrdU for 2 hours. Cells were fixed in 1% formaldehyde and allowed to settle on glass cover slips. After permeabilization with 0.5% Triton-X-100 in PBS DNA was denatured with 2 M HCl for 30 min and samples were neutralized with 0.1 M sodium borate. Detection of EdU was performed as described in the manufacturer's protocol (Click-iT EdU Imaging Kit, Invitrogen). BrdU was detected with a monoclonal anti-BrdU antibody followed by incubation with an Alexa 488 antibody.
RNAi was induced for 12 hours before adding BrdU to cells for further 7 hours. Cells were fixed for flow cytometry analysis and sorted according to their DNA content. Sorted cells were allowed to settle on glass cover slips, DNA was denatured and detection of BrdU was performed as described above.

2.2.8.4 Fluorescence *in situ* hybridization (FISH)

The α/β-tubulin gene cluster on chromosome 1 was used as a marker for polyploidy of large chromosomes in *T. brucei*. The probe was prepared by amplification of the tubulin gene locus using primers CJ116/ CJ117 and labeling of the product with the help of the Biotin-nick

Translation Mix (Roche Diagnostics). The resulting average probe length was approximately 150 bp.

FISH procedures were carried out as described (Ersfeld and Gull, 1997). In brief, $5x10^6$ PCF were fixed in 3.6% formaldehyde for 15 min at RT, washed twice in PBS and allowed to settle on silanized coverslips for 30 min at RT before permeabilization with 0.1% NP-40/PBS for 5 min. Biotin-labeled probe was coprecipitated with herring sperm DNA (0.2 mg/ml) and yeast tRNA (0.2 mg/ml) in hybridization mix. Final hybridization was carried out, after denaturation at 95°C for 5 min, at 37°C for 16 hours in water saturated environment. Washing was done in 50% formamide, 2x SSC for 30 min at 37°C, 10 min in 2x SSC at 50°C, 60 min in 0.2x SSC at 50°C and 10 min in 4x SSC at RT. Cells were incubated with a streptavidin-Cy3 conjugate (Sigma) in 1% BSA/PBS for 1 hour at RT to detect the biotinylated probe.

2.2.8.5 Microscopic analysis

Samples were examined on the Axioplan2 microscope with a 63-fold magnification objective lens (Ph3 Plan Apochromat 63x/1.40) and immersion oil Immersol 518N from Zeiss.

A DeltaVision image restoration system (IX71 Olympus microscope) was used to acquire images. Vertical stacks (0.2 µm steps) were captured using an objective lens with 60-fold magnification (PlanApo N 60x (Olympus)) and immersion oil with a refractive index of 1.520. Deconvolution and pseudo-coloring were performed using softWoRx, ImageJ and Adobe Photoshop software.

Super-resolution imaging with three-dimensional structured illumination microscopy was performed with a DeltaVision OMX v3 (Applied Precision) equipped with a 100x/1.40 NA PlanApo oil immersion objective (Olympus), Cascade II:512 EMCCD cameras (Photometrics) and 405, 488 and 593 nm diode lasers. Samples were illuminated by coherent scrambled laser light directed through a movable optical grating (Dobbie *et al.*, 2011). Image stacks with 15 images per plane (5 phases, 3 angles) and a z-distance of 125 nm were acquired and subjected to a computational reconstruction (softWoRx, Applied Precision).

2.2.9 Flow cytometry

2.2.9.1 Cell cycle analysis

$2x10^7$ cells were centrifuged (1400 g; 10 min; 4°C) and washed once with ice cold PBS. Cells were then resuspended in 1 ml PBS and fixed by adding 2.5 ml ice cold 100% ethanol dropwise. The fixed cells were stored at 4°C for at least 1 hour. The samples were washed

once with PBS and resuspended in 950 µl PBS / 2 mM EDTA. 1 µl RNaseA (10 µg/µl) and 10 µl propidium iodide (1µg/µl) were added, followed by incubation for 30 min at 37°C. The samples were stored at 4°C in the dark until analysis with a FACSCalibur by measuring emission of the dye in the FL-2 channel. The software CellQuest 3.3 and FlowJo 8.8.6 were used for data analysis.

2.2.9.2 Cell cycle based sorting

To obtain populations of different cell cycle phases, cells were sorted according to their DNA content. $1x10^7$ PCF cells were resuspended in 1 ml of PBS/EDTA and stained with 1 µl vybrant orange (final concentration: 5 µM) for 5 min at RT. Analysis and sorting were done with FACSAriaII and the software FACSDiva 6.0 (Becton Dickinson) using the following settings: Flow rate of 3; 70 µm nozzle; filter 585 ± 42 nm. $5x10^6$ cells per cell cycle phase were sorted into a 15 ml Falcon tube with 500 µl of SDM79 medium. Post sort analyses confirmed the quality of sorting. Data were analyzed with the software FlowJo 8.8.6.

2.2.9.3 Luciferase assay

Luciferase activity was determined by measuring light emission resulting from the turnover of luciferin to oxyluciferin. Coenzyme A (included in the reaction buffer) binds oxyluciferin and prevents inhibition of the luciferase by oxyluciferin (Airth *et al.*, 1958). $1x10^6$ cells were harvested (900g; 10 min; RT) and washed with PBS. The pellet was resuspended in 40 µl of lysis buffer and cells were permeabilized by the freeze-thaw-method: Suspension was first frozen in liquid nitrogen and immediately thawed almost completely in a 37°C water bath. This procedure was repeated three times. Afterwards the sample was centrifuged (20,000g; 1 min; 4°C) and stored on ice. 90 µl of reaction buffer were put into a reaction tube and incubated 1 min at RT. 10 µl of cell lysate were added and incubated for exactly 110 sec before luciferase activity was measured for 10 sec with a luminometer.

2.2.10 Mass spectrometry analysis

Histones were separated by 15% SDS-PAGE, stained with Coomassie blue and excised from the gel. Isolated bands were diced into smaller pieces, destained, chemically modified as described (Jasencakova *et al.*, 2010) and digested with trypsin. The resulting peptides were desalted and analyzed by liquid chromatography-MS/MS. All fragment ion spectra were recorded in the linear quadrupole ion trap (LTQ) part of the instrument. Spectra were

analyzed with the Xcalibur and Proteome Discoverer software packages and ion chromatogram areas under verified peaks were quantified.

2.2.11 Chromatin immunoprecipitation

Chromatin immunoprecipitation was applied as published by Siegel *et al.* using magnetic beads coupled to anti-rabbit IgG antibodies (Siegel *et al.*, 2009). 100 µl beads were washed with 1 ml of block solution and resuspended in block solution adding 10 µg of the primary antibody. After over night incubation at 4°C beads were washed and resuspended in 100 µl of block solution. $1x10^8$ PCF cells were fixed in 40 ml of SDM79 with 4 ml formaldehyde solution for 20 min at RT. 2.5 ml of 2 M glycine were added and cells were centrifuged (4000 g; 20 min; 4°C). Supernatant was discarded and cells were lysed for 10 min in 10 ml of lysis buffer 1 at 4°C before they were centrifuged again. Pellet was resuspended in 10 ml of lysis buffer 2, transferred to a 15 ml falcon tube and rocked for 10 min at RT. Another centrifugation step followed, the supernatant was discarded and the pellet was resuspended in 2 ml of lysis buffer 3. Cell lysates were sonicated for 10 cycles of 30 sec on/off intervals each, setting "high". Afterwards 220 µl 10% Triton X-100 were added, the samples were split into two 1 ml aliquots and centrifuged (16,100 g; 10 min; 4°C) to pellet the debris. 50 µl of "input sample" and 100 µl of "size sample" were taken for later analysis. The total volume of the rest of the sample was brought to 3 ml with lysis buffer 3 containing 1% Triton X-100 and was split between two 2 ml microcentrifuge tubes. 50 µl of previous prepared beads and 150 mM NaCl were added to each tube. Samples were incubated over night on rotator at 4°C. The next day IP samples were washed seven times in 1 ml RIPA buffer. Another washing step with 50mM NaCl in TE buffer followed and residual buffer was removed completely. Material was eluted in 200 µl elution buffer at 65°C for 30 min and mixing every 2-5 min. After centrifugation (16,100 g; 1 min; RT) supernatant was transferred to a new tube. To reverse crosslinking, samples were incubated for 12 to 15 hours at 65°C. Afterwards 8 µl of RNaseA (10 mg/ml) were added and incubated at 37°C for 2 hours followed by incubation with 4 µl Proteinase K (20 mg/ml) at 55°C for 2 hours. DNA of samples was purified using a Quiagen PCR purification kit.

DNA was amplified using the whole genome amplification kit from Sigma (20 cycles of amplification). 8 µg of each DNA sample including input was sent to Roche NimbleGen for hybridization on a microarray.

2.2.12 Microarray / Data analysis

The ChIP on chip service from Roche NimbleGen (Madison, USA) was used including the generation of a custom designed array (format 3x720K: 3 identical arrays per glass slide with 720,000 probes per array) containing all sequences of the 11 megabase-size chromosomes of *T. brucei* (strain 927, version 4). Probe length was 50-75 nucleotides. NimbleGen performs ChIP-chip experiments with a two-color protocol by co-hybridizing control and input samples to the same array. Data were analyzed with the help of a bioinformatics specialist (Dr. Manuel Arteaga).

Raw data from the NimbleGen microarrays (.pair format) were read and analyzed using R (http://www.r-project.org) and Bioconductor (http://www.bioconductor.org). All functions were used with default parameters unless stated otherwise. The raw probe signals were transformed into $\log_2$-values and then adjusted with scale normalization as described previously (Yang *et al.*, 2002). Enriched (Cy5) and input (Cy3) normalized $\log_2$-signals were converted into enrichment ratios ($\log_2$(Cy5/Cy3)), individually for each biological replicate. The replicate ratios were averaged to obtain a single estimate for each histone modification (H3, H3K76me1 and H3K76me2).

To examine the differences between the H3K76me1/me2 and H3 $\log_2$-ratios, the $\log_2$-enrichments were scaled (so that the set of $\log_2$-enrichments have mean=0 and standard deviation=1) to allow for an appropriate comparison. Then the H3K76me1/me2 data were further normalized with H3, by subtracting the $\log_2$-ratios. Finally, a moving average (degree 3) was used to smooth all data series to minimize the effect of probes with outlier $\log_2$-ratios. Genomic features were extracted from the TriTryp database (http://tritrypdb.org).

2.2.13 Standard DNA methods

2.2.13.1 Transformation of chemical competent bacteria

Chemical competent bacteria were thawed on ice 15 min prior to transformation. Plasmid DNA or 10 µl DNA from a ligation reaction were added to 100 µl of competent bacteria and incubated for 30 min on ice followed by a heat shock at 42°C for 90 sec. The cells were incubated on ice for 2 min, resuspended in 900 µl LB medium and incubated on a shaker at 37°C for 30 min. The bacteria were plated onto LB-agar plates containing ampicillin for selection and incubated over night at 37°C.

3.2.13.2 Isolation of DNA

Plasmid DNA from *E. coli* was isolated using the NucleoSpin Plasmid or the NucleoBond PC100 kit (Macherey&Nagel) following the instructions of the manufacturer.

Genomic DNA from trypanosomes was isolated using the NucleoSpin Tissue kit (Macherey &Nagel).

3.2.13.3 Amplification of DNA fragments

PCRs were performed in 50 μl reaction mixtures with Phusion polymerase and the following parameters (depending on the primer): 98°C/5 min - [98°C/10 sec - X°C/15 sec - 72°C/X sec] 30x - 72°C/5 min. Colony PCRs and other control PCRs were carried out in 20 μl reaction mixture using Taq polymerase with the following parameters (depending on the primer): 95°C/2 min - [95°C/15 sec - X°C/15 s - 72°C/X sec] 30x - 72°C/5 min.

3.2.13.4 Separation and isolation of DNA fragments

DNA fragments were separated on agarose gels (1% agarose, 1µg/ml ethidium bromide) in TAE buffer with 10 V/cm^2. Samples were mixed before with 6x DNA loading dye. Sizes of DNA fragments were determined by comparison with DNA size markers. DNA was visualized with the Geldoc 2000.

DNA was extracted from agarose gels with the NucleoSpin Extract II kit (Macherey&Nagel) according to the instructions of the manufacturer.

3.2.13.5 Precipitation of DNA with isopropanol

1 volume of isopropanol and 1/10 volume of 3 M sodium acetate (pH 5.2) were mixed with the DNA sample. Centrifugation (20,000 g; 15 min; 4°C) and two washing steps with 70% ethanol followed (20,000 g; 10 min; RT). The pellet was dried in a laminar flow hood and resuspended in sterile dH_2O.

3.2.13.6 Restriction digest and ligation of DNA

DNA was digested with restriction endonucleases according to the instructions of the manufacturer. Ligation was performed in a final volume of 20 µl for 2 hours at RT according to the instructions of the manufacturer.

3.2.13.7 Determination of DNA concentration and DNA sequencing

DNA concentrations were determined with the NanoDrop by measuring the absorption at 260 nm and 280 nm. DNA was sequenced by the sequencing service of the LMU Department Biology I. The reaction volume of 10 µl included 200 ng plasmid, 3.2 pmol primer, BigDye TerminatorV3.1 mix and BigDyeV3.1 5x sequencing buffer. Cycling conditions were 96°C/1 min - [96°C/10 sec - 50°C/15 sec - 60°C/4 min] x 35 - 12°C/∞.

2.2.14 Standard protein methods

2.2.14.1 Preparation of protein lysates

Cells were centrifuged (1400 g; 10 min; 4°C) and washed with PBS. The pellet was resuspended in 1x Laemmli buffer in a cell concentration of $2x10^6$ cells per 10 µl. Samples were heated at 95°C for 10 min and sonicated for 30 sec prior to SDS-PAGE.

2.2.14.2 SDS-PAGE

Proteins were separated by one dimensional discontinuous gel electrophoresis (Laemmli, 1970). 10% or 15% SDS-gels were made following the instructions in Current Protocols in Molecular Biology (Gallagher, 2001). Proteins were separated with 20 mA per gel in Laemmli running buffer.

2.2.14.3 Western blot analysis

Proteins were transferred electrophoretically from SDS gels to polyvinylidene fluoride (PVDF) membranes with the semi-dry technique (Kyhse-Andersen, 1984). Gels were blotted with 0.8 mA/cm^2 for 70 min at RT. The membrane was blocked with 5% dried milk in PBS or 3% BSA in PBS dependent on the used antibody. Primary antibodies were diluted in 5 ml of PBS / 0.1% Tween-20 and incubated for 1 hour at RT. 3 washing steps with PBS / 0.2% Tween-20 followed before the membrane was incubated with the appropriate secondary antibodies diluted in 5 ml of PBS / 0.1% Tween-20 for 1 hour at RT. Finally, the membrane was washed again 3 times. The antigens were visualized with the Odyssey Infrared scanner (LI-COR) and quantification of signal intensities was performed with the Odyssey 2.1.12 software.

3 Results

3.1 Changes of the H3K76 methylation pattern during cell cycle

It was previously reported that H3K76me2 is mainly associated with mitosis and cytokinesis, while H3K76me3 is detectable throughout the cell cycle (Janzen *et al.*, 2006b). In order to complete the picture of the H3K76 methylation pattern during the cell cycle, an antibody specific for H3K76me1 was first to be generated; the specificity of the anti-H3K76me1 antibody was confirmed by peptide competition assays (Niklas Schandry, bachelor thesis).

A potential cell cycle-dependent regulation of H3K76me1, similar to that of H3K76me2, was analyzed by indirect immunofluorescence (IF). To determine the phase of the parasite in the cell cycle, the nuclear (N) and the mitochondrial genome (kinetoplast, K) were stained with DAPI. Replication and segregation of the kinetoplasts precede those of the nuclei; therefore, they can be used as markers to determine the phase of an individual cell in the cell cycle (Siegel *et al.*, 2008a; Woodward and Gull, 1990). H3K76me1 was detected in cells of the G2/M phase and in cytokinetic cells, whereas cells of the G1- and S- phase did not display H3K76me1 (Fig 6A). 55% of cells being in the G2/M phase and ~40% of cytokinetic cells showed H3K76me1 (Fig 6D). In comparison, H3K76me2 was detected in only 20% of G2/M phase cells and in up to 100% of post-mitotic cells (Figs 6B and 6D), whereas H3K76me3 appeared not to be cell cycle-regulated (Figs 6C and 6D). Thus, H3K76me1 and -me2 were both detected in G2/M phase and cytokinetic cells, but H3K76me1 seemed to precede H3K76me2. Furthermore, replicating cells seemed to be devoid of H3K76me1 and H3K76me2. To test whether H3K76me1 and replication are mutually exclusive, a cell cycle marker for the S phase was used. Since the S phase is not defined precisely by the nuclear and kinetoplast configuration, the proliferating cell nuclear antigen (PCNA) served as marker for replication foci (Fig 7A). Distinguishable foci of TY-tagged PCNA were detected in >90% of cells with an elongated kinetoplast (Fig 7B, 1NeK, S phase), and in 20% of cells with one nucleus and one kinetoplast (Fig 7B, 1N1K, G1/S phase). Importantly, all PCNA-positive cells were negative for H3K76me1 and -me2.

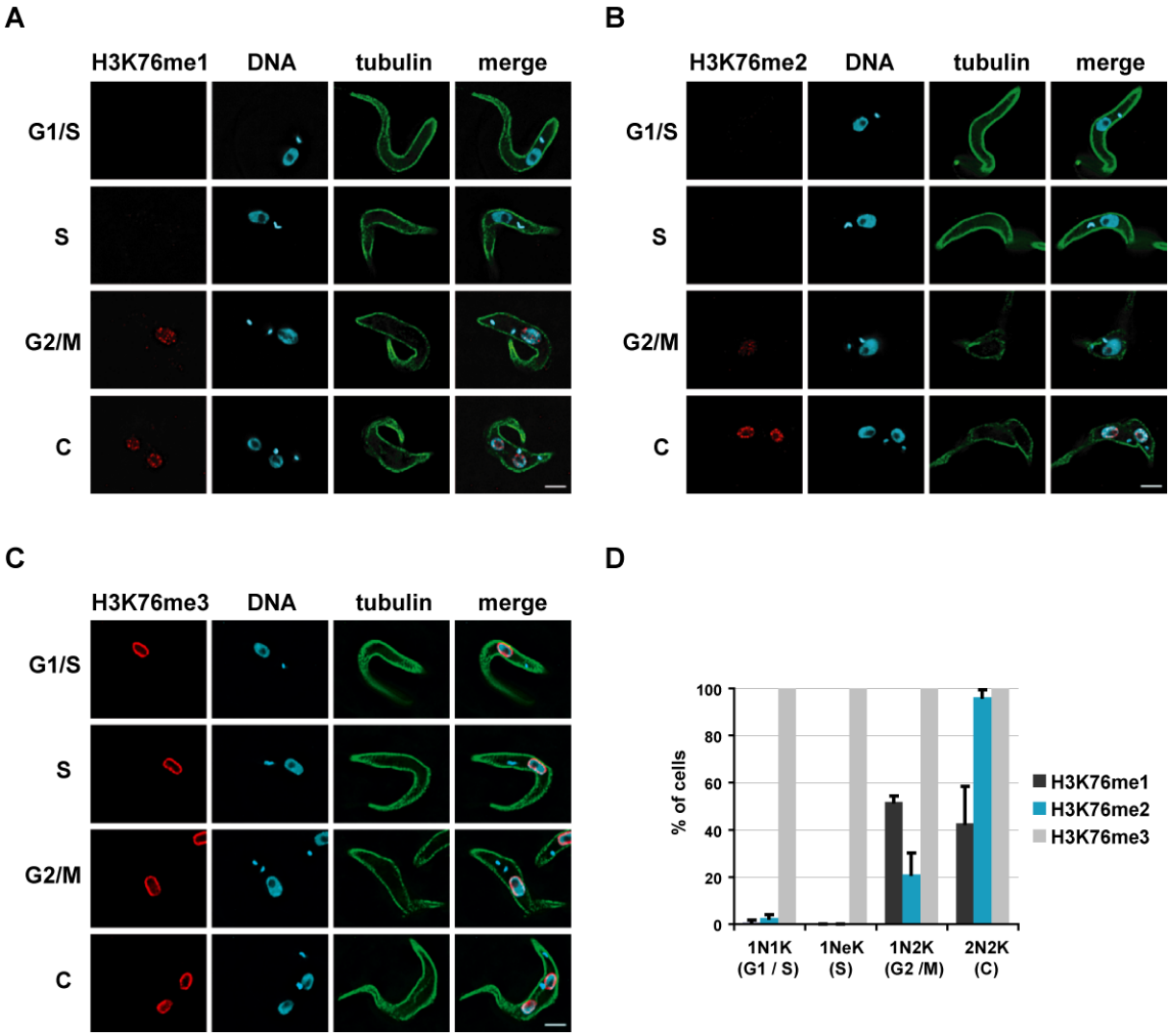

Figure 6: Cell cycle-dependent H3K76 methylation in PCF of *T. brucei*. Indirect IFA using antibodies specific for (**A**) H3K76me1, (**B**) H3K76me2, (**C**) H3K76me3 (red) and alpha-tubulin (green) to visualize the shape of cells. DNA (blue) was stained with DAPI. Cells were assigned to different cell cycle phases based on nucleus/kinetoplast configuration as indicated. Scale bars represent 3 µm. (**D**) Quantification of different cell cycle-dependent methylation states. Three independent experiments were analyzed.

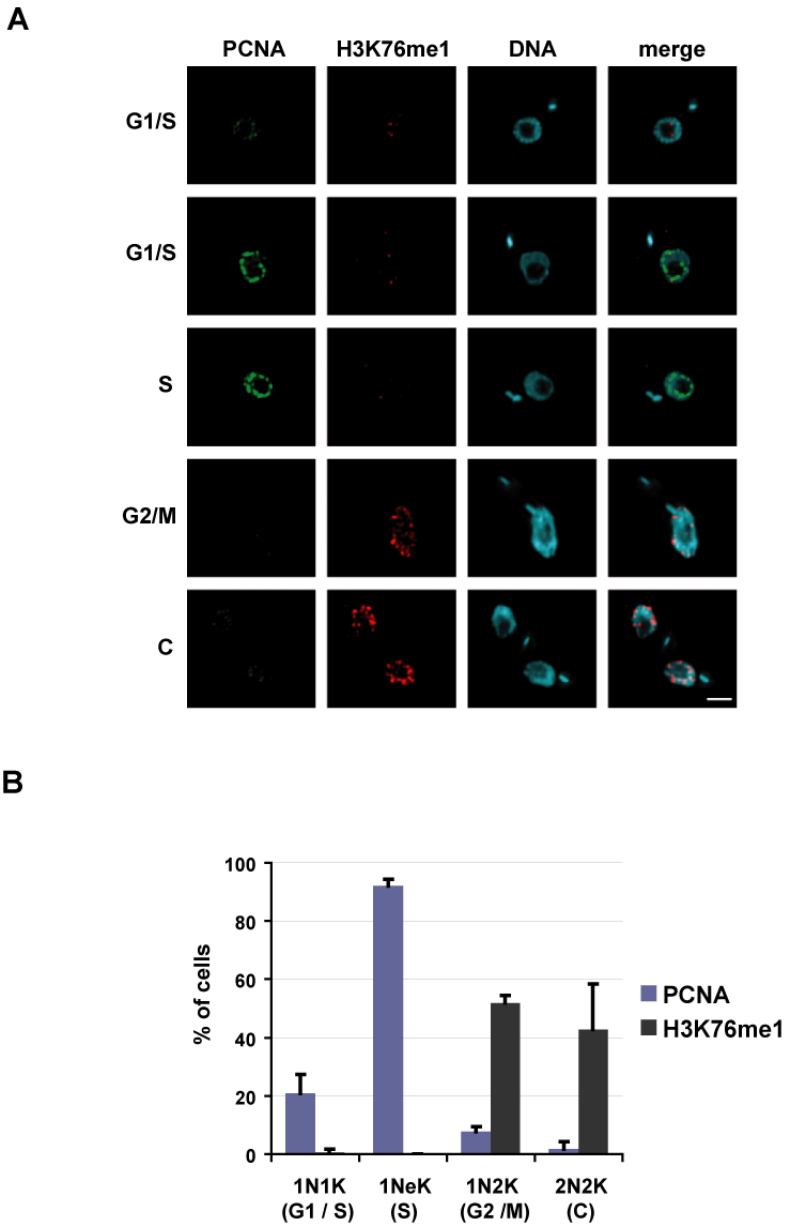

Figure 7: H3K76me1 is absent in S phase cells and precedes H3K76me2. (**A**) Indirect IFA of PCF in different cell cycle phases expressing PCNA-TY (green) and H3K76me1 (red). DNA was stained with DAPI. Scale bar represents 2 µm. (**B**) Quantification of cell cycle-dependent expression of PCNA-TY and H3K76me1. Three independent experiments were analyzed.

In summary, H3K76me1 is restricted to the G2/M phase and cytokinesis similar to H3K76me2. However, H3K76me1 precedes H3K76me2, but does not coincide with expression of PCNA. Thus, replication and H3K76me1/me2 exclude each other.

First, the data suggest that methylation of H3K76 occurs sequentially starting with monomethylation followed by dimethylation. Second, *de novo* H3K76 methylation of histones, which are incorporated into the chromatin fiber during the S phase, starts probably

in the G2 phase. It is difficult to determine the time point when H3K76 becomes trimethylated, because H3K76me3 is detectable throughout the cell cycle (Fig 6C).

Indirect IFA can be misleading due to interfering factors that might mask binding sites for antibodies. Putative cell cycle-regulated binding proteins of methylated H3K76 might be responsible for the observed H3K76 methylation pattern.
To exclude this possibility, H3K76me2 was analyzed in lysates of cells from different cell cycle phases by Western blot analysis. Suitable methods to synchronize trypanosomes during the cell cycle are not available. Although nucleotide depletion with hydroxyurea arrests the cells in the S phase, and removal of this agent leads to cell cycle progression (Chowdhury *et al.*, 2008), the cell population starts to grow asynchronously few hours after release. Hence, generation of a homogenous G1-population by chemical synchronization is not possible. Therefore, sorting of cells based on DNA content was applied (Siegel *et al.*, 2008a). Cells were stained with the fluorescent dye vybrant orange and 2 x 10^6 cells of G1-, S- and G2/M-populations were sorted. Purity of different cell populations was controlled by post sort analyses confirming that homogenous populations were obtained for G1 and S phase cells (Fig 8A). The cell cycle profile of G2/M phase sorted cells displayed an additional peak (Fig 8A, right panel) representing a low percentage of G1 phase cells. This was probably evoked by cell-doublets characteristic for late cytokinesis and therefore assigned to the G2/M population due to their double DNA content. Conceivably, such cell-doublets were separated during the sorting process and appeared afterwards as G1 cells.
Sorted cells were lysed and total protein extracts were analyzed by Western blot using antibodies specific for H3K76me2 and H3 as loading control (Fig 8B). Weak signals of H3K76me2 were detected in G1 and S phase cells, however G2/M phase cells showed a three-fold stronger signal for H3K76me2 (Fig 8B, right panel). In lysates of the total population, the H3K76me2 signal was slightly stronger than in G1 phase cells reflecting that only ~30% of cells of the total population are in G2/M phase. Additionally, indirect IFA of sorted populations was performed. H3K76me2 was mainly detected in cells during mitosis and cytokinesis (Fig 8C) in agreement with the Western blot analysis.
Hence, Western blot analysis confirmed cell cycle-regulated appearance of H3K76me2 which peaks in G2/M phase.

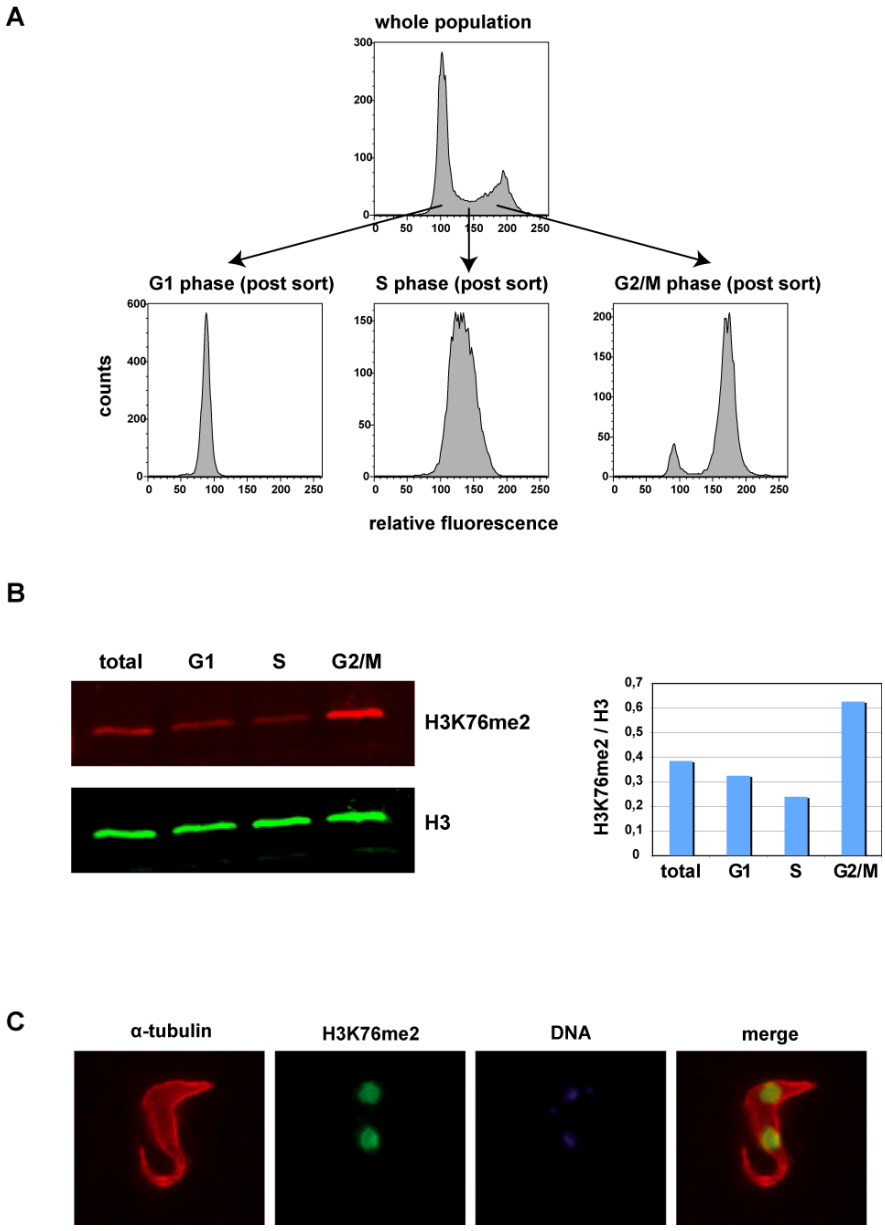

Figure 8: H3K76me2 signals in cells of different cell cycle phases after sorting. (**A**) Cell cycle profiles of cells before and after sorting. Cells of different cell cycle phases (G1, S and G2/M) were sorted according to DNA content. (**B**) Western blot analysis of cell lysates of total population and sorted G1, S, G2/M cells with antibodies specific for H3K76me2 and H3 as a control. Quantification of H3K76me2 level is shown in the right graph. (**C**) Indirect IFA of a cytokinetic cell after cell sorting. H3K76me2 was detected as expected.

The data of indirect IFA and Western blot experiments suggest the following model of regulation of H3K76 methylation (Fig 9): H3K76 is methylated in a cell cycle-dependent manner by the histone methyltransferases DOT1A and DOT1B (Fig 9). The DOT1 enzymes can only methylate histones in a nucleosomal context (Feng *et al.*, 2002; Janzen *et al.*, 2006b); therefore, newly incorporated histones are not methylated at H3K76 during S phase

but become monomethylated during G2 phase and successively further methylated during mitosis.

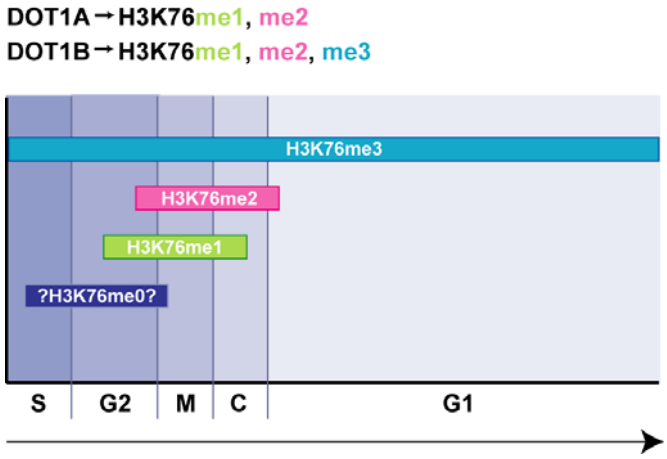

Figure 9: Model of cell cycle-dependent H3K76 methylation. Newly incorporated histones are not methylated during the S phase at H3K76, but become successively methylated by DOT1A and DOT1B starting in G2 phase. DOT1B is solely responsible for H3K76me3 which is present throughout the cell cycle. The temporal presence of unmodified H3K76 is hypothesized.

To date, the underlying kinetic of H3K76 methylation as well as the enzymatic activities of DOT1A and DOT1B have not been explored. In order to obtain first insights, the relative levels of all H3K76 methylation states (me1, me2 and me3) were quantified by mass spectrometry. Therewith, also the presence of unmethylated H3K76 was to be proven.

Histone H3 of whole cell lysates was separated by gel electrophoresis and excised from Coomassie-stained gels. Isolated bands were trypsin-digested and subjected to mass spectrometry (Fig 10A). 63% of H3K76 displayed trimethylation, 31% showed no methylation and only very small amounts of H3K76 were mono- or dimethylated (2 and 4%, respectively) (Fig 10A). These small percentages of H3K76me1 and -me2 were surprising as most of G2/M and cytokinetic cells showed strong signals in indirect IFA. However, the strength of immunofluorescence signals depends on antibody affinity, and signals derived from different antibodies cannot be directly compared. According to the mass spectrometry results, only small areas of the genome seemed to be enriched with H3K76me1 and -me2.

To quantify methylation levels during the cell cycle, cells of all cell cycle phases were analyzed individually. Cells were sorted according to their DNA content, and populations of G1, S and G2/M phase were processed and analyzed as described before. In G1 cells, H3K76me1/me2 signals were either absent or fairly weak (1.4% H3K76me2; Fig 10B); most of H3K76 was trimethylated (95%). In S phase cells, 50% of H3K76 was trimethylated and

50% was unmethylated probably reflecting the proportion of new histones in S phase cells. G2/M phase cells showed 4% H3K76me1 and -me2, 60% H3K76me3 and 30% unmethylated H3K76 (Fig 10B). Values of unmethylated H3K76 and H3K76me3 of G2/M populations varied strongly due to technical problems of unknown character. The two evaluable experiments generated values of 52% and 12% for unmethylated H3K76, or 37% and 82% for H3K76me3, respectively. The mean value is illustrated in Figure 10B. Further experiments are necessary to clarify these strong deviations. Despite of this, values for H3K76me1 and H3K76me2 were reproducibly low and corroborated the observation in total cell lysates. An asynchronous cell culture was composed of 55-60% G1 phase cells, 10-15% S phase cells and ~30% G2/M phase cells. Thus, data from cells of individual cell cycle phases were consistent with that obtained from total populations with only minor variation.

Importantly, these data support the hypothesis that incorporated H3 is unmodified at K76 during S phase. Only a small percentage of new H3K76 becomes methylated in G2/M phase. Most of it remains unmethylated to the end of mitosis, but seems to become rapidly trimethylated at the beginning of the G1 phase. This suggests a strong up-regulation of DOT1B at the end of mitosis or beginning of G1 phase. H3K76 was completely methylated in the G1 phase before the methylated histones were diluted out again during replication in the following cell cycle.

The surprisingly low percentage of H3K76me1 and H3K76me2 raised the question whether these methylation states show a distinct distribution in the nucleus. High-resolution microscopy was applied to analyze the nuclear localization of H3K76me1 and H3K76me2 in detail.

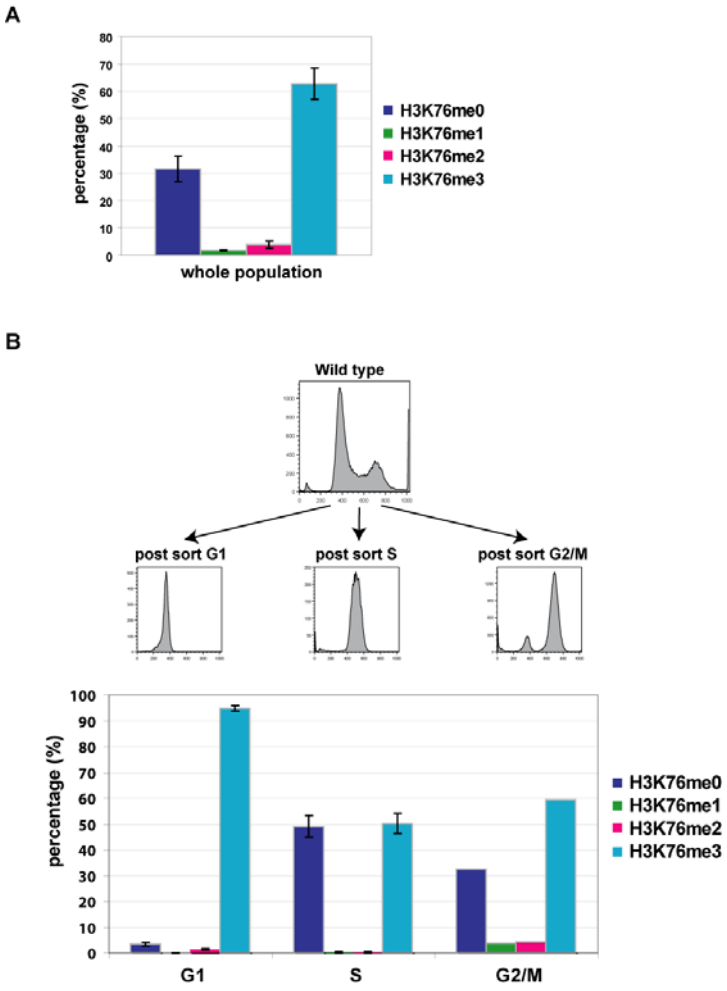

Figure 10: Mass spectrometry analysis of different H3K76 methylation states. (**A**) Histone H3 of total cell lysates (n=8) was separated by SDS gel electrophoresis and examined for H3K76 methylation. Mean value and standard deviation are shown. (**B**) Same analysis was done with cells of different cell cycle phases obtained by DNA content-based cell sorting. Mean values, and if applicable standard deviations of three (G1 and S phase) or two (G2/M phase) independent experiments are shown.

3.2 Nuclear localization of H3K76me1 and H3K76me2

The recent development of super resolution light microscopy methods (Schermelleh *et al.*, 2010) enables detailed analysis of cellular structures and distribution of different molecules in the cell. Thus, immunofluorescence studies can help to understand the functional context of cellular components.

Microscopic analysis of H3K76me1 and -me2 detected signals in a punctuated pattern throughout the nucleus except the nucleolus (Fig 11A). The nucleolus contains only minor amounts of DNA, and this compartment is devoid of histones. Signals of H3K76me1/me2 overlapped with those of H3 as expected, but most H3 signals showed no colocalization with

the H3K76 methylation signals (Fig 11A). There was no striking difference in nuclear distribution pattern between the H3K76me1 and -me2 (Fig 11A). Direct colocalization studies were not applicable, because the antibodies of H3K76me1 and -me2 were both generated in rabbits. As H3K76me1 and -me2 are expressed in G2 phase and mitosis, cells of both cell cycle phases were analyzed. However, the localization pattern did not change visibly, neither for H3K76me1 nor H3K76me2 during these cell cycle phases (data not shown). Figure 11A illustrates a post-mitotic cell showing H3K76me1 and a cell in G2 phase showing H3K76me2. The distribution of tagged PCNA-TY was explored as control for the localization of a nuclear protein, which was described as replication marker in trypanosomes (Kaufmann *et al.*, 2012). PCNA-TY showed similar punctuated signals, which are distributed equally in the nucleus (Fig 11B).

In summary, high-resolution microscopy revealed that localization of H3K76me1 and -me2 was not restricted to specific compartments in the nucleus. The localization pattern of both methylation states looked quite similar and did not change between G2 phase and mitosis. Thus, the function of H3K76 methylation is not associated with distinct nuclear compartments and remains to be explored. A random genomic association of H3K76me1 and -me2 is conceivable, but cannot be analyzed microscopically. This issue was investigated by another approach (chromatin immunoprecipitation) described later in this thesis.

Analysis of nuclear localization failed to unravel functional details about H3K76 methylation. However, the striking cell cycle-dependent appearance of H3K76 methylation point to a role in cell cycle regulation. Therefore, further analyses applying biochemical mutants focussed on the establishment of this cell cycle-regulated pattern and its function during the cell cycle. The pattern of H3K76 methylation might be established by cell cycle-dependent expression of the respective enzymes, DOT1A and DOT1B.

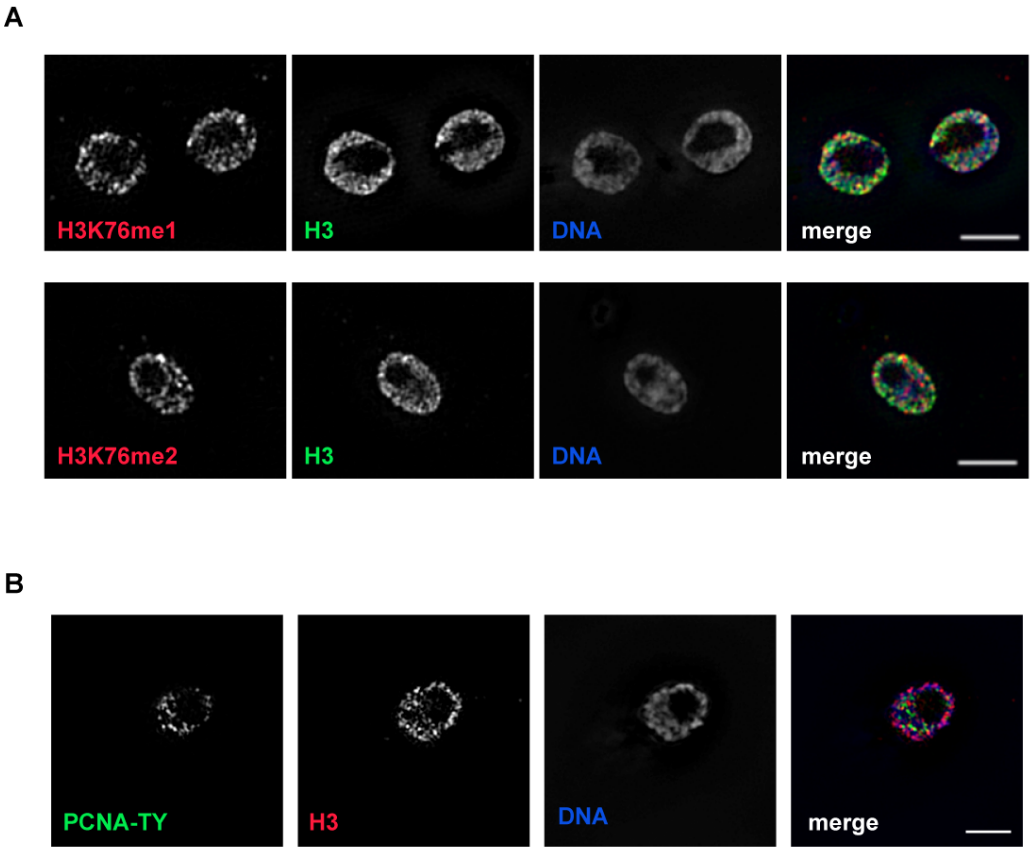

Figure 11: Nuclear localization of H3K76 methylation and PCNA. High-resolution microscopy of PCF stained with antibodies specific for (**A**) H3K76me1 (upper panel) or H3K76me2 (lower panel) in red or (**B**) the TY-epitope to detect TbPCNA-TY (green). Histone H3 was detected simultaneously with antibodies raised in a guinea pig (**A**, green) or rabbit (**B**, red). DNA was stained with DAPI (blue). Scale bars represent 2 µm.

3.3 Regulation of the histone methyltransferases DOT1A and DOT1B

Both DOT1A and DOT1B bring about methylation of H3K76. DOT1A catalyzes H3K76me1 and -me2 as opposed to DOT1B which additionally mediates H3K76me3 (Janzen *et al.*, 2006b), as shown with reconstituted nucleosomes *in vitro* (Gülcin Dindar, personal communication) and in a heterologous expression system in yeast (Frederiks *et al.*, 2010).

A potential cell cycle-dependent regulation of the DOT1 enzymes was investigated by analysis of their RNA levels. This study did not reveal any significant regulation of the DOT1 RNA levels (Ferdinand Bucerius, personal communication). Approaches to address the regulation of the DOT1 protein levels failed because specific antibodies against the enzymes could not be raised, and endogenously tagged DOT1B was not detectable by IFA or Western blot analysis. To overcome technical obstacles, a cell line was generated which expresses a fusion protein of DOT1A or DOT1B with luciferase. Enzymatic activity of luciferase was

measured by detection of bioluminescence which is generated in an oxidative reaction with luciferin and ATP. This approach is highly sensitive and thereby allowed indirect analysis of DOT1A and DOT1B expression. The luciferase gene was introduced by *in situ* tagging of *DOT1A* or *DOT1B* generating a fusion gene located in the endogenous genomic loci of *DOT1A* or *DOT1B* (Fig 12A). The endogenous 3´UTRs were replaced by plasmid delivered 3´UTRs. The strategy succeeded to correctly fuse the luciferase gene to *DOT1A* in a procyclic cell line, which was confirmed by PCR analysis (Fig 12B). Cells were sorted according to their DNA content, and a luciferase assay was performed with the same cell number from each cell cycle phase. Luciferase activity could be measured in cells indicating expression of the DOT1A-luciferase fusion protein (Fig 12C, total population). Only a moderate difference in luciferase activity was observed between cells of different cell cycle phases (Fig 12C). Luciferase activity of G1 and S phase cells showed similar values, whereas luciferase was 1.4-fold more active in G2/M cells, which could be due to the duplication of nuclei and cellular material during mitosis. The data suggests that luciferase and therefore DOT1A expression does not change significantly during cell cycle progression.

In order to test if the tagged allele of *DOT1A* was functional, it was tried to delete the remaining wild-type allele, but this was not successfully. However, deletion of one *DOT1A* allele in wild-type cells also failed indicating essentiality of both alleles. Therefore, the *DOT1A-luciferase* allele was likely to be active and normally regulated. H3K76me1 and H3K76me2 levels were regulated normally as analyzed by Western blot and indirect IFA (data not shown), further supporting that the tagged DOT1A was functional.

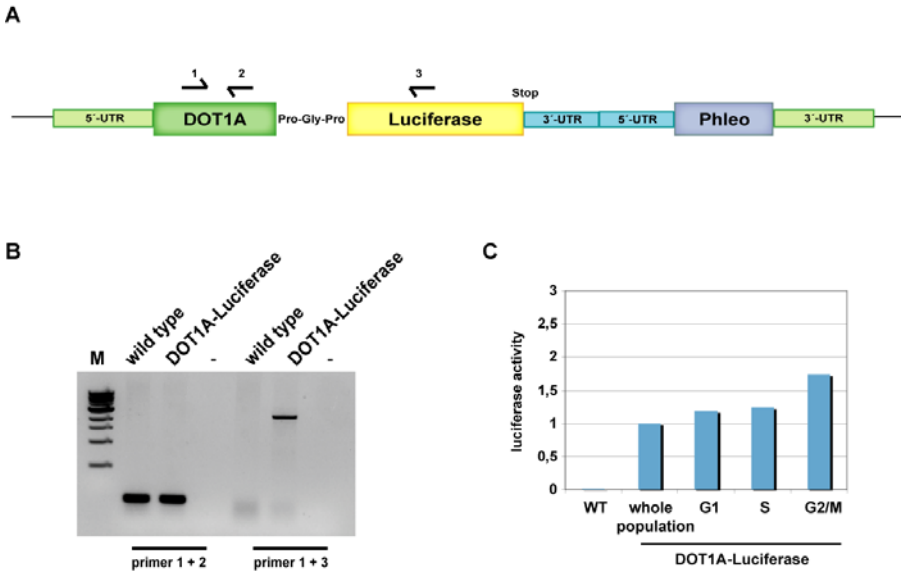

Figure 12: Regulation of DOT1A-luciferase expression during the cell cycle. (**A**) Schematic representation of the tagged *DOT1A* allele indicating primers (black arrows) used for integration control. The integrated construct contains the luciferase gene and the gene for phleomycin resistance (Phleo). (**B**) Integration control PCR using different primer combinations. (**C**) Luciferase assay of wild-type and sorted DOT1A-luciferase populations. DOT1A-luciferase activity showed no significant difference between cells of different cell cycle phases. Mean values of two independent experiments are shown.

An analogues strategy failed to generate a DOT1B-luciferase expressing cell line, and another approach was chosen. A DOT1B-luciferase fusion protein was ectopically introduced into a cell line lacking wild-type *DOT1B* alleles (ΔDOT1B), which are not essential for survival. The fusion gene was flanked by endogenous *DOT1B*-UTRs. In the ΔDOT1B strain, H3K76me3 is absent, whereas H3K76me1 and H3K76me2 levels are increased (Fig 13A; Janzen *et al.*, 2006b). If DOT1B fused to luciferase is functional, regulation of H3K76 methylation should be restored.

Western blot analysis revealed a restored H3K76me3 level in the strain expressing the fusion protein (Fig 13A, left panel) similar to a rescue-cell line expressing DOT1B ectopically without luciferase tag (Fig 13A, left panel). Interestingly, H3K76me1 and -me2 were decreased 3-fold and 1.3-fold, respectively, in comparison to the ΔDOT1B cell line, but were still more abundant than in wild-type cells (Fig 13A, right panel). In agreement, indirect IFA demonstrated a higher percentage of H3K76me1/me2 positive cells of each cell cycle phase in DOT1B-luciferase expressing cells (Fig 13B). 45% of 1N2K, 100% of 2N2K and 12% of 1N1K cells showed H3K76me1 in the DOT1B-luciferase line, whereas in wild-type cells 50% of 1N2K and 50% of 2N2K cells were positive for H3K76me1 (Fig 13B, left panel). When

DOT1B was absent, H3K76me1 was expressed in 75% of 1N2K, 100% of 2N2K, 70% of 1N1K and 25% of 1NeK cells. H3K76me2 was present in each ΔDOT1B cell independent of the cell cycle phase (Fig 13B, right panel). The number of cells displaying H3K76me2 was significantly reduced in DOT1B-luciferase cells and was nearly restored to wild-type levels in most cell cycle phases (Fig 13B, right panel). However, 60% of 1N1K DOT1B-luciferase cells were H3K76me2 positive. In summary, DOT1B-luciferase seemed to establish an intermediate pattern of H3K76 methylation level, which approximated the wild-type situation. These data suggest that DOT1B fused to luciferase is capable to catalyze H3K76 methylation, although the enzymatic activity is impaired. Luciferase activity of the DOT1B-luciferase fusion protein did not change dramatically in cells of different cell cycle phases, except a slight increase in S phase cells (Fig 13C) suggesting that the fusion protein was not regulated. Neither the DOT1A- nor the DOT1B-luciferase fusion proteins showed cell cycle-regulated expression. Hence, methyltransferase activity seems not to be regulated by expression level, but might be modulated by other factors, such as co-regulators or post-translational modifications of the DOT1 enzymes.

To test whether the cell cycle-regulated H3K76 methylation pattern is important for cell cycle progression, manipulation of H3K76 methylation was the next step in my study. Since H3K76 methylation is probably solely dependent on the DOT1 enzymes, mutation of the enzymes most likely impacts the methylation pattern. Previously it was shown, that deletion of *DOT1B* leads to loss of H3K76me3, but is not essential for cell cycle progression (Janzen *et al.*, 2006b). However, depletion of *DOT1A* by RNAi indicated severe cell cycle phenotypes (Janzen *et al.*, 2006b).

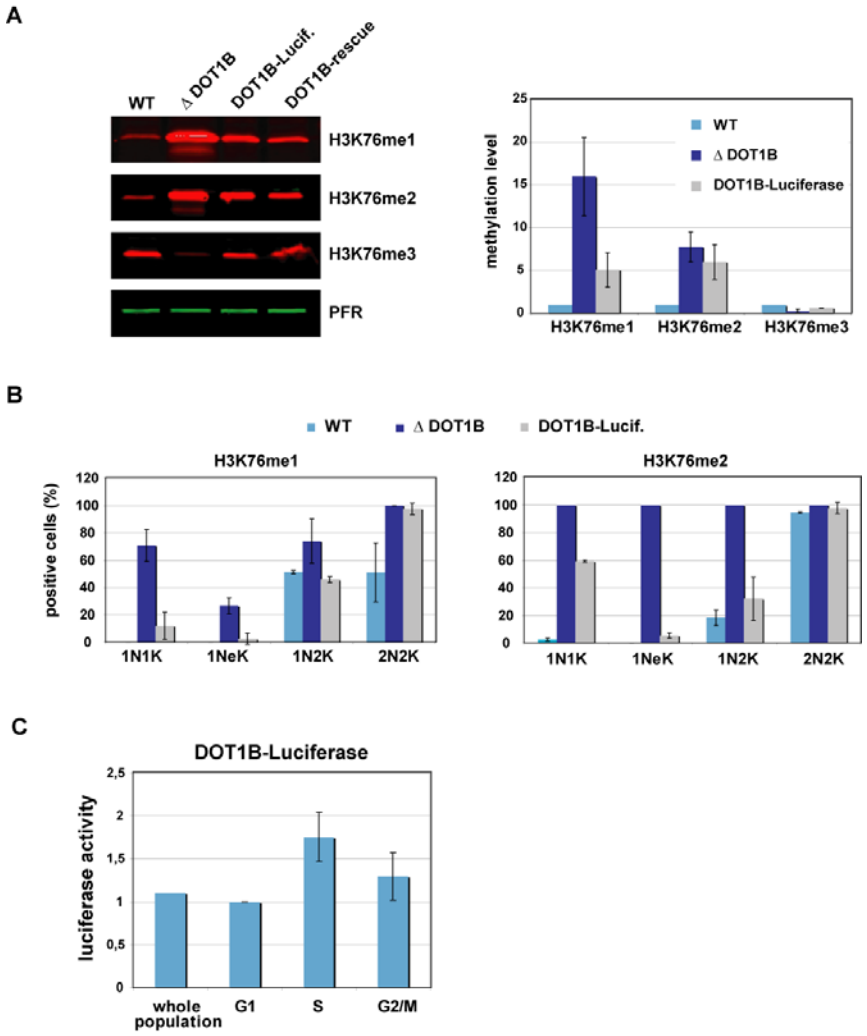

Figure 13: Characterization of the DOT1B-luciferase cell line. (**A**) Representative Western blot analysis of H3K76 methylation levels in different cell lines. PFR was used for normalization (right panel). Mean values and standard deviation of three independent experiments are shown. (**B**) Quantification of cell number positive for H3K76me1 (left) or H3K76me2 (right) of indirect IFA. Different cell cycle phases were distinguished by DAPI staining (1N1K, 1NeK, 1N2K and 2N2K). Mean value and standard deviation of three independent experiments are shown. (**C**) Luciferase assay of the total population and different cell cycle phases of DOT1B-luciferase cells obtained by DNA content-based cell sorting. Mean value of two (whole population) or three (G1, S and G2/M) independent experiments and, where appropriate, standard deviations are shown.

3.4 Depletion of DOT1A by RNAi

DOT1A is an essential enzyme in trypansosomes in contrast to DOT1B. In BSF, down-regulation of *DOT1A* by RNAi creates a cell population that contains half of the DNA content of a diploid wild-type cell, which is an exceptional observation in trypanosomes.

In these experiments, RNAi was based on a construct carrying the whole ORF of *DOT1A*, which was transcribed from two opposing T7-Polymerase promoters resulting in sense and antisense RNA. To establish another independent system in BSF and additionally in PCF, a new RNAi construct was introduced, which contained sense and antisense sequences of the *DOT1A* ORF building a hairpin when transcribed. In this case, RNAi targets only 460 bp of the *DOT1A* ORF.

To test whether down-regulation of *DOT1A* with the new construct causes the same phenotype as in previous experiments both life cycle stages of *T. brucei* were investigated. Depletion of *DOT1A* was lethal in both life cycle stages in accordance to previous experiments. Cell growth of PCF ceased completely 48 hours post induction (data not shown). As expected, a decrease in H3K76me1 (just shown for BSF) and H3K76me2 could be detected after induction (Fig 14A). Interestingly, the H3K76me3 level did not show any significant change suggesting that depletion of *DOT1A* had no detectable influence on H3K76me3.

The previously observed cell cycle phenotype in BSF could be reproduced with the new RNAi construct. 30% of cells showed 1n DNA content 24 hours after induction (Fig 14B, right panel). RNAi directed against GFP sequences was performed in a GFP-expressing cell line as a control. Knockdown of GFP caused no cell cycle-related phenotypes (Figure S1 in appendix).

PCF cells displayed a different cell cycle phenotype. About 15% of cells contained half of the DNA content of a wild-type cell 48 hours after induction (Fig 14B, left panel, 1n). Simultaneously, cells with DNA content below 1n increased to 30% of the total population 48 hours post induction (Fig 14B, left panel, arrow). These cells contain no nucleus, but one kinetoplast, and are called “zoids” (Robinson *et al.*, 1995). Zoid formation is characteristic for cell cycle mutants in PCF. They can undergo cytokinesis without previous karyokinesis generating enucleated cells, because a checkpoint is lacking (Ploubidou *et al.*, 1999).

In summary, down-regulation of *DOT1A* with an alternative construct reproduced the cell cycle phenotype observed in BSF before. In addition, a similar, but not identical phenotype was detected in PCF indicating that DOT1A has a similar function in both life cycle stages of trypanosomes.

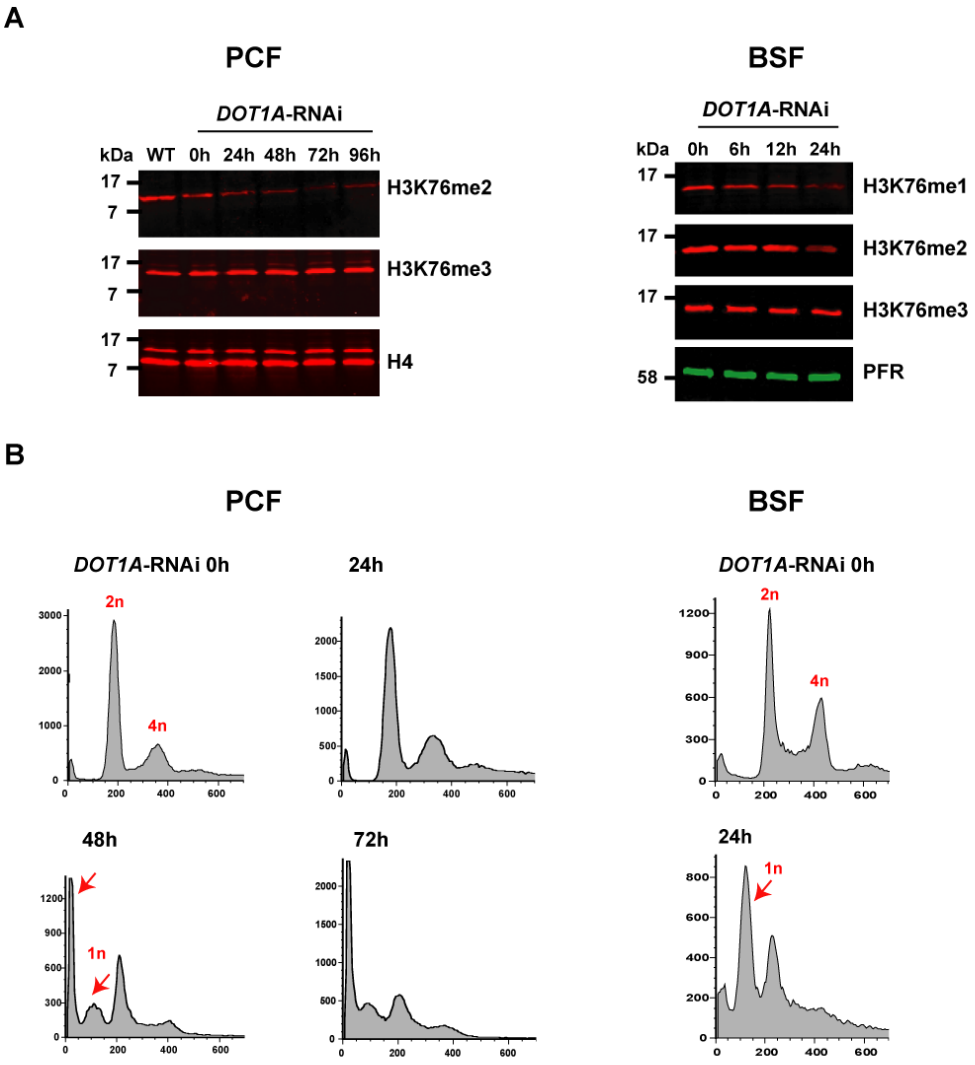

Figure 14: Depletion of *DOT1A* by RNAi causes similar cell cycle phenotypes in BSF and PCF. (**A**) Western blot analyses of PCF (left) and BSF (right) cells after induction of *DOT1A* RNAi. H3K76me1 (just shown for BSF) and H3K76me2 signals decreased after induction, whereas H3K76me3 level remained unchanged. H4 (PCF) or PFR (BSF) was used as loading control. (**B**) Flow cytometry analyses based on DNA staining with PI revealed cell cycle phenotypes in both PCF (left) and BSF (right). In PCF emergence of cells with 1n DNA content was observed as in BSF; additional high amounts of enucleated cells were generated in PCF.

3.5 Replication phenotype by DOT1A-RNAi

The appearance of cells with half DNA content was remarkable and posed one question: Where do these cells originate from? In principle there are two possibilities: first, cells can become haploid by the second cell division during meiosis, a process not described in trypanosomes, yet. Second, cells could loose half of the DNA by karyokinesis and cell division without previous replication of their DNA, which is usually prevented by a

checkpoint in other eukaryotes. In trypanosomes, artificially blocked replication by aphidicolin prevents mitosis, but not cytokinesis (Ploubidou *et al.*, 1999). Because checkpoint control in trypanosomes is different compared to higher eukaryotes, detailed analysis is required to explain cell cycle-related phenotypes in trypanosomes. A defect in replication might be the source of the observed aberrant cells after depletion of *DOT1A* and is the subject of further analyses.

The nucleus and kinetoplast configuration during the cell cycle was analyzed in detail by DAPI staining. After induction of *DOT1A*-RNAi, nucleus/kinetoplast configurations (1N1K, 1NeK, 1N2K and 2N2K) were determined and compared to those of non-induced cells. 68% of cells showed 1N1K, 12% 1NeK, 12% 1N2K and 8% 2N2K configuration before induction of RNAi (Fig 15). No significant differences were detected after down-regulation of *DOT1A*, except a slight increase in 1N2K cells up to 20% 24 hours post induction (Fig 15). The mainly unchanged nucleus to kinetoplast configuration 24 hours after DOT1A depletion was in contrast to the severe cell cycle phenotype visible at this time point. The data indicated that there is no cell cycle arrest after *DOT1A*-RNAi induction, although the DNA content of cells is reduced as detected by flow cytometry analysis (Fig 14B). This suggests that cells progress through S phase without replicating their nuclear DNA ending in 1N1K cells with half of the DNA content of a normal G1 phase cell. According to this, the observed 1N2K cells probably have a non-replicated genome but nevertheless pass through karyokinesis. The slight increase in the 1N2K population after *DOT1A*-RNAi induction might indicate a delay in the process of this unusual karyokinesis.

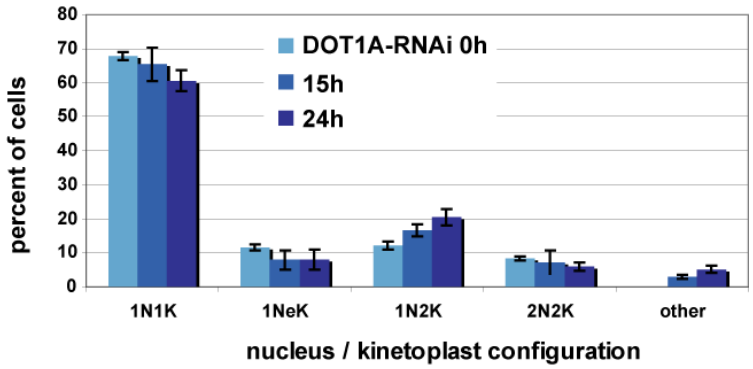

Figure 15: Cell cycle analysis of DOT1A depleted cells (BSF) based on DAPI staining. Distribution of different nucleus/ kinetoplast configurations was determined in non-induced, 15 hours and 24 hours induced cell populations. Mean values and standard deviations of three independent experiments are shown.

To unravel whether replication is indeed affected by depletion of *DOT1A*, 5-bromo-2-deoxyuridine (BrdU)-labeling of newly synthesized DNA was applied. After induction of *DOT1A*-RNAi, a population with 1n DNA content was detectable by PI staining followed by flow cytometry analysis as expected (Fig 16A, lower panel). 12 hours post induction, cells were labeled with BrdU for 7 hours, and the emerging 1n population was sorted for indirect IFA with a BrdU-specific antibody (Fig 16A, lower panel, bracket). Surprisingly, none of these cells showed BrdU-incorporation suggesting that these cells progressed through mitosis and cytokinesis without previous DNA replication. As a control, non-induced cells with 2n DNA content (G1 phase cells) were sorted and analyzed (Fig 16A, upper panel, bracket). Almost 100% of this population showed BrdU incorporation. These data suggest that depletion of *DOT1A* abolishes replication completely but does not prevent karyokinesis, which then leads to cells with a 1n DNA content. Karyokinesis without preceding replication has not been described before in trypanosomes and will be the subject of further analysis.

In addition, 19 hours after induction cells with 2n DNA content were sorted and analyzed as described above (Fig 16B, bracket). Cells with 2n DNA content are usually in the G1 phase and show 1N1K configuration (Fig 16A, upper panel). However, after *DOT1A* depletion, the 2n population consisted mostly of 1N2K cells with an irregular nucleus, and the majority showed no BrdU incorporation (Fig 16B). In some cells, DNA replication seemed to be not completely blocked without affecting the severe cell cycle phenotype of the total population. These unusual G1 phase cells further support the hypothesis of a defect in replication, which surprisingly does not lead to a cell cycle arrest.

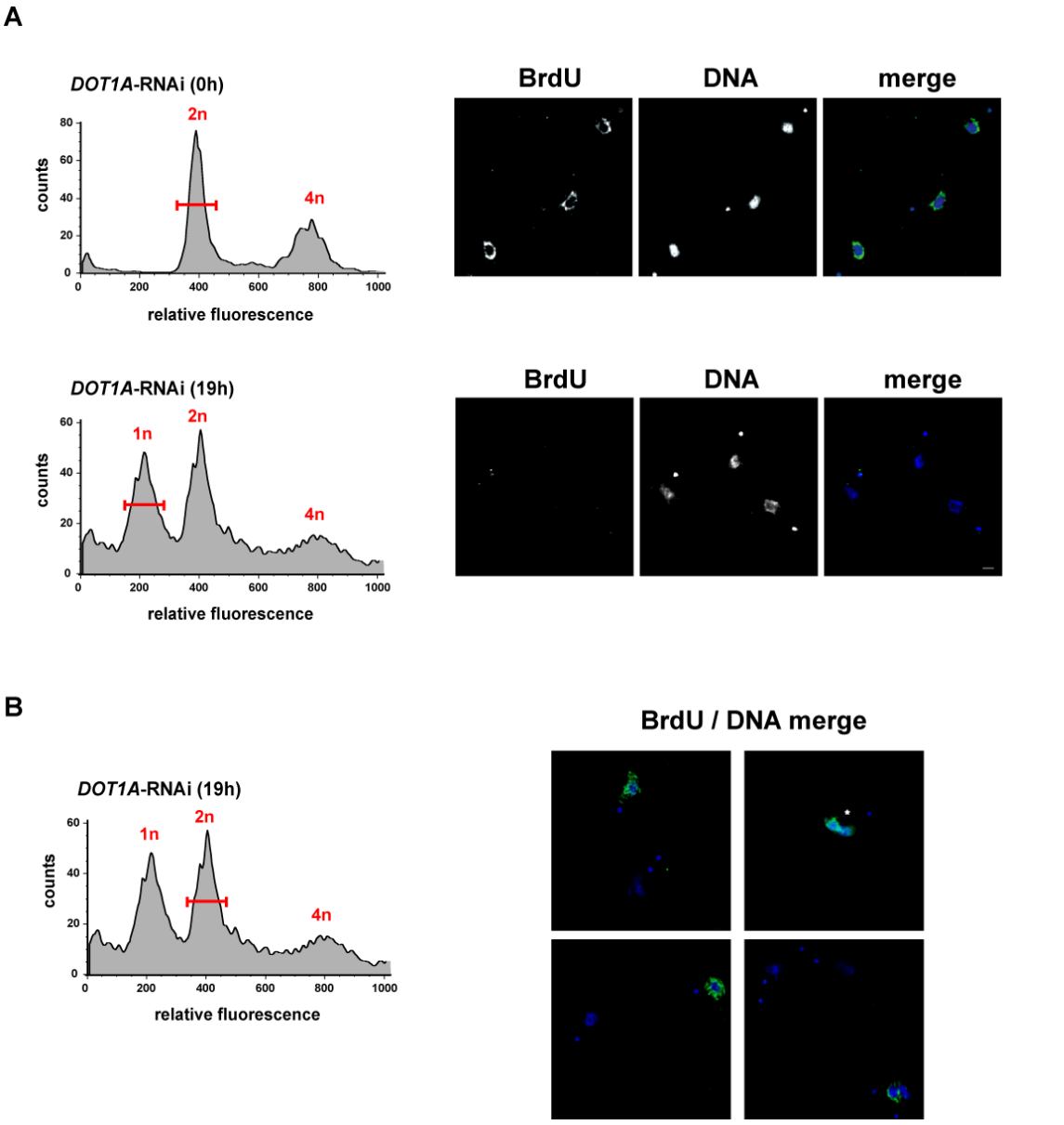

Figure 16: RNAi-mediated depletion of DOT1A inhibits replication. (**A**) Flow cytometry analysis of propidium iodide stained non-induced BSF cells (upper left panel) and cells 19 hours post induction of *DOT1A*-RNAi (lower left panel). Non-induced cells with a DNA content of 2n and DOT1A-depleted cells with a DNA content of 1n (both indicated by a red bracket) were sorted, and incorporation of BrdU (green) was analyzed (right panels). Cells were incubated with BrdU for 7 hours before fixation. DNA was stained with DAPI (blue). Scale bar, 2 µm. (**B**) Same analysis as in (A) of DOT1A-depleted cells with a DNA content of 2n.

In DOT1A depleted cells, H3K76me1 and -me2 is reduced and seems to be important for replication regulation. Thus, I addressed the question whether disturbance of the H3K76 methylation pattern by over-expressing DOT1A might cause a reciprocal phenotype and leads to increased initiation of replication.

3.6 DOT1A over-expression disturbs accurate H3K76 methylation levels and causes cell cycle defects

To analyze the effects of DOT1A over-expression on cell cycle progression, an inducible T7 RNA polymerase-driven expression system was used (Wirtz *et al.*, 1999). A peptide-tagged DOT1A-TY fusion protein was expressed, as a specific antibody for trypanosome DOT1A is not available. In contrast to yeast, DOT1A over-expression was lethal in *T. brucei*. Within 24 hours post induction, growth of the population ceased almost completely (Fig 17A). To monitor cell cycle profiles, tetracycline-induced cells were stained with PI and analyzed by flow cytometry (Fig 17B). Cell cycle profiles of non-induced cells were indistinguishable from those of wild-type cells with approximately 45% of the cells in G1 phase, 11% in S phase and about 28% in G2/M phase. However, after induction, two additional populations could be detected: enucleated cells (so called "zoids", Fig 17B, lower panel, arrow) and a population with an apparent aneuploid DNA content (Fig 17B, > 4n). Emergence of enucleated cells has been observed after DOT1A depletion as well. Cytokinesis without karyokinesis resulted in one daughter cell without nucleus and the other with a nucleus of 4n DNA content. 16 h post induction of DOT1A over-expression, 7% of zoids were detected, and aneuploid cells increased dramatically to almost 50% of the population while the G1 phase population decreased.

The numbers of nuclei and kinetoplasts per cell were determined up to 16 hours post induction (Fig 17C). In agreement with the flow cytometry analysis, a decrease of 1N1K cells (G1 or S phase) could be detected (from 55% to 20%). Simultaneously, the percentage of 1N2K (G2 phase) cells increased up to 50%, while the proportion of 1NeK cells (S phase) did not change significantly. 2N2K cells (post mitotic) decreased and were not detectable 16 hours post induction. At this time point, 5% of enucleated zoids were observed in accordance with the flow cytometry data. Strikingly, none of the cells showed multiple nuclei or kinetoplasts. This strongly supports the hypothesis that karyokinesis is inhibited and the DNA content increases constantly in individual nuclei leading to the generation of cells with aneuploid nuclei.

To evaluate the effect of DOT1A over-expression on H3K76 methylation levels, quantitative Western blot analysis was performed using antibodies specific for H3K76me1, -me2 or -me3 (Fig 17D). Surprisingly, H3K76me1 and H3K76me2 levels of total cell lysates remained unchanged 24 hours post induction and did not increase, although over-expression of DOT1A-TY could be detected (Fig 17D, upper panel). The level of H3K76me3 did not increase, too.

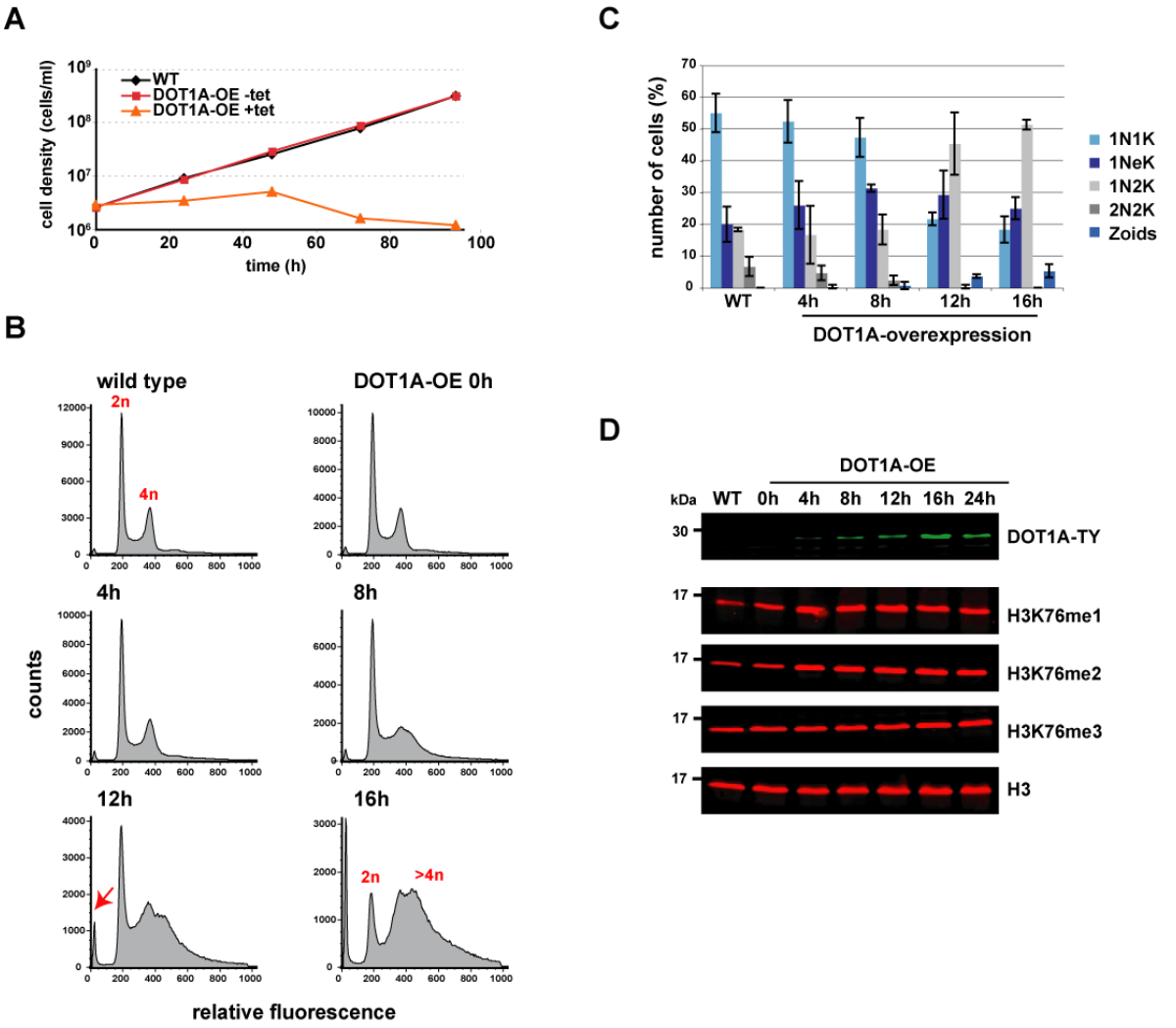

Figure 17: DOT1A over-expression causes a cell cycle defect and alters H3K76 methylation pattern. (**A**) Cumulative growth curves of WT, non-induced and induced DOT1A over-expressing cell lines (PCF). (**B**) Flow cytometry analysis of PI stained DOT1A over-expressing cells. Relative amount of DNA content is indicated. The population of enucleated cells ("zoids") is marked by an arrow. (**C**) Quantitative analysis of number of nuclei (N) and kinetoplasts (K) in WT and DOT1A over-expressing cells. Mean values of three independent experiments are presented with standard deviation (100 cells were analyzed each). (**D**) Western blot analysis of DOT1A-TY expression and different H3K76 methylation states in DOT1A over-expressing cells. Histone H3 was used as loading control.

To analyze the temporal appearance of the H3K76 methylation pattern after DOT1A over-expression, individual cells were analyzed by indirect IFA. In wild-type populations, about 2% of 1N1K cells, 20% of 1N2K cells and 95% of 2N2K cells showed H3K76me2 (Fig 18A). 8 hours after induction of DOT1A over-expression, 70% of 1NeK cells were positive for H3K76me2 which was in striking contrast to 1NeK cells of wild-type populations never displaying H3K76me2 signals (Fig 18B). The proportion of 1N2K cells positive for H3K76me2 increased up to 80% 8 hours post induction (Fig 18A). On the other hand, only

50% of the 2N2K cells were H3K76me2 positive 4 hours post induction. At later time points, the amount of 2N2K cells was very low and could not be analyzed. These results revealed that H3K76me2 was detectable earlier in the cell cycle after DOT1A over-expression and shifted into S phase. However, H3K76me2 disappeared earlier in the cell cycle as well (probably by becoming trimethylated). In the post mitotic phase only 50% of 2N2K cells were positive for H3K76me2, in contrast to wild-type cells, where H3K76me2 was detectable in nearly every 2N2K cell and additionally in 2% of 1N1K cells, which have probably just completed cytokinesis.

In summary, the temporal occurrence of H3K76me2 was shifted during the cell cycle by DOT1A over-expression, although the overall H3K76me2 level of total cell populations was not increased as detected by Western blot analysis (Fig 17D). In accordance to the premature H3K76me2 pattern, H3K76me1 also occurred earlier in the cell cycle in induced cells as a precursor of H3K76me2 (Fig 18C and D). The abnormal H3K76 methylation pattern could be the source for the observed cell cycle phenotype, which is examined in more detail below.

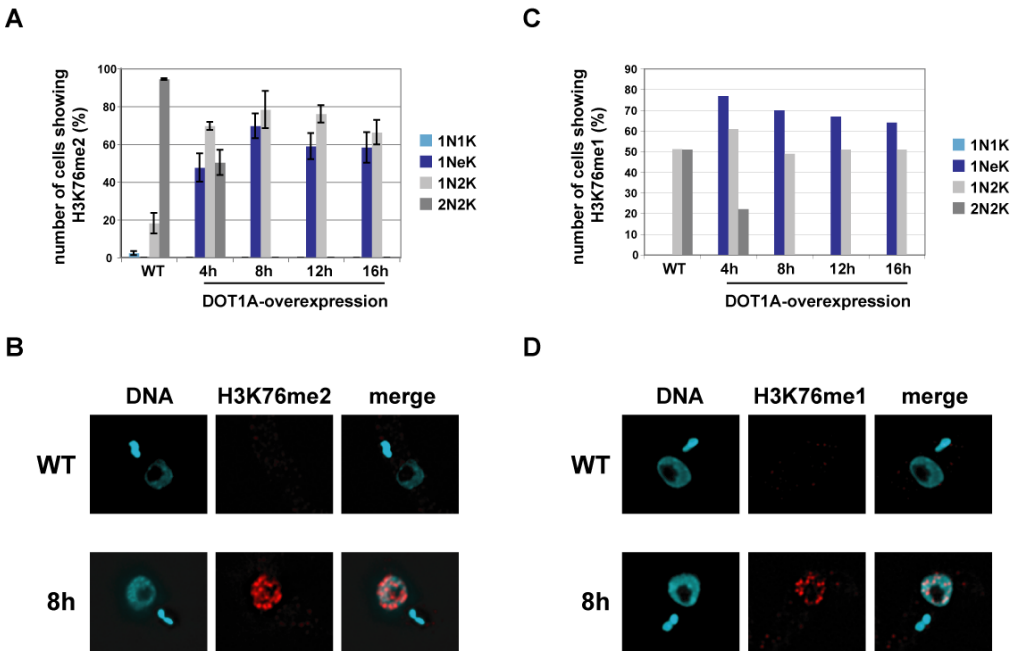

Figure 18: H3K76 methylation pattern after DOT1A over-expression in individual cells during the cell cycle. (**A**) Percentage of cells in different cell cycle phases positive for H3K76me2. Cell cycle stages were distinguished by DAPI staining. Mean values of three independent experiments are presented with standard deviation (n > 70 for each cell cycle phase). 2N2K cells were analyzed only for wild-type and induced cells 4 hours post induction due to the reduced amount of 2N2K cells after longer induction periods. (**B**) Example of a DOT1A over-expressing S phase cell (lower panel) showing H3K76me2 prematurely in contrast to a wild-type S phase cell (upper panel). (**C**), (**D**) Analogue analyses as shown in (A) and (B) for H3K76me1.

3.7 Over-expression of a DOT1A-mutant attenuates lethal cell cycle phenotype

To demonstrate that the development of the cell cycle phenotype is dependent on methyltransferase activity of DOT1A, a catalytic mutant of DOT1A (DOT1A-G138R) was over-expressed. The central glycine of the conserved GxGxG motif which is essential for catalytic activity of Dot1 enzymes in other organisms (Cheng *et al.*, 2005; Cheng and Zhang, 2007) was mutated to arginine (Frederiks *et al.*, 2010). The DOT1A mutant showed only residual activity on trypanosomal nucleosomes *in vitro* (G. Dindar, personal communication). Although expression levels of the DOT1A mutant were comparable to over-expressed wild-type DOT1A (Fig19A), only minor changes of cell cycle profiles were detected at later time points after induction of ectopic expression (Fig 19B).

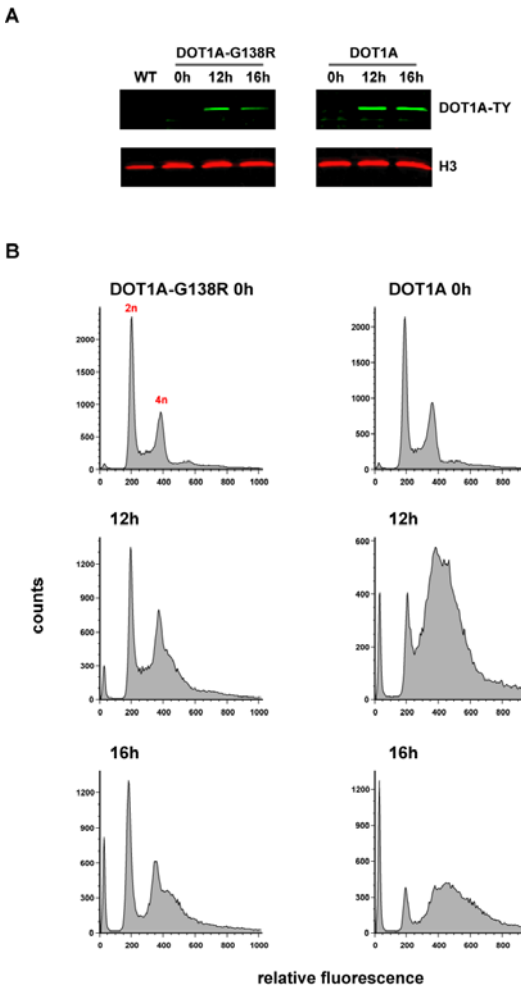

Figure 19: Over-expression of a DOT1A-G138R mutant. (**A**) Western blot analysis of DOT1A-G138R mutant (left panel) and wild-type DOT1A over-expression (right panel). Histone H3 was used as loading control. (**B**) Flow cytometry analysis of PI-stained DOT1A-G138R mutant (left panel) and wild-type DOT1A over-expressing cells (right panel). Relative amount of DNA content is indicated.

3.8 DOT1A over-expression causes continuous replication of nuclear DNA

The FACS profile of DOT1A over-expressing cells did not reveal a sharp peak for the aneuploid cell population; therefore, it is unlikely that the DNA content of these cells was accurately doubled in an additional round of replication. The broad profile rather suggests continuous replication of DNA without proper chromosome segregation and karyokinesis. To test this hypothesis, a protocol was established that allows the detection of DNA synthesis at distinct time points of the cell cycle by incorporation of differently labeled nucleotides. First, newly synthesized DNA was labeled with 5-ethynyl-2-deoxyuridine (EdU) 7 hours post induction for 2 hours. Subsequently, EdU was removed from the cell culture supernatant, cells were incubated for 3 hours without any additive to ensure that all labeled cells exit S phase (which required about 2.5 hours in our laboratory strain), and DNA was labeled again with 5-bromo-2-deoxyuridine (BrdU) for 2 hours. Afterwards, cells were analyzed by fluorescence microscopy (Fig 20). In a wild-type population, cells could be labeled with either EdU or BrdU but never with both (Fig 20A). The distribution of the incorporated BrdU and EdU was different possibly caused by differences in the mobility of an antibody (BrdU-labeling) compared to a small molecule (EdU-labeling).

Individual DOT1A over-expressing cells were clearly labeled with EdU and BrdU, indicating that replication continued for a long time period, although cellular markers suggested that the cells were not in S phase anymore (Fig 20B, 1N2K cell).

In summary, these data support the hypothesis that DOT1A over-expression causes continuous replication, which generates nuclei with increasing DNA content and prevents chromosome segregation and karyokinesis.

To characterize the aneuploid cells in more detail, fluorescence in situ hybridization (FISH) was performed with a probe specific for the tubulin gene array (Fig 21). Cells of G1, G2 phase and cytokinetic cells used as control showed distinguishable signals for the tubulin gene locus as expected (Fig 21A). 2 signals were detectable in most G1 phase cells, and G2 phase cells showed either 2 or 4 signals. The lower panel of Figure 21A shows 4 distinguishable signals representing segregated chromosomes in a cell that completed karyokinesis. In contrast, cells of aneuploid populations contained enlarged nuclei with several clearly distinguishable signals 16 hours post induction of wild-type DOT1A over-expression (Fig 21B) which suggests multiple re-initiation events of the same locus within one S phase.

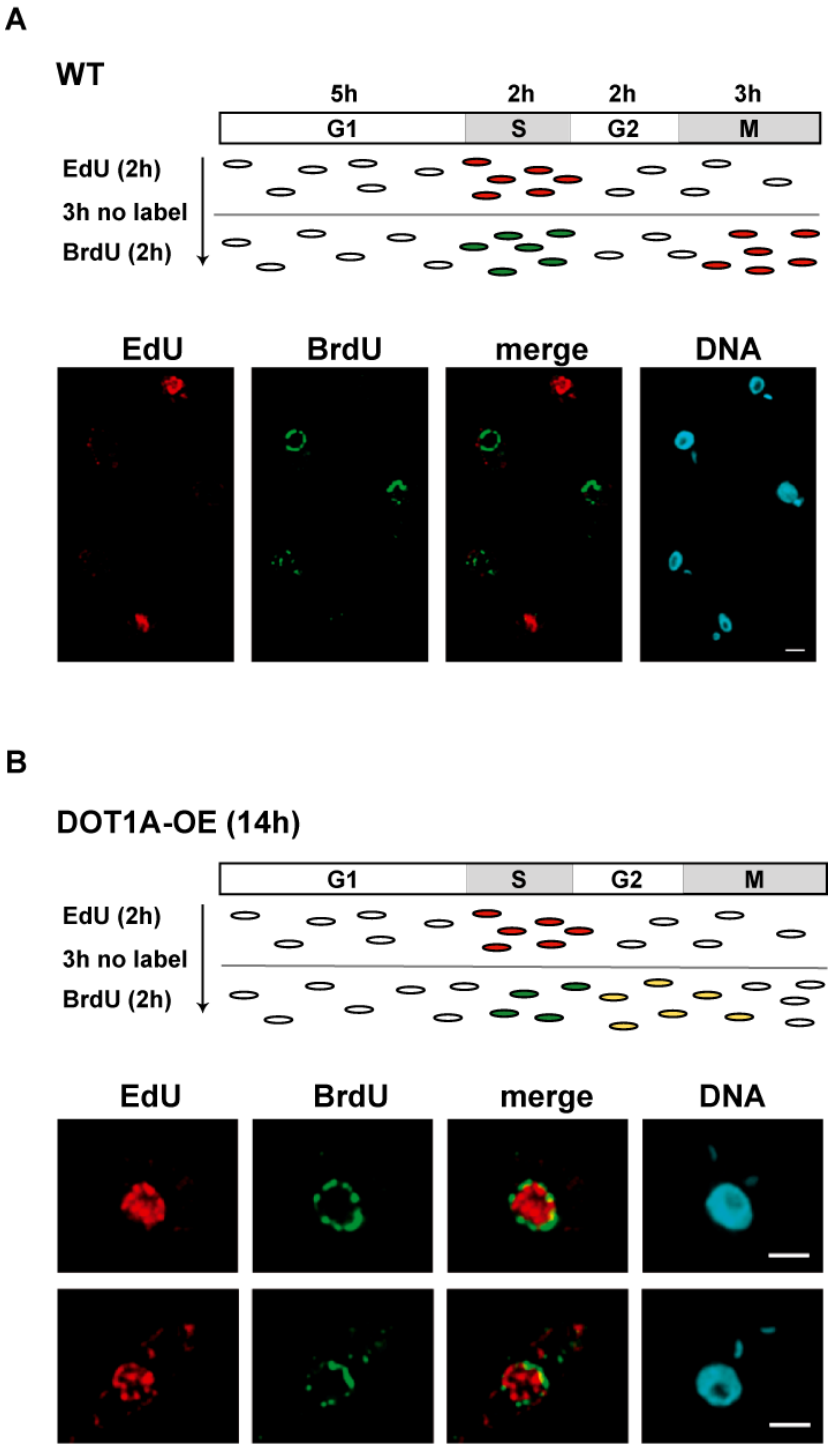

Figure 20: DOT1A over-expression causes continuous replication of nuclear DNA. Incorporation analysis of EdU and BrdU in replicated DNA during S phase of (**A**) wild-type and (**B**) DOT1A over-expressing cells (14 h post induction). Top panels show a schematic representation of the experimental design. One cell cycle is displayed. Labeled cells are shown as colored ovals. Bottom panels show IFA of labeled trypanosomes. Detection of EdU (red) is based on a "click reaction"; BrdU (green) was detected by an antibody. DNA was stained with DAPI. Scale bars, 2 µm.

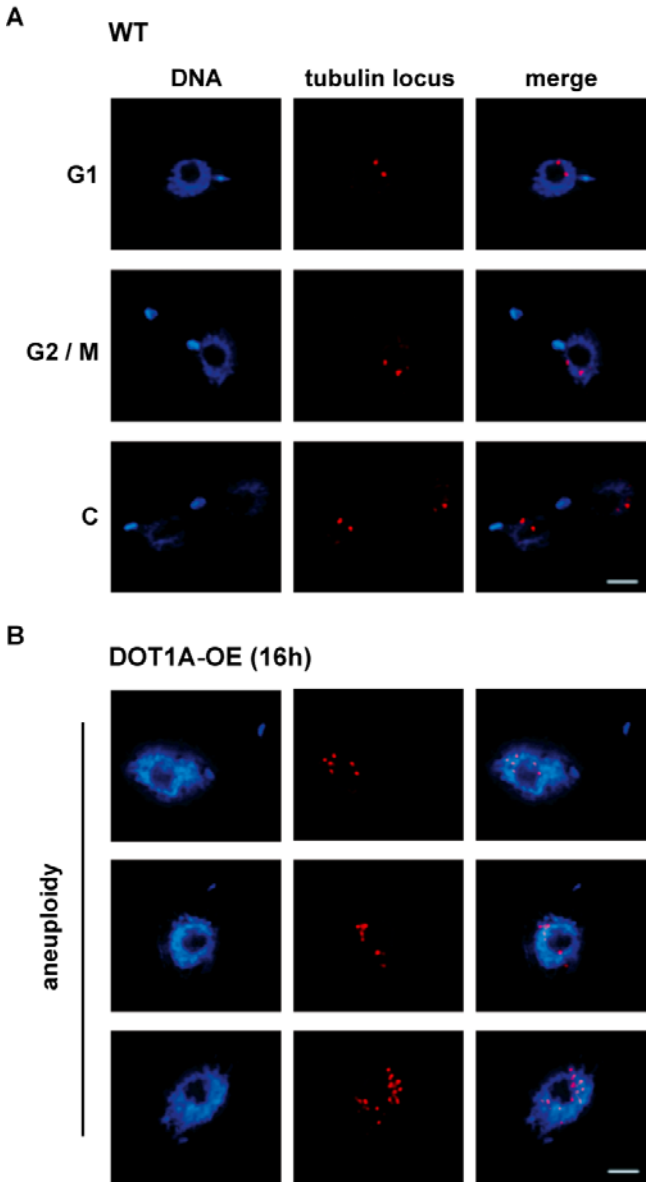

Figure 21: DOT1A over-expression causes re-initiation of replication. Fluorescence *in situ* hybridization analysis of (**A**) wild-type and (**B**) DOT1A over-expressing cells. A probe specific for the tubulin gene array (red) was used for hybridization. DNA was stained with DAPI. Aneuploid nuclei showed several distinguishable signals of the tubulin locus. Scale bars, 2 µm.

The data obtained so far suggest that the H3K76me1 and -me2 pattern has to be regulated carefully for proper replication regulation in trypanosomes. If *DOT1A* is depleted, and therefore the levels of H3K76me1 and H3K76me2 decrease, replication is impaired which produces cells with reduced DNA content. In contrast, DOT1A over-expression causes the reciprocal phenotype. H3K76me1 and H3K76me2 appear prematurely in S phase, and replication occurrs on a continuous basis generating cells with increased DNA content, which are not capable to process through karyokinesis. The role of H3K76me3 remains elusive, particularly because loss of H3K76me3 by *DOT1B* deletion does not cause any cell cycle-

related phenotype (Janzen *et al.*, 2006b). Nevertheless, DOT1B-dependent methylation was considered as well, because DOT1B is also able to mediate H3K76me1 and -me2 (Frederiks *et al.*, 2010). Therefore, DOT1B over-expression might also lead to premature H3K76 methylation and affect replication in a similar way to DOT1A over-expression.

3.9 The role of DOT1B in cell cycle control

H3K76me1 and -me2 is increased in *DOT1B* deleted cells, possibly because the conversion to H3K76me3 does not take place. As a consequence, H3K76me2 becomes detectable throughout the cell cycle (Janzen *et al.*, 2006b). Interestingly, ΔDOT1B cells do not show any cell cycle-related phenotype.

To test if DOT1B over-expression leads to premature H3K76 methylation and affects replication as well, an analogue inducible system was used as for DOT1A over-expression which introduces a peptide-tagged TY-DOT1B fusion product (Wirtz *et al.*, 1999). Induction of DOT1B over-expression was lethal, similar to DOT1A over-expression. Growth of the population ceased almost completely within 48 hours (Fig 22A). In contrast to DOT1A over-expression, H3K76 methylation ratios changed by DOT1B over-expression as detected by quantitative Western blot analysis using antibodies specific for the different methylation states (Fig 22B). H3K76me1 and H3K76me2 levels decreased to ~35% of wild-type levels 24 h post induction, which correlated with the onset of the growth phenotype (Fig 22B, lower panel). H3K76me3 did not increase dramatically which reflects that most of H3K76 is trimethylated already in an asynchronously growing population as previously revealed by mass spectrometry (Fig 10).

Next, cell cycle profiles were analyzed to find a potential phenotype. Indeed, cell cycle profiles looked very similar to that of DOT1A over-expressing cells including the emergence of enucleated cells (Fig 22C, lower panel, arrow) and a population with aneuploid DNA content (Fig 22C, > 4n). 24 h post induction, an increase of aneuploid cells to almost 40% of the population was detected while the G1 phase population decreased dramatically.

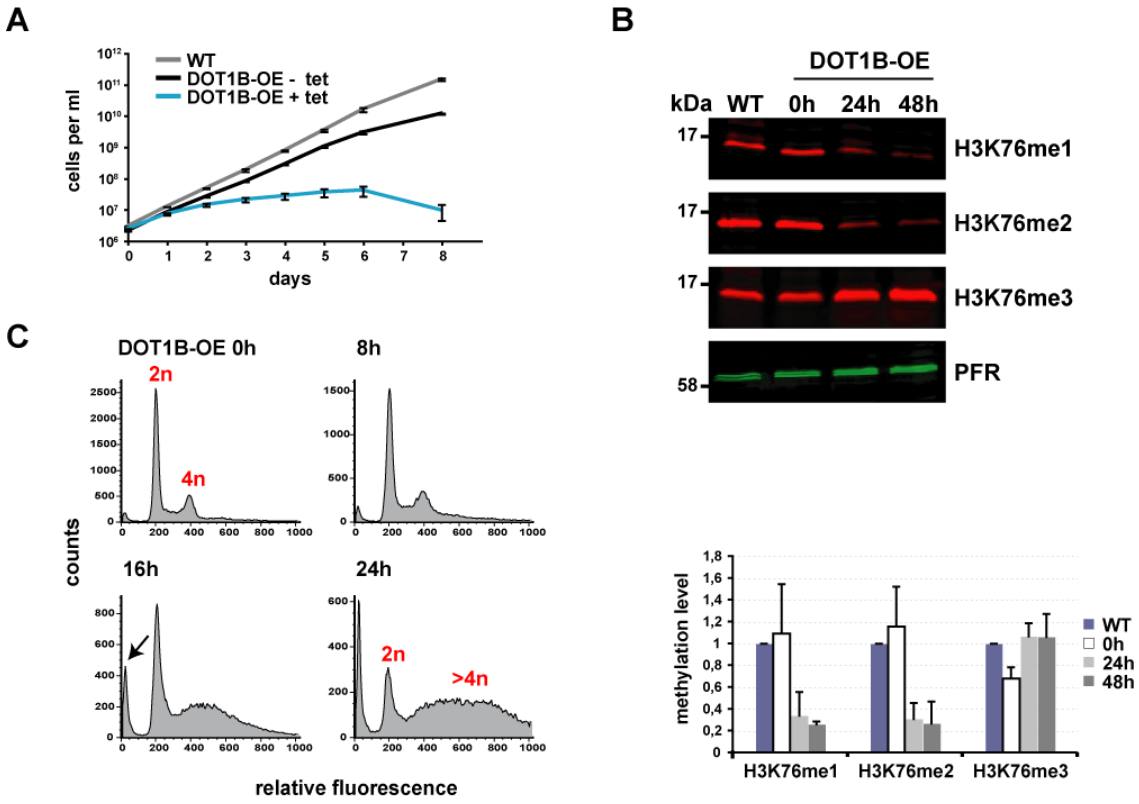

Figure 22: DOT1B over-expression generates aneuploid cells. (**A**) Cumulative growth curves of WT, non-induced and induced DOT1B over-expressing cell lines. Mean values of three independent experiments are presented with standard deviation (**B**) Quantitative Western blot analysis of different H3K76 methylation states in DOT1B over-expressing PCF cells. PFR was used for normalization. One of three representative blots is shown (top panel). Quantification of three independent experiments is shown below. WT methylation levels were set to one. (**C**) Flow cytometry analysis of PI-stained DOT1B over-expressing cells. Relative amount of DNA content is indicated. The population of enucleated cells ("zoids") is marked by an arrow.

The generation of zoids (18%, 24 h post induction) could be observed directly by indirect IFA using antibodies against H3K76me2 and α-tubulin (Fig 23A). Induced cells showed no signals for H3K76me2, but progressed through cytokinesis without previous karyokinesis. This produced up to 45% of zoids detected by DAPI staining 3 days post induction of DOT1B over-expression (Fig 23B). Although the 2n peak (G1 phase cells) in the FACS profile dropped dramatically after 24 hours, only a faint decrease of 1N1K could be detected. The number of 1N2K cells remained stable as well (Fig 23B) suggesting that most of these observed 1N1K and 1N2K cells had an unusually high DNA content. Furthermore, a decrease of 2N2K cells was detectable. This strongly supports the hypothesis that the parasite's cell cycle progression continues although karyokinesis is inhibited, and the DNA content

increases constantly in individual nuclei leading to the generation of cells with aneuploid nuclei.

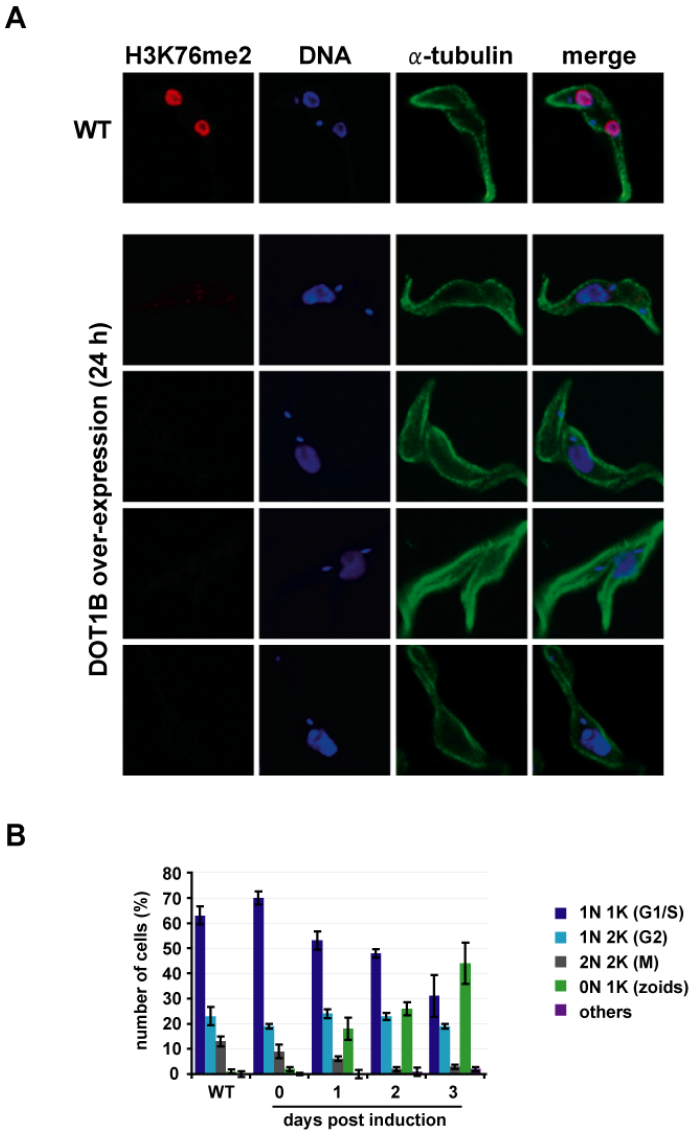

Figure 23: DOT1B over-expressing cells progress through cytokinesis without preceding karyokinesis. (**A**) Indirect IFA of WT and DOT1B over-expressing cells using antibodies for H3K76me2 and α-tubulin to visualize the shape of cells. DNA was stained with DAPI. (**B**) Quantitative analysis of number of nuclei (N) and kinetoplasts (K) in WT and DOT1B over-expressing cells. Mean values of three independent experiments are presented with standard deviation (100 cells were analyzed each).

3.10 DOT1B over-expression causes continuous replication of nuclear DNA

To test whether DOT1B over-expression results in continuous replication as well, cells were doubly labeled with EdU and BrdU. As previously shown, cells of the wild-type population

could be labeled with either EdU or BrdU but not with both (Fig 24A). Individual DOT1B over-expressing cells were clearly double-labeled with EdU and BrdU, indicating that replication continued (Fig 24B) which had been previously observed for DOT1A over-expression.

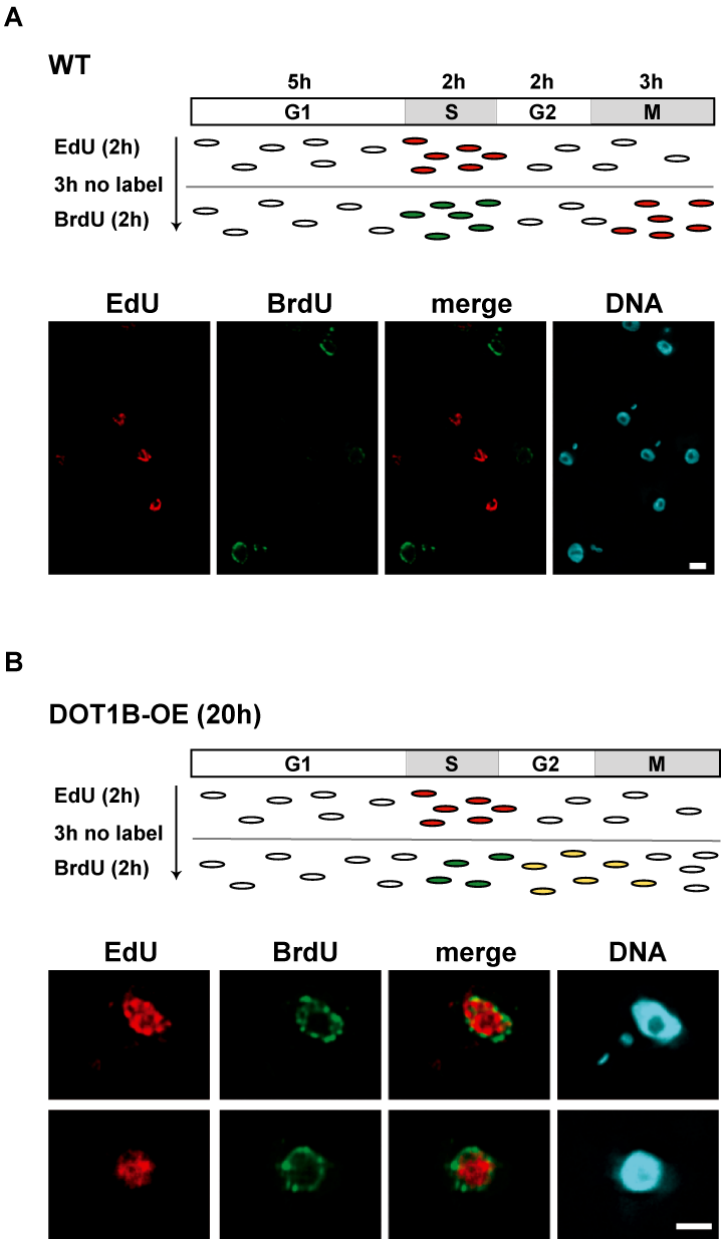

Figure 24: DOT1B over-expression causes continuous replication of nuclear DNA. Incorporation analysis of EdU and BrdU in newly replicated DNA of (**A**) WT and (**B**) DOT1B over-expressing cells (20 h post induction). Top panels show a schematic representation of the experimental design. One cell cycle is displayed as a bar. Labeled cells are shown as colored dots. Bottom panels show IFA of labeled trypanosomes. Detection of EdU (red) is based on a "click reaction"; BrdU (green) was detected by an antibody. DNA was stained with DAPI. Scale bars, 2 µm.

In comparison, the phenotypes of DOT1A and DOT1B over-expressing cells looked quite similar despite of some minor differences. In DOT1B over-expressing cells, more zoids were produced and the 1N2K population remained stable, while this population increased after DOT1A over-expression. This suggests that the majority of cells is arrested in 1N2K configuration after DOT1A over-expression, probably due to the ongoing replication and failure in karyokinesis. This is not observed in DOT1B over-expressing cells which seem to progress through the cell cycle despite ongoing replication. Direct comparison of both genetically manipulated systems is not possible, because expression levels of the DOT1 proteins might vary, and therefore slightly different phenotypes can be generated with respect to time point post induction and severity of the phenotype.

3.11 Titration of tetracycline as inductor for DOT1B over-expression

To test whether phenotypes vary with different amounts of expressed DOT1B, increasing tetracycline concentrations were used for induction. Cell cycle profiles were analyzed 24 hours post induction. Indeed, the severity of the phenotype was dependent on tetracycline concentration: with low tetracycline concentrations (1-10 ng/ml tetracycline), cell growth was not affected, and cell cycle profiles were indistinguishable from non-induced cells 24 hours post induction (Fig 25). With 100 ng/ml tetracycline, cells showed impaired growth and a cell cycle phenotype consisting of zoids and aneuploid cells (Fig 25, lower panel). Higher tetracycline concentration (1 µg/ml) resulted in a higher percentage of zoid formation and more aneuploid cells with continuing increased DNA content. The data showed that the phenotype varied in severity in a dose-dependent manner of tetracycline.

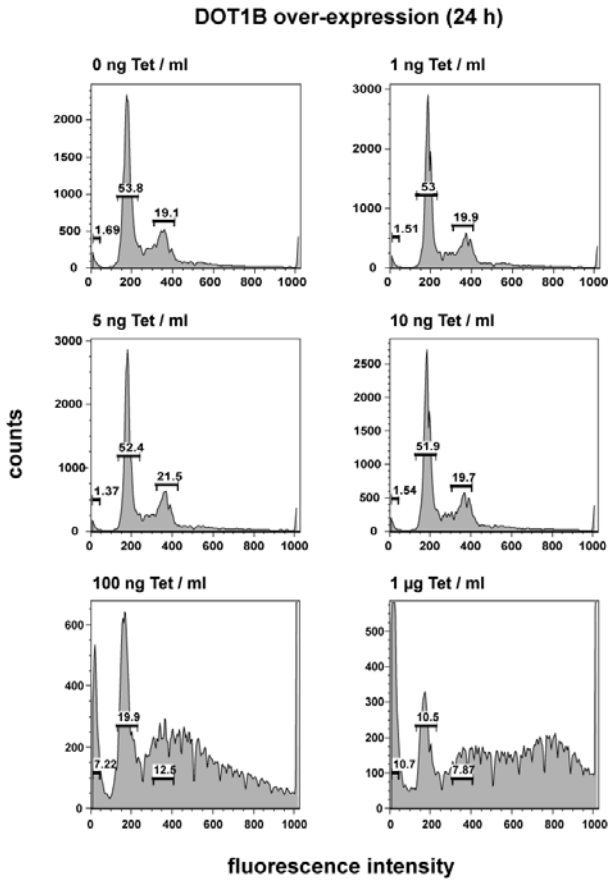

Figure 25: Flow cytometry analyses of DOT1B over-expressing cells using different tetracycline concentrations. The effect of tetracycline (Tet) was analyzed 24 hours after induction. Analysis was based on PI staining.

3.12 Comparison between DOT1A and DOT1B over-expression

In summary, the data revealed that DOT1A as well as DOT1B over-expression caused continuous replication, which generated nuclei with increasing DNA content. Importantly, over-expression of the enzymes had different effects on H3K76 methylation pattern: DOT1A over-expression resulted in premature emergence of H3K76me1 and H3K76me2 in the cell cycle. Both modifications were detected in S phase in DOT1A over-expressing cells in contrast to wild-type cells, where they were visible in G2 and M phase cells. The time window of H3K76me1 and H3K76me2 expression during the cell cycle was not extended by DOT1A over-expression. This is in contrast to DOT1B over-expression which led to decreasing amounts of H3K76me1 and H3K76me2. Probably, incorporated unmodified histones were prematurely mono- and dimethylated by DOT1B, similar to the situation in DOT1A over-expressing cells. However, the premature emergence of H3K76me1 and -me2 could not been shown in DOT1B over-expressing cells, probably because the conversion to

H3K76me3 followed immediately. The emergence of H3K76me1/me2 might become very transiently with induction time of DOT1B over-expression, which could be a reason for the decreased levels of H3K76me1 and -me2. Western blot analysis did not detect changes in the H3K76me3 level upon DOT1A and DOT1B over-expression, probably because most of H3K76 is already trimethylated in wild-type cells (Fig 10). According to the model, unmodified H3K76 levels should be decreased upon DOT1A and DOT1B over-expression which was analyzed by mass spectrometry analysis for DOT1B over-expressing cells (Fig 26). Indeed, the amount of unmethylated H3K76 decreased 3-fold 24 hours after DOT1B over-expression and simultaneously, a similar fold increase was detected for H3K76me3 (Fig 26).

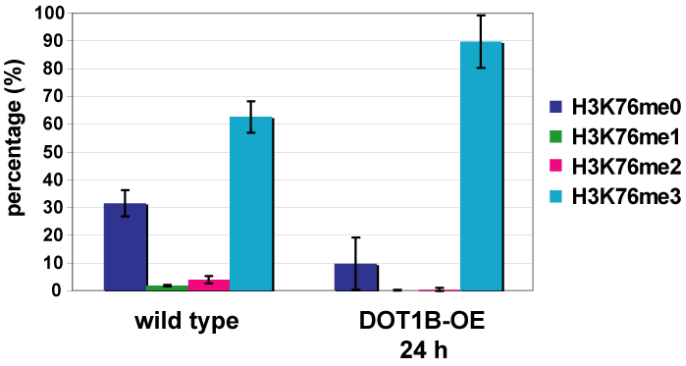

Figure 26: Mass spectrometry analysis comparing H3K76 methylation states in wild-type and DOT1B-OE cells. Histone H3 separated from total cell lysates of wild-type or 24 hours DOT1B over-expressing cells was examined for H3K76 methylation. Mean values and standard deviations of at least three independent experiments are shown.

In summary, depletion of DOT1A as well as over-expression of both DOT1 enzymes led to severe replication defects in a reciprocal manner. After DOT1A depletion, replication was not initiated, whereas continuous replication could be detected after over-expression of DOT1A and also DOT1B. These data suggest that *de novo* H3K76-methylation of newly incorporated histones has to be regulated coordinately to ensure accurate replication initiation in *T. brucei*. How does H3K76 methylation mediate replication control? One explanation is that H3K76 methylation may mark the loci in the genome where replication is initiated. These origins of replication are not well defined in most eukaryotes and have not been described in trypanosomes, yet. To find such potential association of H3K76me1 and -me2 with distinguishable domains or specific DNA sequences, a genome-wide analysis by chromatin immunoprecipitation was performed.

3.13 Genome-wide distribution of H3K76 mono- and dimethylation

Chromatin was immunoprecipitated with specific antibodies for H3K76me1 and -me2, and purified DNA was hybridized on a custom-made microarray to identify genomic regions enriched in H3K76 methylation. An antibody specific for H3 was used in parallel. The array covered all 11 megabase-size chromosomes of *T. brucei* (strain 927, version 4) with 720K probes of 50-75 nucleotides length each. To reduce the number of poor-performing probes, a frequency filter was applied which removed probes containing 15mers that were very common in the sequence. Usually probes with 15mer frequencies greater than 100 were eliminated, and more than 10 matches between a probe and the genome were normally not allowed for final probe selection. In this case, coverage in repetitive regions was requested and the selection criteria were relaxed by allowing up to 400 matches between a probe and the genome, and the permitted 15mer frequency were increased to 300 (probes with 15mer frequencies this high will have a much higher signal than the other probes, increasing the dynamic range of signals on the array). With these modifications in the array design, it was possible to cover most of the repetitive regions which are normally not considered.

The raw probe signals were transformed into $\log_2$-values. Immunoprecipitated (Cy5) and input (Cy3) normalized $\log_2$-signals were converted into enrichment ratios ($\log_2$ [Cy5/Cy3]) individually for each biological triplicate. The replicate ratios were averaged to obtain a single estimate for each histone modification (H3, H3K76me1 and H3K76me2).

No obvious difference could be detected between mean $\log_2$ ChIP signals of H3K76 methylation and H3 (Fig 27 and Fig S2 in appendix). However, some genomic regions showed a striking depletion of H3 and H3K76me1/me2. These regions contained well-defined Pol II transcription start sites (TSS). TSS in combination with transcription termination sites (TTS) border the large polycistronic transcription units, which are characteristic for the trypanosomal genome. TSS and TTS are associated with nucleosomes consisting of histone variants and enrichment in specific post-translational histone modifications (Siegel *et al.*, 2009). For example, H4K10 acetylation and the histone variants H2AZ and H2BV are highly enriched at TSS, whereas the variants H3V and H4V are mainly found at TTS. Furthermore, partial nucleosome depletion is characteristic for TSS (Stanne and Rudenko, 2010). Importantly, H3 as well as H3K76me1/me2 depletion by a factor of 16 was clearly reproduced at TSS (Fig 27 and Fig S2 in appendix) indicating that immunoprecipitation with the different antibodies operated well.

Log_2 ratios of H3 were subtracted from those of the modified histones to correct for the differences in nucleosomal density,

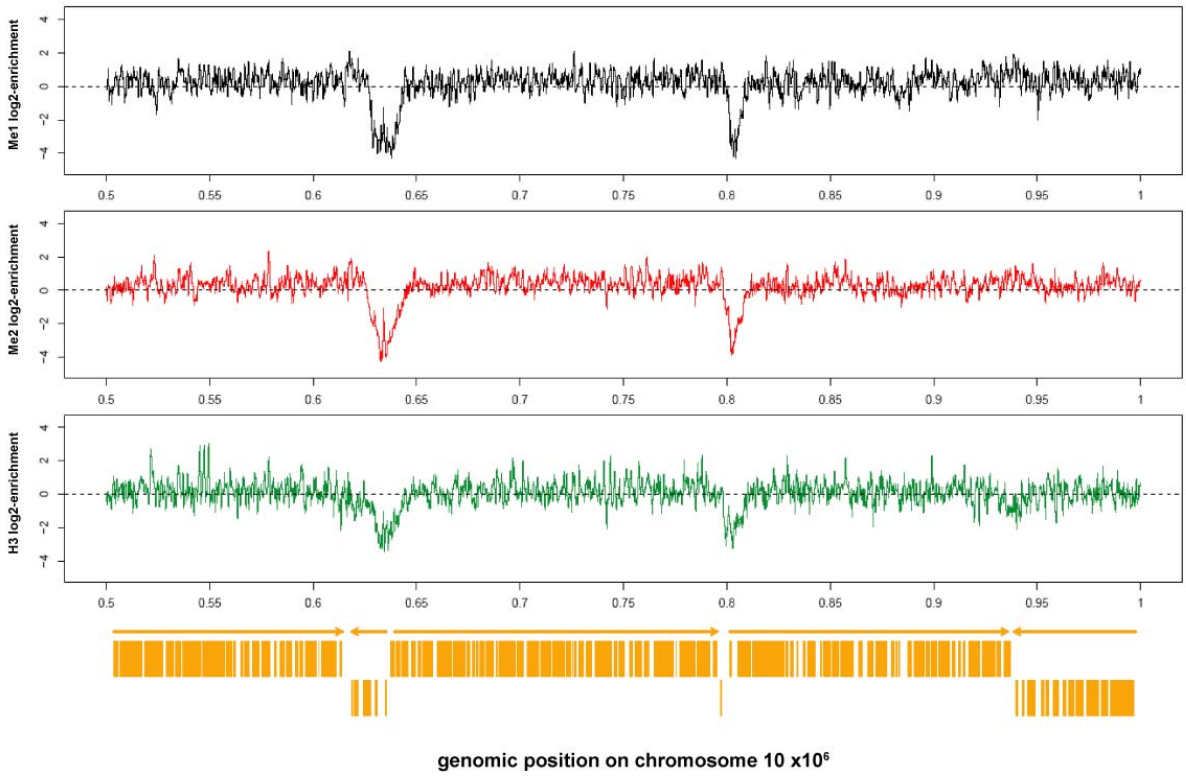

Fig 27: Distribution of H3K76me1, -me2 and histone H3. The genomic distribution of H3K76me1 (black), H3K76me2 (red) and H3 (green) is displayed for representative regions of chromosome 10. Orange boxes represent ORFs and orange arrows indicate the direction of transcription. See Figure S2 in appendix for data of complete chromosome 10 (on enclosed DVD).

Genome-wide analysis could not reveal any sequence-specific association of H3K76 methylation. However, after normalization with H3-data, enrichment of H3K76me1 and H3K76me2 was detected in functional domains, mainly coinciding with TTS (Fig 28 and Fig S3 for all chromosomes). A peak profile was defined to quantify H3K76me1/me2 enrichment with following criteria:

1. ≥ 4-fold enrichment
2. ≥ 5 adjacent probes display the threshold value
3. ≥ 5 kb peak width

On chromosome 10, 24 peaks were found with at least 5-fold increase of H3K76me1, and 28 peaks of at least 4-fold H3K76me2- enrichment matched the defined profile (Fig 29). The average peak profiles of H3K76me1 and H3K76me2 looked similar with a mean peak width of about 7.4 kb (Fig 29). H3K76me1 seemed to be more enriched with a mean $\log_2$ value of 2.4 (means 5.76-fold enrichment) than H3K76me2 with a mean $\log_2$ value of 2 (means 4-fold enrichment).

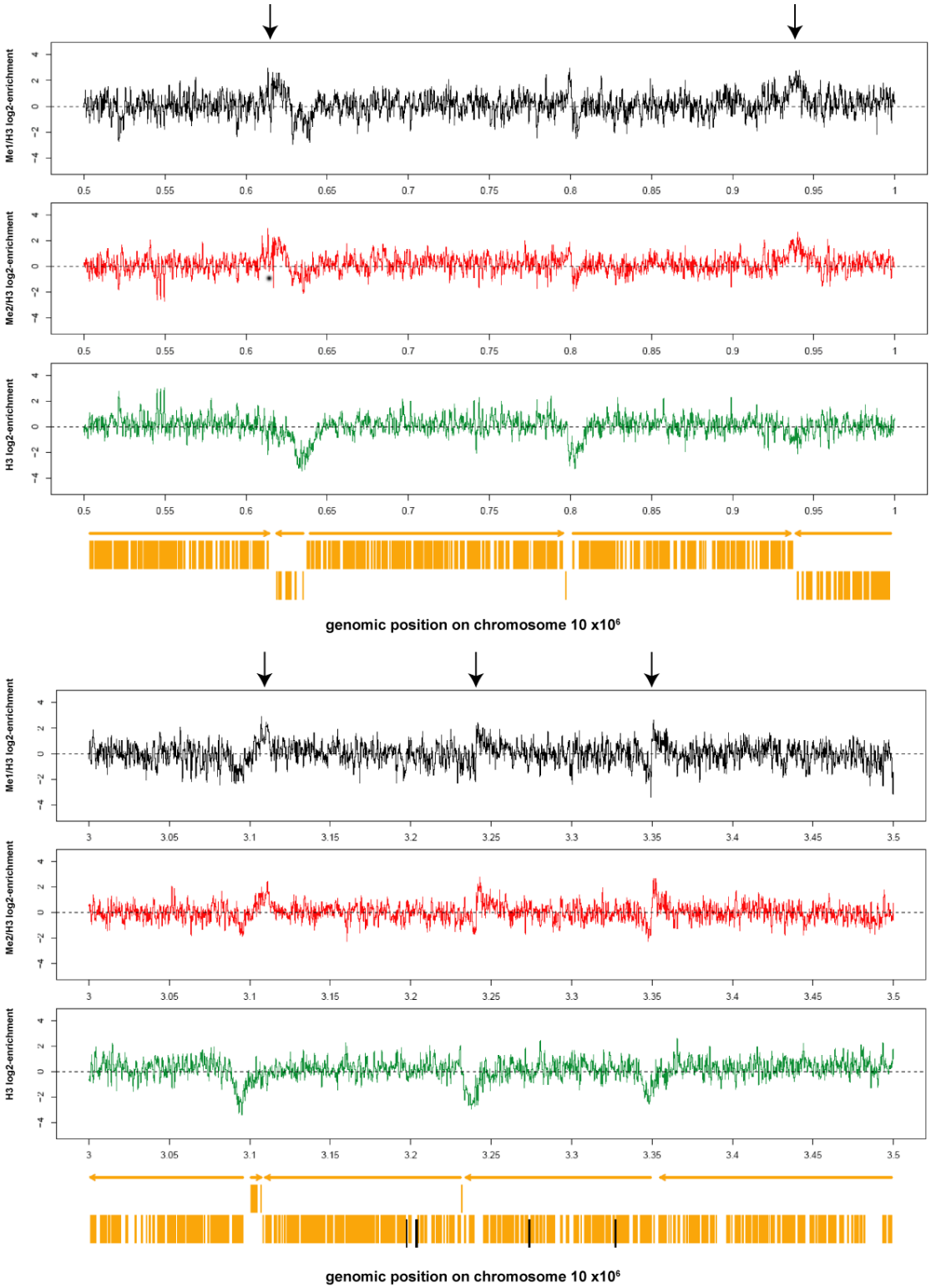

Fig 28: Distribution of H3K76me1 and -me2 normalized to H3 distribution. Representative parts of chromosome 10 illustrate the distribution of H3K76me1 (black), H3K76me2 (red) and H3 (green). Orange boxes represent ORFs and orange arrows indicate the direction of transcription. Positions of H3K67me1 and -me2 enrichment ($\log_2 > 2$) are marked by black arrows. For data of all chromosomes see Figure S3 in appendix (on enclosed DVD).

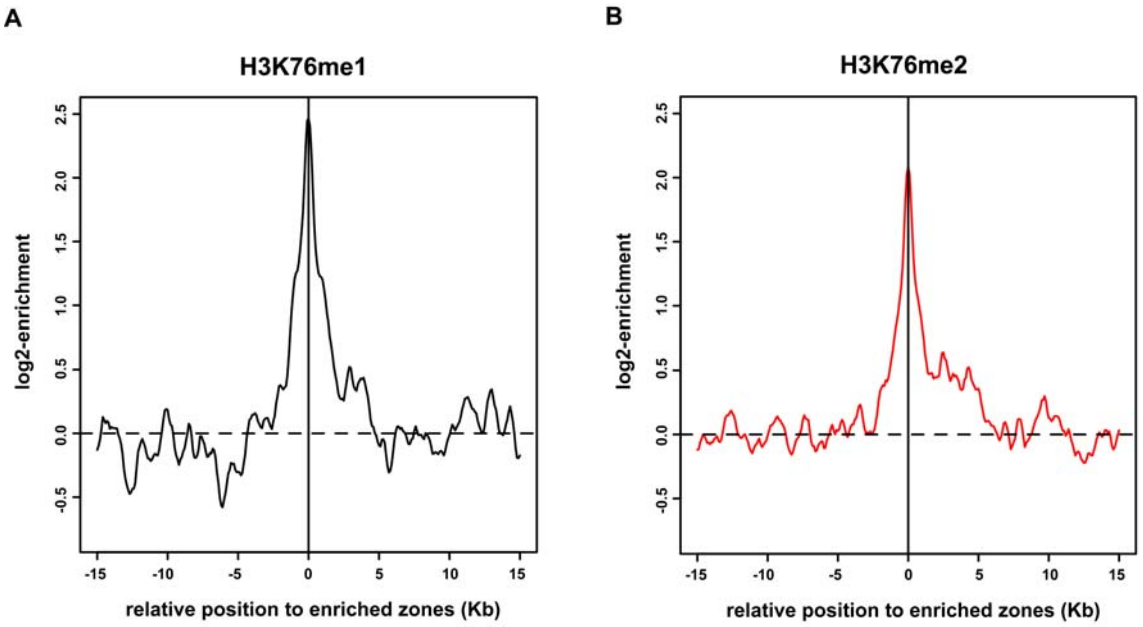

Fig 29: Mean shapes of H3K76me1 and H3K76me2 enrichment at selected regions on chromosome 10. Peak profiles were created by averaging the H3K76me1/me2 log_2-ratios of 24 peaks for H3K76me1 or 28 peaks for H3K76me2 in a ±15 kb neighborhood centered at the middle position of each enriched zone. Calculation was done with a window size of 500 bp and sliding the window in steps of 100 bp. The average log_2-ratios at each step were obtained with a 5% trimmed mean to avoid the effects of outliers.

A closer view revealed that 6 out of 24 H3K76me1-peaks were located within convergent TTS (Fig 30A), and 8 were found at internal TTS/TSS (Fig 30C). Most of the divergent TSS, except for 4, were not enriched in H3K76me1 (Fig 30A and D), whereas 6 areas of enrichment did not correlate with transcription initiation or termination. An accurate annotation list of internal TTS was not available, and the genomic locations of these sites were estimated using genome plots (http://tritrypdb.org). Therefore, genomic location of peaks was compared with location of the TTS/TSS ± 5kb. It was not possible to distinguish between internal TSS and internal TTS because they are located close to each other.

28 peaks with at least 4-fold H3K76me2 enrichment could be identified. 10 of these peaks were located at convergent TTS (Fig 30A), and 5 were found at internal TTS/TSS (Fig 30C). 2 divergent TSS were enriched in H3K76me2 (Fig 30A and D), and 11 peaks did not show a correlation with TTS or TSS on chromosome 10.

Overall, 75% of H3K76me1- and 60% of H3K76me2-peaks matched with TSS or TTS. 60% or even 100% of the convergent TTS on chromosome 10 were enriched in H3K76me1 or H3K76me2, respectively. 80% or 50% of the internal TTS/TSS sites showed association with

H3K76me1 or H3K76me2, respectively. Less percent of divergent TSS correlated with H3K76me1 and -me2 enrichment (36% and 18%, respectively) on chromosome 10.

In summary, ChIP results revealed a link for H3K76me1 and -me2 with functional genomic domains, particularly with the TTS. An influence of H3K76 methylation on transcriptional regulation was not observed in trypanosomes and is therefore unlikely. Instead, manipulation of H3K76 methylation led to distinct replication phenotypes as described above in this thesis. Recently, origins of replication were identified in *Trypanosoma brucei* and were associated with some TSS and TTS (Tiengwe *et al.*, 2012a). Therefore, H3K76 methylation could characterize origins of replication, and accurate timing of *de novo* H3K76 methylation might be the critical mark for proper replication regulation.

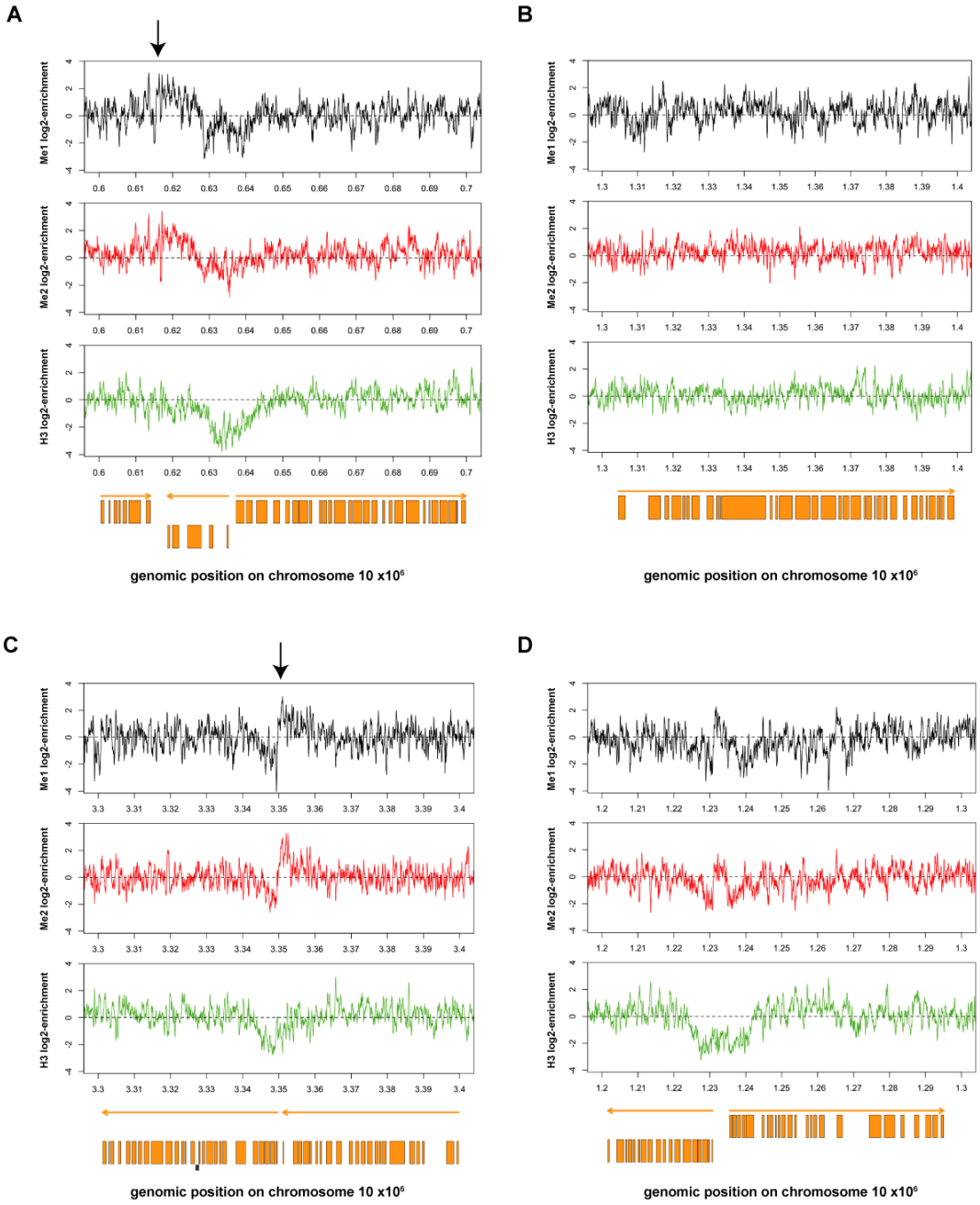

Fig 30: Enrichment of H3K76me1 and -me2 at transcription termination sites. Distribution of H3K76me1 (black) and H3K76me2 (red) are normalized to H3-distribution (green). Orange boxes represent ORFs and orange arrows indicate the direction of transcription. Displayed are examples for chromosome 10 of (**A**) a convergent transcription termination site (TTS) followed by a divergent transcription start site (TSS), (**B**) an internal part of a polycistronic unit, (**C**) an internal TSS/TTS and (**D**) a divergent TSS. Enrichment ($\log_2 > 2$) of H3K76me1/me2 was detected in TTS (marked by black arrows).

4 Discussion

4.1 Function of H3K76 methylation during replication

Several conclusions can be drawn based on my results: DOT1A and DOT1B are responsible for a cell cycle-dependent H3K76 methylation pattern, whereby newly incorporated histones become successively methylated, which is detectable after the onset of G2 phase. Only a low percentage (up to 4%) of all H3K76 is mono- and dimethylated. The rest of H3K76 remains unmodified or is converted to trimethylated H3K76. A direct link of H3K76 methylation states to replication control is apparent, because manipulation of the H3K76 methylation pattern leads to different replication phenotypes in several mutants. The lower methylation states seem to act as important cell cycle markers, whereas loss of H3K76me3 in a ΔDOT1B cell line does not affect replication or cell cycle regulation. How can a histone modification be involved in replication regulation? Interestingly, such an association has already been described. H4K20 methylation by the histone methyltransferase PR-Set7 is directly linked to replication control in mammalian cells (Wu and Rice, 2011).

4.1.1 Histone methylation is involved in replication regulation in mammals

Similar to H3K76 methylation, both H4K20me1 and the PR-Set7 protein level oscillate during the cell cycle, with their highest abundance in late G2 phase (Rice, 2002). Expression of a degradation-resistant PR-Set7 mutant or forced over-expression of wild-type PR-Set7 result in DNA re-replication in G2 phase-arrested cells (Tardat *et al.*, 2010). Coincidentally, H4K20me1 appears prematurely at several origins during S phase. Furthermore, targeting of PR-Set7 to a non-origin locus in the genome increases H4K20me1 at this site and causes recruitment of several pre-RC protein complexes like ORC and MCM. Absence of PR-Set7 and H4K20me1 results in improper DNA replication (Tardat *et al.*, 2007), due to a reduction of chromatin-bound pre-RC proteins. These data strongly suggest that H4K20me1 functions in replication licensing in mammals. Kuo and colleagues showed that ORC1 directly interacts with H4K20me2 through its bromo-adjacent-homology (BAH) domain in higher eukaryotes (Kuo *et al.*, 2012). In addition, they found that H4K20me2 is also enriched at replication origins.

Could H3K76 methylation execute similar function in trypanosomes as H4K20me1/me2 in higher eukaryotes? Several observations support this hypothesis. First, the phenotypes generated by over-expression of PR-Set7 resemble those of DOT1A (DOT1B) over-

expression, which are characterized by re-replication of DNA in both cases. Second, knockdown of *DOT1A* leads to severe replication defects, potentially similar to defects by PR-Set7 knockdown, which results in a reduction of pre-RC components loading (Tardat *et al.*, 2010). Although alternative targets of the DOT1 methyltransferases cannot be completely excluded, the data obtained so far suggest that H3K76 methylation is involved in replication in *T. brucei*. An indirect effect on H4K18 methylation (the homologous residue to mammalian H4K20 in trypanosomes) can be excluded, because H4K18 methylation levels do not change after manipulation of DOT1A expression (Fig S4 in appendix).
In summary, H3K76 methylation could have a similar function in replication in *T. brucei* as H4K20 methylation in mammals.

4.1.2 Model of replication regulation in *T. brucei*

In eukaryotes, the "licensing model" of replication control suggests three consecutive steps: (1) the pre-RC complex assembles at origins during late mitosis and G1 phase, (2) the ability to license new replication origins is down-regulated before entry into S phase, by down-regulation of ORC, Cdc6 and Cdt1, which are required for loading but not for continued association of MCM on DNA, and (3) initiation of replication displaces the Mcm complex from origins, which necessitates re-establishment of licensing by binding of Orc and Mcm complexes during the next cell cycle. The proper timing of origin licensing is critical to prevent re-replication or multiple uncoordinated rounds of DNA synthesis per cell cycle (Arias and Walter, 2007). The regulation of licensing involves carefully coordinated interactions of CDKs and licensing factors like Cdt1 (Blow and Dutta, 2005).
There is clear evidence that the cell cycle is also regulated by cyclins and CDKs in trypanosomes (Hammarton, 2007), but the mechanisms of replication regulation are completely unknown. Database searches suggest that Cdt1 homologues are absent in *T. brucei*, but Orc1/Cdc6 homologues and other proteins of the replication complex have been identified recently (Godoy *et al.*, 2009; Dang *et al.*, 2011). Neither expression and localization, nor chromatin binding of Orc1 appear to be the mechanism of replication regulation in *T. brucei* (Godoy *et al.*, 2009).

H3K76me1 and -me2 might function in licensing of replication origins in trypanosomes. The following model suggests that H3K76 methylation creates a chromatin environment advantageous for DNA binding of the pre-RC complex. H3K76 methylation is only possible in a nucleosomal context (Janzen *et al.*, 2006b). Hence, unmodified histones are incorporated

into chromatin followed by accumulative H3K76me1 in G2 phase and H3K76me2 in mitosis. This is also the time point when the pre-RC complex assembles in all other eukaryotes. H3K76me1 and -me2 are not detectable during S phase, where formation of the pre-RC complex is inhibited in eukaryotes and probably also in trypanosomes.

The timing of H3K76 methylation is important for replication progression, as abnormal appearance in the DOT1A mutants leads to replication defects (Fig 31). Down-regulation of *DOT1A* reduces H3K76me1 and H3K76me2 to a nearly undetectable level (Fig 31B), which hypothetically impairs pre-RC binding to origins of replication during mitosis. Therefore replication cannot take place in the following S phase. In DOT1A over-expressing mutants, histones are methylated prematurely during S phase (Fig 31C), leading potentially to pre-RC complex re-formation at origins and repetitive rounds of DNA replication during the same S phase. DOT1B over-expression causes DNA re-replication similar to DOT1A over-expression, which suggests that H3K76 is methylated prematurely as well. However, the lower methylation states are not detectable in DOT1B over-expressing cells, indicating that H3K76me1 and -me2 might occur transiently due to high turnover to trimethylated H3K76. This transient state might suffice to mark chromatin as replication competent and to stimulate the replication process.

In wild-type cells, H3K76 is fully trimethylated by DOT1B shortly after cytokinesis (Fig 31A), which erases H3K76me1 and -me2 marks. Thus, pre-RC formation is terminated. The conversion to H3K76me3 is not essential for the regulation of replication, because replication is not affected in ΔDOT1B cells (Janzen *et al.*, 2006b). Although H3K76me2 appears cell cycle-independent in these cells, replication is controlled normally. H3K76me1 also increases in these cells, but remains cell cycle-regulated and is undetectable in S phase (data not shown). This hints to H3K76me1 as critical factor for replication regulation in trypanosomes.

In summary, the data suggest that H3K76 methylation is involved in the activation of origin licensing in trypanosomes. If this is true, an association of H3K76 methylation with origins of replication is expected.

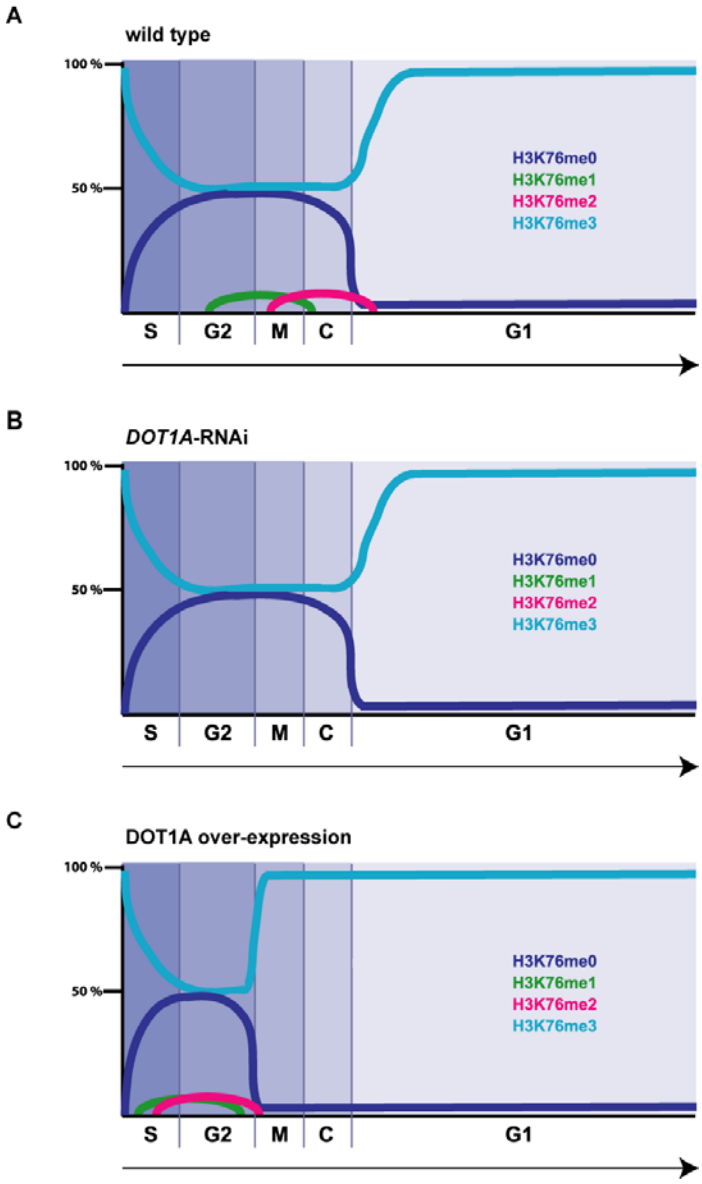

Figure 31: Model of H3K76 methylation during the cell cycle. Percentages of different H3K76 methylation states are indicated during the course of the cell cycle based on mass spectrometry and immunofluorescence data. The appearance of H3K76me1 and -me2 in wild-type cells (**A**) is manipulated after down-regulation of *DOT1A* by RNAi (**B**) and over-expression of DOT1A (**C**), causing severe replication defects.

4.2 Origins of replication

The analysis of direct association between H3K76 methylation and origins of replication was not possible, because origins had not been identified in trypanosomes until the end of my PhD thesis. Just recently, a first publication described the identification of origins in *T. brucei* (Tiengwe *et al.*, 2012a).

In *S. cerevisiae*, DNA replication origins are specified by a consensus sequence, the autonomously replicating sequence (ARS; Stinchcomb *et al.*, 1979), whereas in *S. pombe* such consensus sequences are lacking and origins consist of AT-rich islands (Segurado *et al.*, 2003). In metazoans, functional replication origins do not show defined DNA consensus sequences and more potential origins are present than are actually bound by replication-initiating proteins. For example, about 30,000 origins per cell cycle are active in human cells. Thus, the involvement of chromatin factors in the selection of these origins is required (Cayrou *et al.*, 2010). Histone acetyltransferase complexes provide an environment favorable for the association of Mcm complexes to chromatin. For example, the mammalian HBO1 (histone acetyltransferase binding to ORC1) is responsible for H4K5, K8 and K12 acetylation and seems to be required for pre-RC formation at origins (Burke *et al.*, 2001; Iizuka and Stillman, 1999).

Attempts to find replication origins in *T. brucei* have just been initiated and quite recently, origins could be detected through mapping of Orc1/Cdc6 binding sites by ChIP-chip analysis (Tiengwe *et al.*, 2012a). To establish whether these binding sites correspond with active replication origins, a technique called marker frequency analysis sequencing (MFAseq) was employed, which compares the copy number of marker sequences in replicating (early to mid S phase) and non-replicating cells (G2 phase). Tiengwe and colleagues revealed an association of Orc1/Cdc6 binding with transcription start or termination sites (TSS and TTS, respectively). About 70% of divergent TSS, 96% of internal TSS/TTS sites and 40% of convergent TTS showed evidence for Orc1/Cdc6 binding. The MFAseq analysis identified a total of 42 active origins (late-firing origins are not represented), which are always located at the boundaries of transcription, in accordance with Orc1/Cdc6 binding. 19 of the identified origins are found at divergent TSS, 3 are associated with convergent TTS and the rest correlate to internal TSS/TTS (Tiengwe *et al.*, 2012a). In summary, origins of replication seem to be located at the boundaries of transcription units and do not show any specific consensus sequence in *T. brucei*.

An association of replication origins with transcription has been discovered in human cells before. In HeLa cells, origins consist of GC-rich regions mostly overlapping with transcriptional regulatory elements localized around TSS (Cadoret *et al.*, 2008; Karnani *et al.*, 2010). The chromatin structure characterizes origins of replication in different organisms. For example, H3K4me2 and -me3 are enriched at origins in HeLa cells or *Arabidopsis thaliana* (Costas *et al.*, 2011; Karnani *et al.*, 2010).

In my thesis, the genome-wide localization of H3K76 methylation was explored by ChIP-chip analysis and also revealed a link to the boundaries of transcription units, mainly to TTS. 60% of convergent TTS and 80% of the internal TSS/TTS on chromosome 10 showed an association with H3K76me1. In addition, 100% of convergent TTS and 50% of the internal TSS/TTS correlated to H3K76me2. Only 36% and 18% of divergent TSS were enriched for H3K76me1 or H3K76me2, respectively. Taking Orc1/Cdc6 localization data into consideration, an association of H3K76me1 and -me2 with origins of replication is likely. Orc1/Cdc6 seems to bind preferentially at TSS and to a lesser extend to the TTS (Tiengwe *et al.*, 2012a). However, MFAseq analysis demonstrated clearly that TTS (convergent as well as internal) and active replication origins correlate in *T. brucei* (Tiengwe *et al.*, 2012a). These data suggest that H3K76me1 and -me2 mark replication origins, predominantly at TTS. Whether this epigenetic feature is essential for the function of each individual origin remains to be analyzed in further experiments.

In summary, H3K76 is highly mono- and dimethylated at TTS at the end of polycistronic units, which could potentially favor assembly of pre-RC complexes during the origin licensing in trypanosomes. To fully unravel the mechanism of replication regulation by H3K76 methylation, the spatial and temporal context of its appearance needs to be investigated in more detail.

4.3 Novel function of H3K76 methylation in trypanosomes?

H3K76 methylation seems to have a different function in trypanosomes from the structurally homologous H3K79 methylation in other eukaryotes. H3K79 methylation has been studied in many organisms and is important in various biological processes such as transcriptional regulation or DNA repair (see introduction). A direct link to replication regulation has not been described so far. My thesis` data suggest such a function in *T. brucei*, although the mechanism of replication regulation by H3K76 methylation is still unclear. Two possibilities are conceivable: First, a direct interaction of H3K76me1 or -me2 with components of the pre-RC complex as it was shown for H4K20me2 and ORC1 (Kuo *et al.*, 2012) or second, a more general effect, which generates an open chromatin structure accessible for binding of replication complexes, similar to the function of H4K10 acetylation, which is responsible for the open chromatin state at TSS.

How is the distinct localization of H3K76me1 and -me2 at the transcription boundaries established? One explanation is that the methylation activities of DOT1A and/or DOT1B may be specifically targeted to origins of replication. Interaction partners of DOT1A and DOT1B

have not been found in trypanosomes yet, but DOT1L was purified from a protein complex (DotCom), which is composed of different transcription factors in human cells (Mohan *et al.*, 2010). During leukemogenesis, human DOT1L is targeted to specific loci by interaction with MLL (mixed-lineage leukemia) fusion partners and activates gene transcription (Chang *et al.*, 2010; Krivtsov *et al.*, 2008; Mueller *et al.*, 2009). Thus, trypanosomal DOT1A and/or DOT1B may also be targeted to specific genomic loci through the interaction with other factors, perhaps inside a protein complex.

In addition to the spatial context, the timing of H3K76 methylation during the cell cycle seems to be absolutely essential for proper replication control, as phenotypes of DOT1 mutants have demonstrated. In yeast, H3K79 methylation reflects cell cycle length on a global level. H3K79 of new and old histones is progressively methylated during the cell cycle by Dot1, which works in a distributive manner (De Vos *et al.*, 2011). The methylation degree is also affected by histone dilution during replication. Therefore the overall degree of H3K79 methylation is dynamic and depends on the residence time of histones within the chromatin. De Vos and colleagues suggested that the accumulation of H3K79 methylation on ageing histones functions as a timer mechanism for the cell. This enables coupling of cell cycle length to changes in chromatin modification and finally can affect gene regulation. A timer function might exist for H3K76 in trypanosomes as well, where the appearance of H3K76me1 and -me2 during distinct cell cycle phases is necessary for proper cell cycle regulation, and where the progressive methylation in specific periods of the cell cycle resembles the situation in yeast.

In summary, the results of my thesis indicate a novel role for H3K76 methylation in replication regulation, which might be specific for trypanosomes. This is one example where a conserved process has been adapted to fulfill a different purpose in trypanosomes, compared to other eukaryotes. Detailed mechanistic analysis of replication regulation in trypanosomes is necessary to fully unravel the function of H3K76 methylation in this process. Such a function of H3K76 methylation might exist also in other protozoan parasites or even in higher eukaryotes as a redundant pathway for replication regulation.

4.4 Outlook

The underlying mechanism of replication regulation by H3K76 methylation is still unclear and needs to be explored. Pre-RC assembly could be analyzed in the different DOT1 mutants

with the help of co-immunoprecipitation assays of different replication proteins, which have been characterized recently in trypanosomes (Dang and Li, 2011). Peptide pulldowns could be useful to identify binding partners of the different H3K76 methylation states. However, the nucleosomal context of a modification is often necessary to establish specific interaction (Altaf *et al.*, 2007). Therefore, peptide pulldown experiments lacking the nucleosomal context often fail (Frederiks *et al.*, 2011). Purified nucleosomes from trypanosome cells are mostly trimethylated on H3K76 or show a mixture of different H3K76 methylation states. To improve analysis of pulldown assays, differently H3K76-methylated nucleosomes could be reconstituted *in vitro.* This method involves the expression of recombinant histones from trypanosomes, following purification and *in vitro* assembly of nucleosomes by adding DNA (Luger *et al.*, 1999).

H3K76 methylation may participate in cross-talk to other PTMs or other parts of the nucleosome. For example, enhanced H3K79 methylation has been already correlated to ubiquitination of H2B on lysine 123 in yeast or lysine 120 in humans (Sun and Allis, 2002; McGinty *et al.*, 2008). H2B ubiquitination directly stimulates H3K79 methylation in humans. This was analyzed *in vitro* with chemically modified H2B, which was ubiquitinated site-specifically (McGinty *et al.*, 2008). Thus, with newly developed chemical methods, *in vitro* systems including reconstituted nucleosomes could also help to find other PTMs that influence H3K76 methylation.

How is the cell cycle-regulated pattern of H3K76 methylation established? How is H3K76me2 restricted to mitosis and cytokinesis during the cell cycle? In order to answer these questions, it is also important to unravel the structural basis for the different enzymatic activities of DOT1A and DOT1B. *In vitro* methylation assays with reconstituted nucleosomes as substrates can help to study the activity and specificity of recombinant DOT1 proteins. Methyltransferases can work either via a processive or a distributive kinetic mechanism to generate different methylation states. Processive enzymes do not dissociate from their substrate and perform consecutive rounds of methylation independent of preceding methylation states. Distributive enzymes dissociate from their substrate after each round of methylation and, therefore, the introduction of higher methylation states depends on the preceding lower state. Both a distributive and a processive mechanism of methylation had been proposed based on crystal structures of yeast and human Dot1 enzymes (Min *et al.*, 2003; Sawada *et al.*, 2004). Later, the yeast Dot1 was shown to work distributively *in vivo* (Frederiks *et al.*, 2008). In trypanosomes, initial *in vitro* experiments indicated that DOT1A and DOT1B are distributive like in yeast (Gülcin Dindar, personal communication). However,

the very low amounts of H3K76me1 and H3K76me2 (2 and 4%, respectively) in comparison to the highly abundant H3K76me3 (63%) raise the question if DOT1B may work processively in trypanosomes, unlike in yeast. Unmodified H3K76 is rapidly converted to H3K76me3 after G2/M phase, without detectable levels of H3K76me1 and -me2, which also favors the hypothesis of a processive mechanism for DOT1B. In addition, this implies a massive up-regulation of DOT1B protein level or its activity after mitosis. A potential regulation of the enzymes was analyzed in my thesis by luciferase fusion proteins and enzymatic activity measurements of luciferase in different cell cycle stages. Both enzymes, DOT1A and DOT1B, seem not to be cell cycle-regulated. However, not the proteins themselves but their methylation activity could be regulated through post-translational modification or interactions with other proteins. This should be subject of further analyses.

Interaction partners of DOT1A and DOT1B are unknown but it would be very interesting to identify a complex associated with these methyltransferases, as it was already shown for DOT1 enzymes in other eukaryotes (Mohan *et al.*, 2010). Interaction studies could also clarify whether there are potential alternative substrates of the DOT1 enzymes in trypanosomes. Indeed, some histone methyltransferases catalyze methylation of several histone residues or even of non-histone substrates (Huang and Berger, 2008). For example, the enzyme Set1 is responsible for methylation of H3K4, but also methylates the kinetochore protein Dam1 in *S. cerevisiae* and thereby influences chromosome segregation (Zhang *et al.*, 2005).

Manipulation of the DOT1 enzymes causes enormous replication phenotypes, which do not prevent cell cycle progression in trypanosomes. Here are also still open questions to be answered. For example, both DOT1A and DOT1B over-expression cause continuous replication, potentially due to premature *de novo* methylation during S phase. Premature H3K76 methylation was shown in DOT1A over-expressing cells, but could not be detected in DOT1B over-expressing cells. Probably the lower methylation states appear only transiently, but can induce continuous replication before being rapidly converted to the trimethylated state. This should be studied in more detail.

The phenotype of DOT1A depletion raises some interesting questions as well: Inhibition of replication does not result in cell cycle arrest, but cells go through cytokinesis distributing half of their DNA content to each of the daughter cell. Is checkpoint control disrupted in these cells? Are these cells haploid? Is a specific mechanism, like meiosis, triggered accidentally? Studying these questions in further experiments will help to decipher the complete mechanism of H3K76 methylation by the DOT1 enzymes in *T. brucei*.

Bibliography

Airth, R.L., Rhodes, W.C. and Mc, E.W. (1958) The function of coenzyme A in luminescence. *Biochim Biophys Acta*, **27**, 519-532.

Alibu, V.P., Storm, L., Haile, S., Clayton, C. and Horn, D. (2005) A doubly inducible system for RNA interference and rapid RNAi plasmid construction in *Trypanosoma brucei*. *Mol Biochem Parasitol*, **139**, 75-82.

Alsford, S. and Horn, D. (2004) Trypanosomatid histones. *Molecular Microbiology*, **53**, 365-372.

Alsford, S., Kawahara, T., Isamah, C. and Horn, D. (2007) A sirtuin in the African trypanosome is involved in both DNA repair and telomeric gene silencing but is not required for antigenic variation. *Mol Microbiol*, **63**, 724-736.

Altaf, M., Utley, R.T., Lacoste, N., Tan, S., Briggs, S.D. and Cote, J. (2007) Interplay of chromatin modifiers on a short basic patch of histone H4 tail defines the boundary of telomeric heterochromatin. *Mol Cell*, **28**, 1002-1014.

Arias, E.E. and Walter, J.C. (2007) Strength in numbers: preventing rereplication via multiple mechanisms in eukaryotic cells. *Genes Dev*, **21**, 497-518.

Bastin, P., Bagherzadeh, Z., Matthews, K.R. and Gull, K. (1996) A novel epitope tag system to study protein targeting and organelle biogenesis in *Trypanosoma brucei*. *Mol Biochem Parasitol*, **77**, 235-239.

Bell, S.P. and Dutta, A. (2002) DNA replication in eukaryotic cells. *Annu Rev Biochem*, **71**, 333-374.

Biebinger, S., Wirtz, L.E., Lorenz, P. and Clayton, C. (1997) Vectors for inducible expression of toxic gene products in bloodstream and procyclic *Trypanosoma brucei*. *Mol Biochem Parasitol*, **85**, 99-112.

Bitoun, E., Oliver, P.L. and Davies, K.E. (2007) The mixed-lineage leukemia fusion partner AF4 stimulates RNA polymerase II transcriptional elongation and mediates coordinated chromatin remodeling. *Hum Mol Genet*, **16**, 92-106.

Blow, J.J. and Dutta, A. (2005) Preventing re-replication of chromosomal DNA. *Nat Rev Mol Cell Biol*, **6**, 476-486.

Borst, P., Bitter, W., Blundell, P.A., Chaves, I., Cross, M., Gerrits, H., van Leeuwen, F., McCulloch, R., Taylor, M. and Rudenko, G. (1998) Control of VSG gene expression sites in *Trypanosoma brucei*. *Mol Biochem Parasitol*, **91**, 67-76.

Briggs, S.D., Xiao, T., Sun, Z.W., Caldwell, J.A., Shabanowitz, J., Hunt, D.F., Allis, C.D. and Strahl, B.D. (2002) Gene silencing: trans-histone regulatory pathway in chromatin. *Nature*, **418**, 498.

Brun, R. and Schonenberger. (1979) Cultivation and in vitro cloning or procyclic culture forms of *Trypanosoma brucei* in a semi-defined medium. Short communication. *Acta Trop*, **36**, 289-292.

Burke, T.W., Cook, J.G., Asano, M. and Nevins, J.R. (2001) Replication factors MCM2 and ORC1 interact with the histone acetyltransferase HBO1. *J Biol Chem*, **276**, 15397-15408.

Cadoret, J.C., Meisch, F., Hassan-Zadeh, V., Luyten, I., Guillet, C., Duret, L., Quesneville, H. and Prioleau, M.N. (2008) Genome-wide studies highlight indirect links between human replication origins and gene regulation. *Proc Natl Acad Sci U S A*, **105**, 15837-15842.

Calderano, S.G., de Melo Godoy, P.D., Motta, M.C., Mortara, R.A., Schenkman, S. and Elias, M.C. (2011) *Trypanosoma cruzi* DNA replication includes the sequential recruitment of pre-replication and replication machineries close to nuclear periphery. *Nucleus*, **2**, 136-145.

Cao, R., Wang, L., Wang, H., Xia, L., Erdjument-Bromage, H., Tempst, P., Jones, R.S. and Zhang, Y. (2002) Role of histone H3 lysine 27 methylation in Polycomb-group silencing. *Science*, **298**, 1039-1043.

Cayrou, C., Coulombe, P. and Mechali, M. (2010) Programming DNA replication origins and chromosome organization. *Chromosome Res*, **18**, 137-145.

Chang, M.J., Wu, H., Achille, N.J., Reisenauer, M.R., Chou, C.W., Zeleznik-Le, N.J., Hemenway, C.S. and Zhang, W. (2010) Histone H3 lysine 79 methyltransferase Dot1 is required for immortalization by MLL oncogenes. *Cancer Res*, **70**, 10234-10242.

Cheng, X., Collins, R.E. and Zhang, X. (2005) Structural and sequence motifs of protein (histone) methylation enzymes. *Annu Rev Biophys Biomol Struct*, **34**, 267-294.

Cheng, X. and Zhang, X. (2007) Structural dynamics of protein lysine methylation and demethylation. *Mutat Res*, **618**, 102-115.

Chowdhury, A.R., Zhao, Z. and Englund, P.T. (2008) Effect of hydroxyurea on procyclic *Trypanosoma brucei*: an unconventional mechanism for achieving synchronous growth. *Eukaryot Cell*, **7**, 425-428.

Clayton, C., Adams, M., Almeida, R., Baltz, T., Barrett, M., Bastien, P., Belli, S., Beverley, S., Biteau, N., Blackwell, J.*, et al.* (1998) Genetic nomenclature for *Trypanosoma* and *Leishmania*. *Mol Biochem Parasitol*, **97**, 221-224.

Clayton, C.E. (2002) Life without transcriptional control? From fly to man and back again. *EMBO J*, **21**, 1881-1888.

Conde, F., Refolio, E., Cordon-Preciado, V., Cortes-Ledesma, F., Aragon, L., Aguilera, A. and San-Segundo, P.A. (2009) The Dot1 histone methyltransferase and the Rad9 checkpoint adaptor contribute to cohesin-dependent double-strand break repair by sister chromatid recombination in *Saccharomyces cerevisiae*. *Genetics*, **182**, 437-446.

Costas, C., de la Paz Sanchez, M., Stroud, H., Yu, Y., Oliveros, J.C., Feng, S., Benguria, A., Lopez-Vidriero, I., Zhang, X., Solano, R.*, et al.* (2011) Genome-wide mapping of *Arabidopsis thaliana* origins of DNA replication and their associated epigenetic marks. *Nat Struct Mol Biol*, **18**, 395-400.

Cross, G.A. (1975) Identification, purification and properties of clone-specific glycoprotein antigens constituting the surface coat of *Trypanosoma brucei*. *Parasitology*, **71**, 393-417.

Cvetic, C. and Walter, J.C. (2005) Eukaryotic origins of DNA replication: could you please be more specific? *Semin Cell Dev Biol*, **16**, 343-353.

da Cunha, J.P., Nakayasu, E.S., de Almeida, I.C. and Schenkman, S. (2006) Post-translational modifications of *Trypanosoma cruzi* histone H4. *Mol Biochem Parasitol*, **150**, 268-277.

Dang, H.Q. and Li, Z. (2011) The Cdc45.Mcm2-7.GINS protein complex in trypanosomes regulates DNA replication and interacts with two Orc1-like proteins in the origin recognition complex. *J Biol Chem*, **286**, 32424-32435.

De Vos, D., Frederiks, F., Terweij, M., van Welsem, T., Verzijlbergen, K.F., Iachina, E., de Graaf, E.L., Altelaar, A.F., Oudgenoeg, G., Heck, A.J.*, et al.* (2011) Progressive methylation of ageing histones by Dot1 functions as a timer. *EMBO Rep*, **12**, 956-962.

DiPaolo, C., Kieft, R., Cross, M. and Sabatini, R. (2005) Regulation of trypanosome DNA glycosylation by a SWI2/SNF2-like protein. *Mol Cell*, **17**, 441-451.

Dobbie, I.M., King, E., Parton, R.M., Carlton, P.M., Sedat, J.W., Swedlow, J.R. and Davis, I. (2011) OMX: a new platform for multimodal, multichannel wide-field imaging. *Cold Spring Harb Protoc*, **2011**, 899-909.

Eissenberg, J.C., James, T.C., Foster-Hartnett, D.M., Hartnett, T., Ngan, V. and Elgin, S.C. (1990) Mutation in a heterochromatin-specific chromosomal protein is associated with suppression of position-effect variegation in *Drosophila melanogaster*. *Proc Natl Acad Sci U S A*, **87**, 9923-9927.

Ersfeld, K. and Gull, K. (1997) Partitioning of large and minichromosomes in *Trypanosoma brucei*. *Science*, **276**, 611-614.

Ersfeld, K., Melville, S.E. and Gull, K. (1999) Nuclear and genome organization of *Trypanosoma brucei*. *Parasitol Today*, **15**, 58-63.

Feng, Q., Wang, H., Ng, H.H., Erdjument-Bromage, H., Tempst, P., Struhl, K. and Zhang, Y. (2002) Methylation of H3-lysine 79 is mediated by a new family of HMTases without a SET domain. *Curr Biol*, **12**, 1052-1058.

Fernandes, A.P., Nelson, K. and Beverley, S.M. (1993) Evolution of nuclear ribosomal RNAs in kinetoplastid protozoa: perspectives on the age and origins of parasitism. *Proc Natl Acad Sci U S A*, **90**, 11608-11612.

Figueiredo, L.M., Cross, G.A. and Janzen, C.J. (2009) Epigenetic regulation in African trypanosomes: a new kid on the block. *Nat Rev Microbiol*, **7**, 504-513.

Figueiredo, L.M., Janzen, C.J. and Cross, G.A. (2008) A histone methyltransferase modulates antigenic variation in African trypanosomes. *PLoS Biol*, **6**, e161.

Filion, G.J., van Bemmel, J.G., Braunschweig, U., Talhout, W., Kind, J., Ward, L.D., Brugman, W., de Castro, I.J., Kerkhoven, R.M., Bussemaker, H.J*., et al.* (2010) Systematic protein location mapping reveals five principal chromatin types in Drosophila cells. *Cell*, **143**, 212-224.

Fingerman, I.M., Li, H.C. and Briggs, S.D. (2007) A charge-based interaction between histone H4 and Dot1 is required for H3K79 methylation and telomere silencing: identification of a new trans-histone pathway. *Genes Dev*, **21**, 2018-2029.

Fischle, W., Wang, Y. and Allis, C.D. (2003) Histone and chromatin cross-talk. *Curr Opin Cell Biol*, **15**, 172-183.

Frederiks, F., Stulemeijer, I.J., Ovaa, H. and van Leeuwen, F. (2011) A modified epigenetics toolbox to study histone modifications on the nucleosome core. *Chembiochem*, **12**, 308-313.

Frederiks, F., Tzouros, M., Oudgenoeg, G., van Welsem, T., Fornerod, M., Krijgsveld, J. and van Leeuwen, F. (2008) Nonprocessive methylation by Dot1 leads to functional redundancy of histone H3K79 methylation states. *Nature Structural & Molecular Biology*, **15**, 550-557.

Frederiks, F., van Welsem, T., Oudgenoeg, G., Heck, A.J., Janzen, C.J. and van Leeuwen, F. (2010) Heterologous expression reveals distinct enzymatic activities of two DOT1 histone methyltransferases of *Trypanosoma brucei*. *J Cell Sci*, **123**, 4019-4023.

Gallagher, S.R. (2001) One-dimensional SDS gel electrophoresis of proteins. *Curr Protoc Protein Sci*, **Chapter 10**, Unit 10 11.

Garcia-Salcedo, J.A., Gijon, P., Nolan, D.P., Tebabi, P. and Pays, E. (2003) A chromosomal SIR2 homologue with both histone NAD-dependent ADP-ribosyltransferase and deacetylase activities is involved in DNA repair in *Trypanosoma brucei*. *EMBO J*, **22**, 5851-5862.

Geigy, R., Jenni, L., Kauffmann, M., Onyango, R.J. and Weiss, N. (1975) Identification of *T. brucei*-subgroup strains isolated from game. *Acta Trop*, **32**, 190-205.

Gibson, W., Peacock, L., Ferris, V., Williams, K. and Bailey, M. (2008) The use of yellow fluorescent hybrids to indicate mating in *Trypanosoma brucei*. *Parasit Vectors*, **1**, 4.

Godoy, P.D.d.M., Nogueira-Junior, L.A., Paes, L.S., Cornejo, A., Martins, R.M., Silber, A.M., Schenkman, S. and Elias, M.C. (2009) Trypanosome Prereplication Machinery Contains a Single Functional Orc1/Cdc6 Protein, Which Is Typical of Archaea. *Eukaryotic Cell*, **8**, 1592-1603.

Gunzl, A., Bruderer, T., Laufer, G., Schimanski, B., Tu, L.C., Chung, H.M., Lee, P.T. and Lee, M.G. (2003) RNA polymerase I transcribes procyclin genes and variant surface glycoprotein gene expression sites in *Trypanosoma brucei*. *Eukaryot Cell*, **2**, 542-551.

Hake, S.B., Garcia, B.A., Duncan, E.M., Kauer, M., Dellaire, G., Shabanowitz, J., Bazett-Jones, D.P., Allis, C.D. and Hunt, D.F. (2006) Expression patterns and post-translational modifications associated with mammalian histone H3 variants. *J Biol Chem*, **281**, 559-568.

Hammarton, T.C. (2007) Cell cycle regulation in *Trypanosoma brucei*. *Mol Biochem Parasitol*, **153**, 1-8.

Heitz, E. (1928) Das Heterochromatin der Moose I. *Jahrb Wiss Bot*, **69**, 762-818.

Hirumi, H. and Hirumi, K. (1989) Continuous cultivation of *Trypanosoma brucei* blood stream forms in a medium containing a low concentration of serum protein without feeder cell layers. *J Parasitol*, **75**, 985-989.

Hong, L., Schroth, G.P., Matthews, H.R., Yau, P. and Bradbury, E.M. (1993) Studies of the DNA binding properties of histone H4 amino terminus. Thermal denaturation studies reveal that acetylation markedly reduces the binding constant of the H4 "tail" to DNA. *J Biol Chem*, **268**, 305-314.

Horn, D. and McCulloch, R. (2010) Molecular mechanisms underlying the control of antigenic variation in African trypanosomes. *Curr Opin Microbiol*, **13**, 700-705.

Huang, J. and Berger, S.L. (2008) The emerging field of dynamic lysine methylation of non-histone proteins. *Curr Opin Genet Dev*, **18**, 152-158.

Iizuka, M. and Stillman, B. (1999) Histone acetyltransferase HBO1 interacts with the ORC1 subunit of the human initiator protein. *J Biol Chem*, **274**, 23027-23034.

Ingram, A.K. and Horn, D. (2002) Histone deacetylases in *Trypanosoma brucei*: two are essential and another is required for normal cell cycle progression. *Mol Microbiol*, **45**, 89-97.

Janzen, C.J., Fernandez, J.P., Deng, H., Diaz, R., Hake, S.B. and Cross, G.A. (2006a) Unusual histone modifications in *Trypanosoma brucei*. *FEBS Lett*, **580**, 2306-2310.

Janzen, C.J., Hake, S.B., Lowell, J.E. and Cross, G.A. (2006b) Selective di- or trimethylation of histone H3 lysine 76 by two DOT1 homologs is important for cell cycle regulation in *Trypanosoma brucei*. *Mol Cell*, **23**, 497-507.

Jasencakova, Z., Scharf, A.N., Ask, K., Corpet, A., Imhof, A., Almouzni, G. and Groth, A. (2010) Replication stress interferes with histone recycling and predeposition marking of new histones. *Mol Cell*, **37**, 736-743.

Jenuwein, T., Laible, G., Dorn, R. and Reuter, G. (1998) SET domain proteins modulate chromatin domains in eu- and heterochromatin. *Cell Mol Life Sci*, **54**, 80-93.

Jones, B., Su, H., Bhat, A., Lei, H., Bajko, J., Hevi, S., Baltus, G.A., Kadam, S., Zhai, H., Valdez, R.*, et al.* (2008) The histone H3K79 methyltransferase Dot1L is essential for mammalian development and heterochromatin structure. *PLoS Genet*, **4**, e1000190.

Karnani, N., Taylor, C.M., Malhotra, A. and Dutta, A. (2010) Genomic study of replication initiation in human chromosomes reveals the influence of transcription regulation and chromatin structure on origin selection. *Mol Biol Cell*, **21**, 393-404.

Kaufmann, D., Gassen, A., Maiser, A., Leonhardt, H. and Janzen, C.J. (2012) Regulation and spatial organization of PCNA in *Trypanosoma brucei*. *Biochem Biophys Res Commun*.

Kawahara, T., Siegel, T.N., Ingram, A.K., Alsford, S., Cross, G.A. and Horn, D. (2008) Two essential MYST-family proteins display distinct roles in histone H4K10 acetylation and telomeric silencing in trypanosomes. *Mol Microbiol*, **69**, 1054-1068.

Kim, W., Kim, R., Park, G., Park, J.W. and Kim, J.E. (2011) The deficiency of H3K79 histone methyltransferase DOT1L inhibits cell proliferation. *J Biol Chem*.

Kouzarides, T. (2007) Chromatin Modifications and Their Function. *Cell*, **128**, 693-705.

Krivtsov, A.V. and Armstrong, S.A. (2007) MLL translocations, histone modifications and leukaemia stem-cell development. *Nat Rev Cancer*, **7**, 823-833.

Krivtsov, A.V., Feng, Z., Lemieux, M.E., Faber, J., Vempati, S., Sinha, A.U., Xia, X., Jesneck, J., Bracken, A.P., Silverman, L.B.*, et al.* (2008) H3K79 methylation profiles define murine and human MLL-AF4 leukemias. *Cancer Cell*, **14**, 355-368.

Krogan, N.J., Dover, J., Wood, A., Schneider, J., Heidt, J., Boateng, M.A., Dean, K., Ryan, O.W., Golshani, A., Johnston, M.*, et al.* (2003a) The Paf1 complex is required for histone H3 methylation by COMPASS and Dot1p: linking transcriptional elongation to histone methylation. *Mol Cell*, **11**, 721-729.

Krogan, N.J., Kim, M., Tong, A., Golshani, A., Cagney, G., Canadien, V., Richards, D.P., Beattie, B.K., Emili, A., Boone, C.*, et al.* (2003b) Methylation of histone H3 by Set2 in Saccharomyces cerevisiae is linked to transcriptional elongation by RNA polymerase II. *Mol Cell Biol*, **23**, 4207-4218.

Kumar, D., Minocha, N., Rajanala, K. and Saha, S. (2009) The distribution pattern of proliferating cell nuclear antigen in the nuclei of *Leishmania donovani*. *Microbiology*, **155**, 3748-3757.

Kuo, A.J., Song, J., Cheung, P., Ishibe-Murakami, S., Yamazoe, S., Chen, J.K., Patel, D.J. and Gozani, O. (2012) The BAH domain of ORC1 links H4K20me2 to DNA replication licensing and Meier-Gorlin syndrome. *Nature*.

Kyhse-Andersen, J. (1984) Electroblotting of multiple gels: a simple apparatus without buffer tank for rapid transfer of proteins from polyacrylamide to nitrocellulose. *J Biochem Biophys Methods*, **10**, 203-209.

Laemmli, U.K. (1970) Cleavage of structural proteins during the assembly of the head of bacteriophage T4. *Nature*, **227**, 680-685.

Lazzaro, F., Sapountzi, V., Granata, M., Pellicioli, A., Vaze, M., Haber, J.E., Plevani, P., Lydall, D. and Muzi-Falconi, M. (2008) Histone methyltransferase Dot1 and Rad9 inhibit single-stranded DNA accumulation at DSBs and uncapped telomeres. *EMBO J*, **27**, 1502-1512.

Lowell, J.E. and Cross, G.A. (2004) A variant histone H3 is enriched at telomeres in *Trypanosoma brucei*. *J Cell Sci*, **117**, 5937-5947.

Lowell, J.E., Kaiser, F., Janzen, C.J. and Cross, G.A. (2005) Histone H2AZ dimerizes with a novel variant H2B and is enriched at repetitive DNA in *Trypanosoma brucei*. *J Cell Sci*, **118**, 5721-5730.

Luger, K., Mader, A.W., Richmond, R.K., Sargent, D.F. and Richmond, T.J. (1997) Crystal structure of the nucleosome core particle at 2.8 A resolution. *Nature*, **389**, 251-260.

Luger, K., Rechsteiner, T.J. and Richmond, T.J. (1999) Expression and purification of recombinant histones and nucleosome reconstitution. *Methods Mol Biol*, **119**, 1-16.

Mandava, V., Fernandez, J.P., Deng, H., Janzen, C.J., Hake, S.B. and Cross, G.A.M. (2007) Histone modifications in *Trypanosoma brucei*. *Molecular and Biochemical Parasitology*, **156**, 41-50.

Marahrens, Y. and Stillman, B. (1992) A yeast chromosomal origin of DNA replication defined by multiple functional elements. *Science*, **255**, 817-823.

Martinez-Calvillo, S., Vizuet-de-Rueda, J.C., Florencio-Martinez, L.E., Manning-Cela, R.G. and Figueroa-Angulo, E.E. (2010) Gene expression in trypanosomatid parasites. *J Biomed Biotechnol*, **2010**, 525241.

McGinty, R.K., Kim, J., Chatterjee, C., Roeder, R.G. and Muir, T.W. (2008) Chemically ubiquitylated histone H2B stimulates hDot1L-mediated intranucleosomal methylation. *Nature*, **453**, 812-816.

McKean, P. (2003) Coordination of cell cycle and cytokinesis in *Trypanosoma brucei*. *Current Opinion in Microbiology*, **6**, 600-607.

McKittrick, E., Gafken, P.R., Ahmad, K. and Henikoff, S. (2004) Histone H3.3 is enriched in covalent modifications associated with active chromatin. *Proc Natl Acad Sci U S A*, **101**, 1525-1530.

Min, J., Feng, Q., Li, Z., Zhang, Y. and Xu, R.M. (2003) Structure of the catalytic domain of human DOT1L, a non-SET domain nucleosomal histone methyltransferase. *Cell*, **112**, 711-723.

Minocha, N., Kumar, D., Rajanala, K. and Saha, S. (2011) Characterization of *Leishmania donovani* MCM4: expression patterns and interaction with PCNA. *PLoS One*, **6**, e23107.

Mohan, M., Herz, H.M., Takahashi, Y.H., Lin, C., Lai, K.C., Zhang, Y., Washburn, M.P., Florens, L. and Shilatifard, A. (2010) Linking H3K79 trimethylation to Wnt signaling through a novel Dot1-containing complex (DotCom). *Genes Dev*, **24**, 574-589.

Mueller, D., Bach, C., Zeisig, D., Garcia-Cuellar, M.P., Monroe, S., Sreekumar, A., Zhou, R., Nesvizhskii, A., Chinnaiyan, A., Hess, J.L*., et al.* (2007) A role for the MLL fusion partner ENL in transcriptional elongation and chromatin modification. *Blood*, **110**, 4445-4454.

Mueller, D., Garcia-Cuellar, M.P., Bach, C., Buhl, S., Maethner, E. and Slany, R.K. (2009) Misguided transcriptional elongation causes mixed lineage leukemia. *PLoS Biol*, **7**, e1000249.

Navarro, M. and Gull, K. (2001) A pol I transcriptional body associated with VSG mono-allelic expression in *Trypanosoma brucei*. *Nature*, **414**, 759-763.

Ng, H.H., Xu, R.M., Zhang, Y. and Struhl, K. (2002) Ubiquitination of histone H2B by Rad6 is required for efficient Dot1-mediated methylation of histone H3 lysine 79. *J Biol Chem*, **277**, 34655-34657.

Nguyen, A.T. and Zhang, Y. (2011) The diverse functions of Dot1 and H3K79 methylation. *Genes Dev*, **25**, 1345-1358.

Oberholzer, M., Morand, S., Kunz, S. and Seebeck, T. (2006) A vector series for rapid PCR-mediated C-terminal in situ tagging of *Trypanosoma brucei* genes. *Mol Biochem Parasitol*, **145**, 117-120.

Okuno, Y., Satoh, H., Sekiguchi, M. and Masukata, H. (1999) Clustered adenine/thymine stretches are essential for function of a fission yeast replication origin. *Mol Cell Biol*, **19**, 6699-6709.

Ooga, M., Inoue, A., Kageyama, S., Akiyama, T., Nagata, M. and Aoki, F. (2008) Changes in H3K79 methylation during preimplantation development in mice. *Biol Reprod*, **78**, 413-424.

Overath, P. and Engstler, M. (2004) Endocytosis, membrane recycling and sorting of GPI-anchored proteins: *Trypanosoma brucei* as a model system. *Molecular Microbiology*, **53**, 735-744.

Passarge, E. (1979) Emil Heitz and the concept of heterochromatin: longitudinal chromosome differentiation was recognized fifty years ago. *Am J Hum Genet*, **31**, 106-115.

Pays, E., Vanhollebeke, B., Vanhamme, L., Paturiaux-Hanocq, F., Nolan, D.P. and Perez-Morga, D. (2006) The trypanolytic factor of human serum. *Nat Rev Microbiol*, **4**, 477-486.

Peacock, L., Ferris, V., Sharma, R., Sunter, J., Bailey, M., Carrington, M. and Gibson, W. (2011) Identification of the meiotic life cycle stage of *Trypanosoma brucei* in the tsetse fly. *Proceedings of the National Academy of Sciences*, **108**, 3671-3676.

Peters, A.H., Kubicek, S., Mechtler, K., O'Sullivan, R.J., Derijck, A.A., Perez-Burgos, L., Kohlmaier, A., Opravil, S., Tachibana, M., Shinkai, Y*., et al.* (2003) Partitioning and plasticity of repressive histone methylation states in mammalian chromatin. *Mol Cell*, **12**, 1577-1589.

Ploubidou, A., Robinson, D.R., Docherty, R.C., Ogbadoyi, E.O. and Gull, K. (1999) Evidence for novel cell cycle checkpoints in trypanosomes: kinetoplast segregation and cytokinesis in the absence of mitosis. *J Cell Sci*, **112 (Pt 24)**, 4641-4650.

Rice, J.C. (2002) Mitotic-specific methylation of histone H4 Lys 20 follows increased PR-Set7 expression and its localization to mitotic chromosomes. *Genes & Development*, **16**, 2225-2230.

Robinson, D.R., Sherwin, T., Ploubidou, A., Byard, E.H. and Gull, K. (1995) Microtubule polarity and dynamics in the control of organelle positioning, segregation, and cytokinesis in the trypanosome cell cycle. *J Cell Biol*, **128**, 1163-1172.

Rudenko, G., Cross, M. and Borst, P. (1998) Changing the end: antigenic variation orchestrated at the telomeres of African trypanosomes. *Trends Microbiol*, **6**, 113-116.

San-Segundo, P.A. and Roeder, G.S. (2000) Role for the silencing protein Dot1 in meiotic checkpoint control. *Mol Biol Cell*, **11**, 3601-3615.

Santos-Rosa, H., Schneider, R., Bannister, A.J., Sherriff, J., Bernstein, B.E., Emre, N.C., Schreiber, S.L., Mellor, J. and Kouzarides, T. (2002) Active genes are tri-methylated at K4 of histone H3. *Nature*, **419**, 407-411.

Sawada, K., Yang, Z., Horton, J.R., Collins, R.E., Zhang, X. and Cheng, X. (2004) Structure of the conserved core of the yeast Dot1p, a nucleosomal histone H3 lysine 79 methyltransferase. *J Biol Chem*, **279**, 43296-43306.

Schermelleh, L., Heintzmann, R. and Leonhardt, H. (2010) A guide to super-resolution fluorescence microscopy. *J Cell Biol*, **190**, 165-175.

Schotta, G., Lachner, M., Sarma, K., Ebert, A., Sengupta, R., Reuter, G., Reinberg, D. and Jenuwein, T. (2004) A silencing pathway to induce H3-K9 and H4-K20 trimethylation at constitutive heterochromatin. *Genes Dev*, **18**, 1251-1262.

Schubeler, D. (2004) The histone modification pattern of active genes revealed through genome-wide chromatin analysis of a higher eukaryote. *Genes & Development*, **18**, 1263-1271.

Schulze, J.M., Jackson, J., Nakanishi, S., Gardner, J.M., Hentrich, T., Haug, J., Johnston, M., Jaspersen, S.L., Kobor, M.S. and Shilatifard, A. (2009) Linking cell cycle to histone modifications: SBF and H2B monoubiquitination machinery and cell-cycle regulation of H3K79 dimethylation. *Mol Cell*, **35**, 626-641.

Segurado, M., de Luis, A. and Antequera, F. (2003) Genome-wide distribution of DNA replication origins at A+T-rich islands in *Schizosaccharomyces pombe*. *EMBO Rep*, **4**, 1048-1053.

Shen, S., Arhin, G.K., Ullu, E. and Tschudi, C. (2001) In vivo epitope tagging of *Trypanosoma brucei* genes using a one step PCR-based strategy. *Mol Biochem Parasitol*, **113**, 171-173.

Siegel, T.N., Gunasekera, K., Cross, G.A. and Ochsenreiter, T. (2011) Gene expression in *Trypanosoma brucei*: lessons from high-throughput RNA sequencing. *Trends Parasitol*, **27**, 434-441.

Siegel, T.N., Hekstra, D.R. and Cross, G.A.M. (2008a) Analysis of the *Trypanosoma brucei* cell cycle by quantitative DAPI imaging. *Molecular and Biochemical Parasitology*, **160**, 171-174.

Siegel, T.N., Hekstra, D.R., Kemp, L.E., Figueiredo, L.M., Lowell, J.E., Fenyo, D., Wang, X., Dewell, S. and Cross, G.A. (2009) Four histone variants mark the boundaries of polycistronic transcription units in *Trypanosoma brucei*. *Genes Dev*, **23**, 1063-1076.

Siegel, T.N., Kawahara, T., Degrasse, J.A., Janzen, C.J., Horn, D. and Cross, G.A. (2008b) Acetylation of histone H4K4 is cell cycle regulated and mediated by HAT3 in *Trypanosoma brucei*. *Mol Microbiol*, **67**, 762-771.

Singer, M.S., Kahana, A., Wolf, A.J., Meisinger, L.L., Peterson, S.E., Goggin, C., Mahowald, M. and Gottschling, D.E. (1998) Identification of high-copy disruptors of telomeric silencing in *Saccharomyces cerevisiae*. *Genetics*, **150**, 613-632.

Stanne, T.M. and Rudenko, G. (2010) Active VSG expression sites in *Trypanosoma brucei* are depleted of nucleosomes. *Eukaryot Cell*, **9**, 136-147.

Steger, D.J., Lefterova, M.I., Ying, L., Stonestrom, A.J., Schupp, M., Zhuo, D., Vakoc, A.L., Kim, J.E., Chen, J., Lazar, M.A.*, et al.* (2008) DOT1L/KMT4 recruitment and H3K79 methylation are ubiquitously coupled with gene transcription in mammalian cells. *Mol Cell Biol*, **28**, 2825-2839.

Stevens, J.R., Noyes, H.A., Schofield, C.J. and Gibson, W. (2001) The molecular evolution of Trypanosomatidae. *Adv Parasitol*, **48**, 1-56.

Stinchcomb, D.T., Struhl, K. and Davis, R.W. (1979) Isolation and characterisation of a yeast chromosomal replicator. *Nature*, **282**, 39-43.

Stockdale, C., Swiderski, M.R., Barry, J.D. and McCulloch, R. (2008) Antigenic variation in *Trypanosoma brucei*: joining the DOTs. *PLoS Biol*, **6**, e185.

Strahl, B.D. and Allis, C.D. (2000) The language of covalent histone modifications. *Nature*, **403**, 41-45.

Stuart, K.D., Schnaufer, A., Ernst, N.L. and Panigrahi, A.K. (2005) Complex management: RNA editing in trypanosomes. *Trends Biochem Sci*, **30**, 97-105.

Sullivan, W.J., Naguleswaran, A. and Angel, S.O. (2006) Histones and histone modifications in protozoan parasites. *Cellular Microbiology*, **8**, 1850-1861.

Sun, Z.W. and Allis, C.D. (2002) Ubiquitination of histone H2B regulates H3 methylation and gene silencing in yeast. *Nature*, **418**, 104-108.

Tardat, M., Brustel, J., Kirsh, O., Lefevbre, C., Callanan, M., Sardet, C. and Julien, E. (2010) The histone H4 Lys 20 methyltransferase PR-Set7 regulates replication origins in mammalian cells. *Nature Cell Biology*, **12**, 1086-1093.

Tardat, M., Murr, R., Herceg, Z., Sardet, C. and Julien, E. (2007) PR-Set7 dependent lysine methylation ensures genome replication and stability through S phase. *The Journal of Cell Biology*, **179**, 1413-1426.

Tiengwe, C., Marcello, L., Farr, H., Dickens, N., Kelly, S., Swiderski, M., Vaughan, D., Gull, K., Barry, J.D., Bell, S.D*., et al.* (2012a) Genome-wide Analysis Reveals Extensive Functional Interaction between DNA Replication Initiation and Transcription in the Genome of *Trypanosoma brucei*. *Cell Rep*, **2**, 185-197.

Tiengwe, C., Marcello, L., Farr, H., Gadelha, C., Burchmore, R., Barry, J.D., Bell, S.D. and McCulloch, R. (2012b) Identification of ORC1/CDC6-Interacting Factors in *Trypanosoma brucei* Reveals Critical Features of Origin Recognition Complex Architecture. *PLoS One*, **7**, e32674.

Vassella, E. and Boshart, M. (1996) High molecular mass agarose matrix supports growth of bloodstream forms of pleomorphic *Trypanosoma brucei* strains in axenic culture. *Mol Biochem Parasitol*, **82**, 91-105.

Vickerman, K. (1985) Developmental cycles and biology of pathogenic trypanosomes. *Br Med Bull*, **41**, 105-114.

Wang, Z., Zang, C., Rosenfeld, J.A., Schones, D.E., Barski, A., Cuddapah, S., Cui, K., Roh, T.Y., Peng, W., Zhang, M.Q*., et al.* (2008) Combinatorial patterns of histone acetylations and methylations in the human genome. *Nat Genet*, **40**, 897-903.

Wirtz, E., Leal, S., Ochatt, C. and Cross, G.A. (1999) A tightly regulated inducible expression system for conditional gene knock-outs and dominant-negative genetics in *Trypanosoma brucei*. *Mol Biochem Parasitol*, **99**, 89-101.

Woods, A., Sherwin, T., Sasse, R., MacRae, T.H., Baines, A.J. and Gull, K. (1989) Definition of individual components within the cytoskeleton of *Trypanosoma brucei* by a library of monoclonal antibodies. *J Cell Sci*, **93 (Pt 3)**, 491-500.

Woodward, R. and Gull, K. (1990) Timing of nuclear and kinetoplast DNA replication and early morphological events in the cell cycle of *Trypanosoma brucei*. *J Cell Sci*, **95 (Pt 1)**, 49-57.

Wu, S. and Rice, J.C. (2011) A new regulator of the cell cycle: the PR-Set7 histone methyltransferase. *Cell Cycle*, **10**, 68-72.

Wysocki, R., Javaheri, A., Allard, S., Sha, F., Cote, J. and Kron, S.J. (2005) Role of Dot1-dependent histone H3 methylation in G1 and S phase DNA damage checkpoint functions of Rad9. *Mol Cell Biol*, **25**, 8430-8443.

Yang, Y.H., Dudoit, S., Luu, P., Lin, D.M., Peng, V., Ngai, J. and Speed, T.P. (2002) Normalization for cDNA microarray data: a robust composite method addressing single and multiple slide systematic variation. *Nucleic Acids Res*, **30**, e15.

Zhang, K., Lin, W., Latham, J.A., Riefler, G.M., Schumacher, J.M., Chan, C., Tatchell, K., Hawke, D.H., Kobayashi, R. and Dent, S.Y. (2005) The Set1 methyltransferase opposes Ipl1 aurora kinase functions in chromosome segregation. *Cell*, **122**, 723-734.

Zhang, W., Xia, X., Reisenauer, M.R., Hemenway, C.S. and Kone, B.C. (2006) Dot1a-AF9 complex mediates histone H3 Lys-79 hypermethylation and repression of ENaCalpha in an aldosterone-sensitive manner. *J Biol Chem*, **281**, 18059-18068.

Zhou, H., Madden, B.J., Muddiman, D.C. and Zhang, Z. (2006) Chromatin assembly factor 1 interacts with histone H3 methylated at lysine 79 in the processes of epigenetic silencing and DNA repair. *Biochemistry*, **45**, 2852-2861.

Appendix

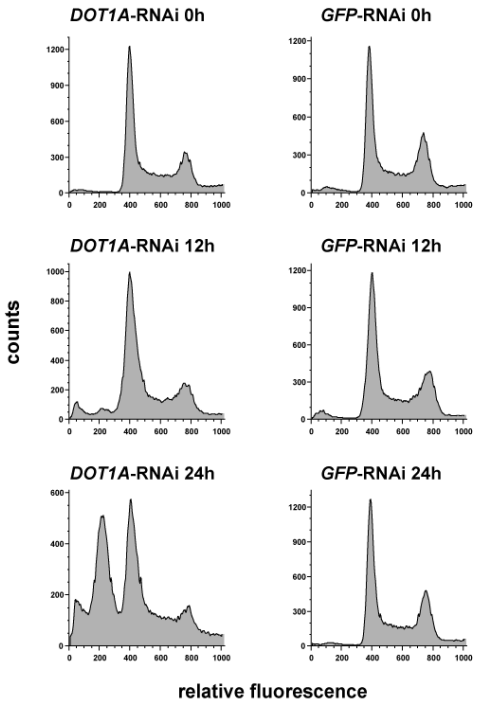

Fig S1: DOT1A-RNAi causes a specific cell cycle phenotype. Flow cytometry analysis of propidium iodide-stained cells transfected with a *DOT1A*-RNAi hairpin construct (left panels) or a *GFP*-RNAi construct as negative control (right panels). Cell cycle profiles of non-induced, 12 hours and 24 hours induced cells are shown. *GFP*-RNAi was transfected into a cell line expressing GFP to control the RNAi. GFP fluorescence was decreased post induction as monitored by FACS (data not shown).

Figures S2 and S3 can be found on enclosed DVD. Based on ChIP-chip results, distribution patterns of H3K76me1, -me2 and H3 are shown for chromosome 10 and genome-wide, respectively.

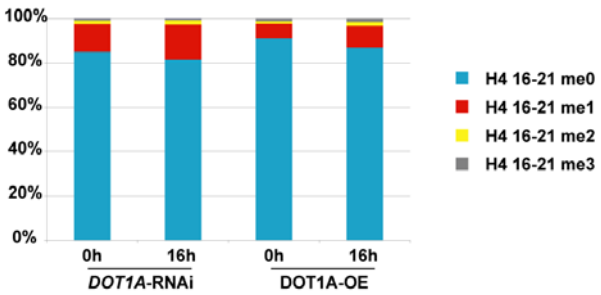

Fig S4: H4K18 methylation levels after manipulation of DOT1A expression. Mass spectrometry analysis of different methylation states of the peptide H4 16-21 in non-induced versus 16 hours induced cells. Histone H4 of whole cell lysates from *DOT1A*-RNAi and DOT1A over-expressing cells was separated by SDS gel electrophoresis and examined for H4 16-21 methylation.

Contents of enclosed DVD

- Figures S2 and S3 (.pdf)
- Gene Construction Kit (GCK) files of plasmids generated during this thesis (.gck)
- Inventory of cell lines and oligonucleotides (.xls)
- PhD thesis (.pdf)
- Figures of this thesis (.ai)

Danksagung

Ich möchte mich sehr herzlich bedanken bei …

… Christian Janzen für das interessante Forschungsprojekt, zahlreiche wissenschaftliche Diskussionen und die tolle Zusammenarbeit und Förderung während meiner gesamten Doktorandenzeit.

… Michael Boshart für alle wissenschaftlichen Diskussionen und die Möglichkeit meine Forschung eingebunden in seiner Arbeitsgruppe zu betreiben.

… Peter Becker für die Erstellung des Zweitgutachtens.

… Manuel Arteaga für seine Hilfe bei der Auswertung der ChIP-Daten.

… allen aktuellen und ehemaligen Mitgliedern der Arbeitsgruppen Janzen und Boshart, die mir jederzeit in vielerlei Hinsicht geholfen haben, und natürlich für alle lustigen und unvergessenen Momente im und außerhalb des Labors!

… Stefan Allmann, George Githure, Daniela Tonn und Jürgen Zschocke für das hilfreiche Korrekturlesen.

… Nils für seine ununterbrochene Unterstützung während der gesamten Zeit.